Final Report

NASA Grant NAS5-28754

KINEMATICS AT THE INTERSECTION OF THE GARLOCK AND DEATH VALLEY FAULT ZONES, CALIFORNIA: INTEGRATION OF TM DATA AND FIELD STUDIES

Principal Investigators:

Kenneth L. Verosub
Roland H. Brady, III
Michael Abrams

Associate Investigators:

Jeff Clayton
Alan Cregan
Bennie W. Troxel

March 1989

Final Report

NASA Grant NAS5-28754

KINEMATICS AT THE INTERSECTION OF THE GARLOCK AND DEATH VALLEY FAULT ZONES, CALIFORNIA: INTEGRATION OF TM DATA AND FIELD STUDIES

Principal Investigators:

Kenneth L. Verosub
(Dept. of Geology, University of California, Davis, CA 95616)

Roland H. Brady, III
(Dept. of Geology, California State University, Fresno, CA 93740)

Michael Abrams
(Jet Propulsion Laboratory, MS 183-501, Pasadena, CA 91109)

Report prepared by:

Roland H. Brady, III
Jeff Clayton
Kenneth L. Verosub
Alan Cregan
Bennie W. Troxel
Michael Abrams

March 1989

TABLE OF CONTENTS

Appendices:

INTRODUCTION

Three elements critical to the analysis of neotectonic processes are the morphology of fault systems, the nature of fault-fault interactions, and the style of deformation along the boundary faults. The southern Death Valley region represents an ideal, if not unique, natural environment for the study of these neotectonic features. The area is situated at the intersection of the Death Valley and Garlock fault zones and has been the locus of vigorous Neogene tectonic activity. In the Death Valley area, remote sensing is an ideal tool for studying the details of neotectonic phenomona because surface exposure is excellent and geologic features are well-preserved in the arid climate.

The purpose of this study is to examine the kinematic relationships at the intersection of the southern Death Valley and Garlock fault zones, to identify and delineate the eastern structural boundary between the Mojave and the Basin and Range geologic terranes, and to construct a model for the evolution of this boundary through time. In order to accomplish this, satellite imagery was combined with field investigations to study six areas in the vicinity of the intersection, or possible extensions, of the fault zones. The information gathered from these areas allowed us to test the various hypotheses that have been proposed to explain the interaction between the Death Valley and Garlock fault zones.

BACKGROUND

This study focussed on the intersection of the Garlock and Death Valley fault zones commencing with features exposed mainly along the Garlock and farther south. These fault zones mark the northern (and possibly the eastern) structural boundary between the Basin and Range and Mojave geologic provinces of southeastern California (Figure 1).

The Basin and Range province is topographically rugged terrain with high mountains and deep valleys. The characteristic structures are seismically-active, northwest-striking normal faults upon which west-vergent extension occurred during late Tertiary time. The role of a number of right-lateral fault

Figure 1. Generalized index map of southern California showing location of the study area in relation to major geologic provinces, faults, and physical features. Major strike-slip faults indicated: GFZ = Garlock fault zone, DVFZ = Death Valley fault zone, LVVSZ = Las Vegas Valley shear zone, SAFZ = San Andreas fault zone, SJFZ = San Jacinto fault zone. AM= Avawatz Mountains, SH= Silurian Hills, SM= Soda Mountains, SL= Soda Lake, BM= Bristol Mountains.

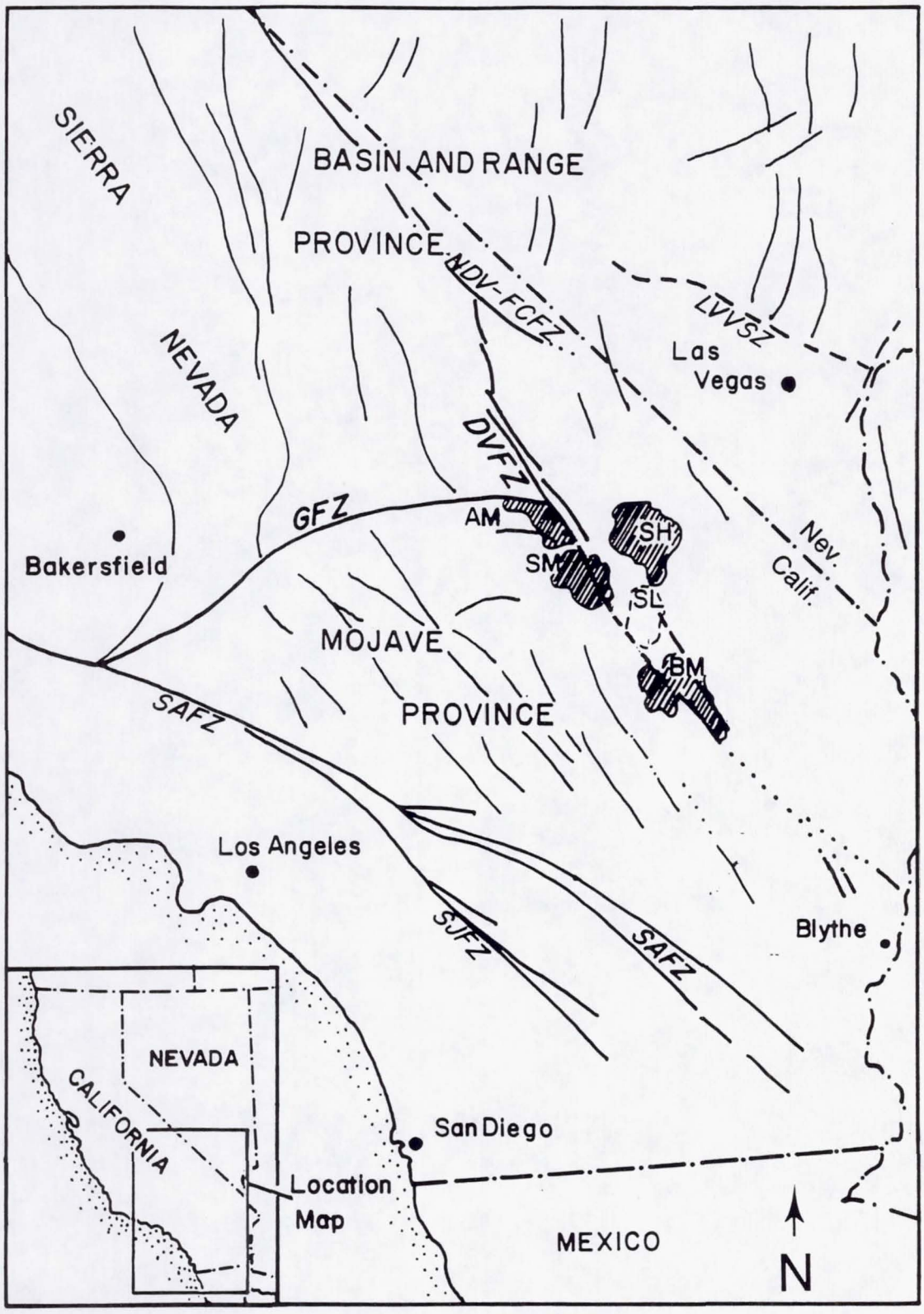
SIERRA
NEVADA
BASIN AND RANGE
PROVINCE
NDV-FCFZ
LVVSZ
Las
Vegas
DVFZ
GFZ
AM
SH
SM
SL
Nev.
Calif.
Bakersfield
MOJAVE
PROVINCE
BM
SAFZ
Los Angeles
SJFZ
SAFZ
Blythe
NEVADA
CALIFORNIA
San Diego
Location
Map
MEXICO
N

systems in the tectonic scheme of this provinceis unclear. One of the largest of these systems is the Northern Death Valley-Furnace Creek fault system.

In contrast to the Basin and Range province, most of the Mojave province is deeply eroded and low-lying. Its main structural features are northwest-striking, right-lateral faults although there are northeast- and east-striking, left-lateral faults and a few reverse and low-angle normal faults (Dibblee, 1980). Many of the lateral faults have been active during Quaternary time (Dokka, 1983; Bird and Rosenstock, 1984).

One of the areas most critical to understanding the structural interaction between the Mojave and Basin and Range provinces is the boundary between them, that is, the Garlock and Death Valley fault zones. Because they are at (or form) this important structural boundary, the Garlock and Death Valley fault zones have been the subjects of significant scientific debate as will be discussed below. Since this study examines the relationship between the Garlock and Death Valley fault zones, the mountain ranges and basins that contained data pertinent to this study were examined in detail (Figure 2). These include from north to south: 1) the Noble Hills on the northwest side of the Avawatz Mountains where the southern Death Valley fault zone emerges from its alluvial cover, 2) the northern Avawatz Mountains at the intersection of the Garlock and Death Valley fault zones, 3) Kingston Wash where the "eastern extension of the Garlock fault" has been suggested to pass, 4) the Soda Mountains which contain the Soda-Avawatz fault zone, a pronounced fault zone on the eastern side of the mountains, 5) Soda Lake which lies southeast of the Soda Mounains and has had an active tectonic history, 6) the Bristol Mountains which were previously not mapped in detail (Basset and Kupfer, 1964) and 7) Ivanpah Valley which was examined for evidence of a possible offset Garlock Fault.

Death Valley Fault Zone

The Death Valley fault system is within the western part of the Basin and Range Province (Figure 1). It consists of three segments that extend 210 km south-southeast from Fish Lake Valley, Nevada, north of Death Valley to the Avawatz Mountains in southern Death Valley, California. The northern

Figure 2. Generalized index map of faults and features examined in this study including the hypothesized "eastern extension of the Garlock fault zone" and the proposed "southern extension of the Death Valley fault zone."

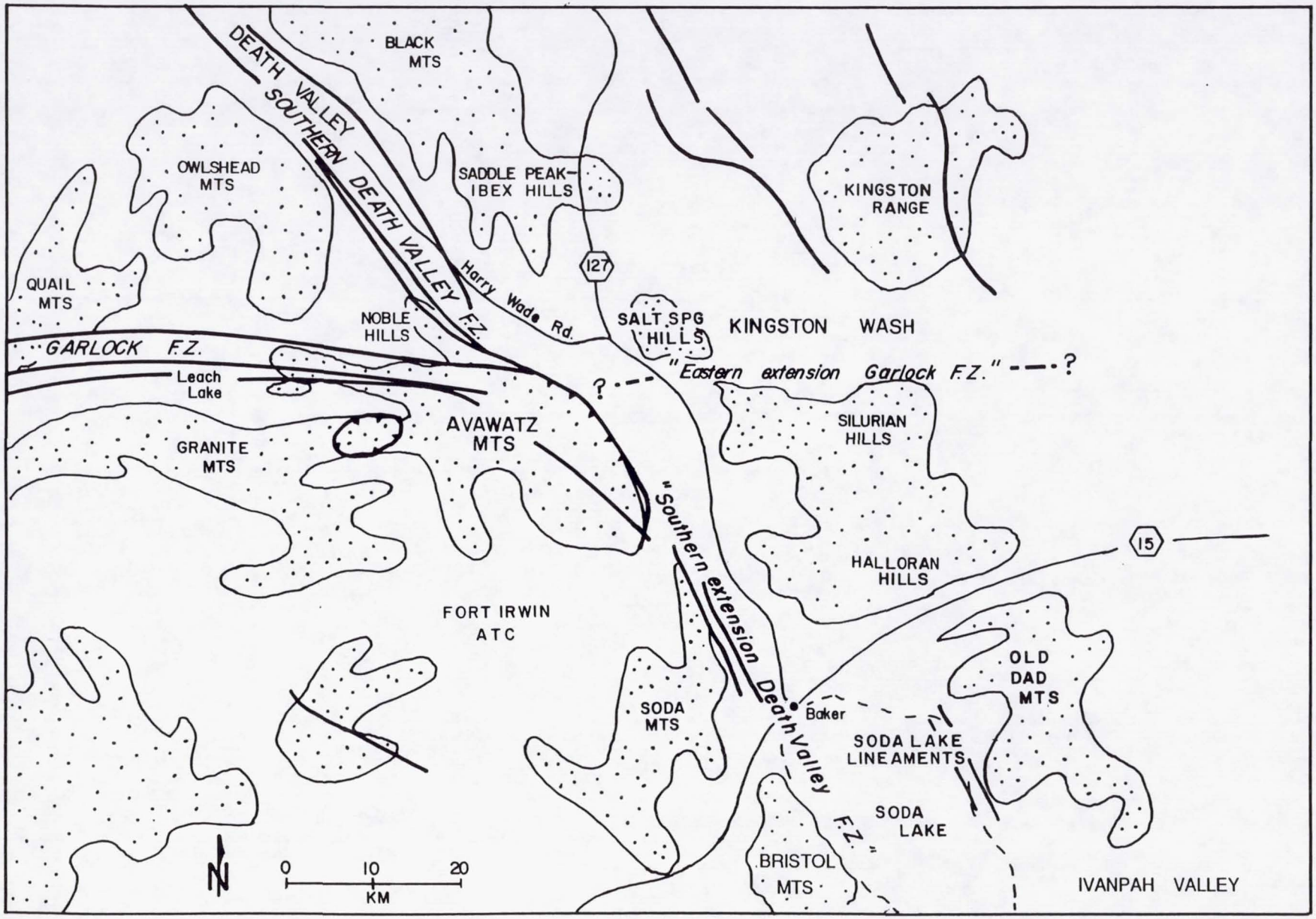
DEATH VALLEY
SOUTHERN DEATH VALLEY F.Z.
BLACK MTS
OWLSHEAD MTS
SADDLE PEAK-IBEX HILLS
KINGSTON RANGE
127
QUAIL MTS
NOBLE HILLS
Harry Wade Rd.
SALT SPG HILLS
KINGSTON WASH
GARLOCK F.Z.
Leach Lake
"Eastern extension Garlock F.Z." ---?
?
AVAWATZ MTS
GRANITE MTS
SILURIAN HILLS
"Southern extension Death Valley F.Z."
15
HALLORAN HILLS
FORT IRWIN ATC
OLD DAD MTS
SODA MTS
Baker
SODA LAKE LINEAMENTS
SODA LAKE
BRISTOL MTS
IVANPAH VALLEY
N
0 10 20
KM

segment, the Northern Death Valley-Furnace Creek fault zone, is mainly a right-lateral shear with as much as 80 km of horizontal displacement (Stewart, 1967; Wright, in press). The central segment of this fault zone passes through Furnace Creek Wash and continues south-southeastward along the northeast side of Furnace Creek Wash into the Amargosa Valley. The southern segment of the Death Valley fault system is the southern Death Valley fault zone. It extends south-southeast from Shoreline Butte in Death Valley to the north edge of the Avawatz Mountains (Noble and Wright, 1954; Troxel and Butler, 1979) and possibly beyond (Stewart, 1967; Troxel, 1968; Dibblee, 1980; Brady, 1984). The southern Death Valley fault zone has several branches; on all of the branches the separation is predominantly right-lateral (Hill and Troxel, 1966; Butler *et al.*, 1988).

The west-dipping central segment of the Death Valley fault system extends 60 km south from the mouth of Furnace Creek Wash to about 30 km north of the Noble Hills in the vicinity of Shoreline Butte. This segment forms the steep eastern edge of central Death Valley and has been considered to be a series of oblique faults on the east side of a pull-apart basin (Burchfiel and Stewart, 1966; Wright *et al.*, 1974). The direction of transport on the central segment is parallel to that on the northern and southern segments with the addition of a significant normal, down-to-the-west component on the hanging wall.

The total amount of slip across the Death Valley fault system is undetermined although major separation is well documented. Stewart (1967) proposed that there had been up to 80 km of separation on the combined fault system. On the other hand, Wright and Troxel (1967) believed the offset along the southern Death Valley fault zone to be less than 8 km. Troxel (1970) later revised this estimate to about 20 km. Since then, the estimate has been increased to about 35 km in accordance with petrologic evidence (Butler *et al.*, 1988). Davis and Burchfiel (1973) asserted the offset was less than 8 km based on a tectonic model, although Brady (1984) produced stratigraphic and petrologic evidence supporting 25-35 km of right separation along the segment of the southern Death Valley fault zone that extends between the Avawatz Mountains and the Halloran Hills.

Branches of the southern Death Valley fault zone are well-exposed in the Confidence Hills, and along the northern edge of the Avawatz Mountains in the Noble Hills (Figure 3). Troxel (1970) and Troxel and Bulter (1979) noted that some of these branches had moved at different times than others and that the branches with the earliest movements were on the southwest side of the zone; however the age of the earliest movement in this area has not been determined. An even older branch of the southern Death Valley fault zone lies farther west along the east flank of the Owlshead Mountains; movement on this branch may have ceased by 14 Ma (Butler *et al.*, 1988).

Abundant evidence exists for late Quaternary activity along the central and southern segments of the southern Death Valley fault zone. In the Confidence Hills and in the Noble Hills, the youngest fault branches are to the northeast indicating that the locus of movement migrated in that direction (Troxel, 1970; Troxel and Butler, 1979; Butler *et al.*, 1988). Northeast of the Noble Hills, on the floor of Death Valley, at least three episodes of folding and faulting have occurred in Pleistocene time (Troxel and Butler, 1979) and surficial features suggest that flexural upwarping is continuing (Troxel, 1970; Butler, 1984).

Garlock Fault Zone

The Garlock fault zone, the second largest on-shore fault in California, separates the Mojave Province to the south from the Basin and Range Province to the north. The fault zone extends 260 km from the San Andreas fault on the west to the area of southern Death Valley on the east (Figure 1). Left-lateral offset of 64 km has been documented across the Garlock fault (Smith, 1962; Smith and Ketner, 1970), and active creep has been measured at Fremont and at Cantil Valleys located along the central portion of the Garlock fault (Clark, 1973). Troxel *et al.* (1972), noted the probability of differential displacement along the Garlock fault.

Although the fault and its traces have been described in detail along much of its length (Smith, 1962; Michael, 1966; Smith and Ketner, 1970; Carter, 1971), the disposition of its eastern end in the southern Death Valley region is unclear (Figure 2). The general features of the intersection of the Death Valley

Figure 3. Generalized geologic map of the Avawatz Mountains. ASFZ= Arrastre Spring fault zone, DLF= Drinkwater Lake fault, GFZ= Garlock fault zone, MSFZ= Mule Spring fault zone, SDVFZ= southern Death Valley fault zone.

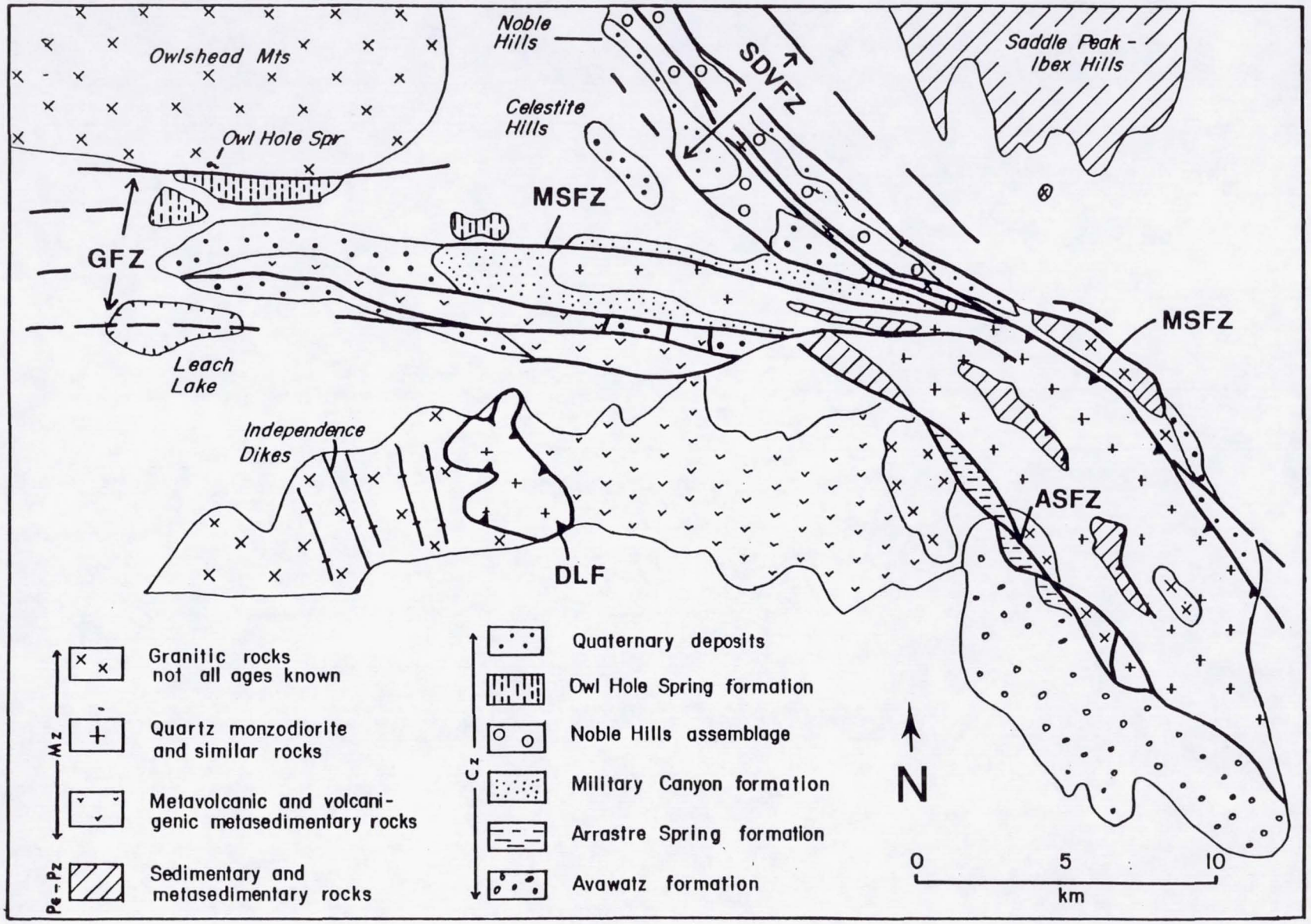
Owlshead Mts
Owl Hole Spr
Noble Hills
Celestite Hills
SDVFZ
Saddle Peak - Ibex Hills
MSFZ
GFZ
Leach Lake
Independence Dikes
DLF
ASFZ
MSFZ
Granitic rocks not all ages known
Quartz monzodiorite and similar rocks
Metavolcanic and volcanigenic metasedimentary rocks
Sedimentary and metasedimentary rocks
Mz
Pe-Pz
Quaternary deposits
Owl Hole Spring formation
Noble Hills assemblage
Military Canyon formation
Arrastre Spring formation
Avawatz formation
Cz
N
0
5
10
km

and Garlock fault zones were first noted by Noble and Wright (1954) and further elaborated by Troxel on the Trona sheet of the Geologic Atlas of California (Jennings *et al.*, 1962). Troxel and Butler (1979) first mapped the area in detail. Farther west, Brady (1986) mapped the eastern part of the Garlock fault zone in detail. Troxel (unpublished data) has since mapped the zone to the southeast end of the Avawatz Mountains. Troxel *et al.* (1979), briefly discussed the Quaternary and Tertiary history of the easternmost part of this fault zone.

Hewett (1954) speculated that the Garlock fault zone may "die out" as a reverse fault on the east flank of the Avawatz Mountains. Troxel and Butler (1979) and Brady and Troxel (1981) documented that the Mule Spring branch of the Garlock fault zone bends nearly 90° from the northern flank to the east side of the Avawatz Mountains. They noted that on the east side, the fault displays reverse-slip, dipping 32-45° towards the west beneath the east flank of the Avawatz Mountains (Figure 3).

Several theories have been proposed for the nature of the interaction between the Death Valley and Garlock fault zones. Jahns and Wright (1960) felt that the Garlock fault simply terminated at the Death Valley fault in the Avawatz Mountains. Davis and Burchfiel (1973) proposed that the fault originated 30-40 km east of the Avawatz Mountains and that it was offset less than 8 km where it crossed the Death Valley fault zone. Stewart (1967) suggested that the Death Valley fault displaced the Garlock fault many kilometers to the south. Troxel and Butler (1979) and Brady (1986a) proposed that the surface of the Garlock fault flattens into an east-directed thrust.

DESCRIPTION OF REMOTE SENSING DATA USED

For our study we obtained three types of remote sensing data: Landsat Thematic Mapper (TM) data; aircraft thermal infrared multispectral scanner data (TIMS); and SPOT satellite panchromatic data.

TM data were obtained in digital form through the Landsat TM project office at the Goddard Space Flight Center. Two different seasons of coverage

were requested: 1) low sun-angle imagery to highlight the structural elements of the landscape and 2) high sun-angle imagery to enhance information about the composition of the surface material. Pertinent information describing the TM quarter scenes is found in Table 1.

TM imagery is acquired as 7 channels of multispectral data in the visible, reflected near-infrared, and thermal wavelength regions (Channel 1=0.45-0.52 μm, Channel 2=0.53-0.60 μm, Channel 3=0.63-0.69 μm, Channel 4=0.76-0.90 μm, Channel 5=1.55-1.75 μm, Channel 6=10.2-12.5 μm, Channel 7=2.08-2.35 μm) with an instantaneous field of view (IFOV) of about 30 m for all channels except the thermal, which has an IFOV of 120 m. A nominal TM scene covers an area of 170 x 185 km. Because of its lower spatial resolution and non-optimal time of data acquisition, the thermal channel was not used in our study.

TIMS acquires 6 channels of data in the 8-12 micron thermal emission region (Channel 1=8.3-8.7 μm, Channel 2=8.8-9.3 μm, Channel 3=9.4-9.9 μm, Channel 4=10.1-11.0 μm, Channel 5=11.0-12.0 μm, Channel 6=12.0-12.6 μm, (Palluconi and Meeks, 1985). TIMS data of the study areas were acquired from NASA's C-130 aircraft on May 13, 1985 at an average elevation of 5500 m above ground level. This produced an IFOV of about 15 m and a swath width of 12 km. TIMS is particularly sensitive to variations in the silica content of surface materials, so that the data is complementary to the lithologic information contained in TM data (Kahle and Goetz, 1983).

Several panchromatic SPOT satellite images were used for structural analyses and were also combined with TM data to enhance the spatial resolution of TM data. The SPOT images were acquired in a single channel in the 0.5-0.8 μm region. Each SPOT scene covers an area of 60 x 60 km, with an IFOV of 10 m. Images are nearly airphoto quality and allow discrimination of small topographic features useful for structural studies.

REMOTE SENSING METHODOLOGY

Image processing for this project was done at the Center for Image Processing and Interactive Computing of the University of California-Davis

Table 1. Thematic Mapper Tapes

TABLE 1. THEMATIC MAPPER TAPES

ID Number	Path-Row	Quads	Date
50155-17445	39-35	1, 3	Aug 03 84
50315-17455	39-35	1, 2, 3, 4	Jan 10 85
40149-17441	39-36	1, 3	Dec 12 84
50155-17452	39-36	1, 3	Aug 03 84
40156-17494	40-35	1, 2, 3, 4	Dec 19 82
50098-17495	40-35	1, 2, 3, 4	Jun 07 84
50274-17520	40-36	1, 2	Nov 30 84
50514-17515	40-36	1, 2, 3, 4	Jul 28 85

and at the Jet Propulsion Laboratory. In the past, the processing of satellite imagery for geological interpretation has focused on the perceptual discrimination of surfaces of varying lithology (Crippen *et al.*, 1987). As a result, the most common processing techniques have involved automatic or interactive classification of different surface types. In this project, a two-dimensional, automatic clustering algorithm was used to partition the six TM bands into thirty-six hexagon-shaped data spaces. Classification of the various alluvial fan surfaces along the northern Avawatz Mountains was attempted using this approach; however, the method was of limited success as the procedure could distinguish only two surface types.

There are three possible reasons why the hexagonal partitions showed such a large overlap in spectral information. First, the ubiquitous presence of a single rock type, in this case the Avawatz quartz monzodiorite, may have served to homogenize the spectral information. Second, windblown dust may have created a fine soil fraction that covered all of the alluvial surfaces, further masking the spectral signature of the alluvial material below (Shipman and Adams, 1987). And finally, the nature of the units may be such that a three-dimensional classification scheme is necessary for useful lithologic discrimination. As a consequence, other processing methods were used including color compositing, principal component analysis, decorrelation stretching, hue-saturation-intensity transformation and band-ratioing. Several of these proved to be more successful at increasing perceptual lithologic discrimination.

For the color composites, a non-linear histogram stretch was used to fill the data range of the TM sensors which have a radiometric resolution of 256 gray levels. For maximum discrimination of lithologic information, color composites were processed as normal images using bands 1, 2 and 3 and as false color images using bands 1, 4 and 7. Unfortunately, this simple method of image enhancement was of limited use. Even though topographic and reflectance information are nearly independent, surface reflectance features combine to produce relatively little color variation using this procedure.

On the other hand, principal component analysis is widely used for enhancing geological information and was a more successful approach.

Because the spectral bands from TM data are highly correlated, principal component analysis can be used to reduce the amount of data required to account for the variance in a scene. This is accomplished by finding a linear transformation which produces orthogonal coordinate axes that are linearly independent of the point distribution function (Gillespie, 1980). This procedure results in the generation of a single image that contains nearly 90% of the scene variance.

In the case of a TM scene which has six bands, the principal component analysis generates six images. The first four principal component images were used to generate several different blue, green and red color composites. The maximum variation in color and brightness was achieved when the color composite consisted of principal component images 1, 2 and 4. In addition, this composite was very useful for depicting geologic detail and for discriminating among at least four diachronous surfaces on a single alluvial fan. In contrast, the automatic classification procedure discussed above uses only the first two principal component images, which may be the reason for its limited success.

One disadvantage of the principal component transformation is the inherent distortion of perceived colors. To avoid difficulties arising from the unrealistic colors, a decorrelation stretch that involves linearly stretching the principal component images parallel to the principal axes was used. The effect of this stretch was to maximize the data space provided by the radiometric resolution of the TM sensors (Gillespie *et al.*, 1986). The stretch was followed by a retransformation of each image back to its original coordinate system for display as a color composite. With this method much of the original color information is retained, but the variance is maximized making interpretation easier.

Of particular value in discriminating between various alluvial fan surfaces were decorrelated images generated from a statistical analysis of data selected from areas covered by alluvium. To achieve this specificity in the principal component analysis and the decorrelation stretch, data were selected from fan surfaces of various ages along the east flank of the Avawatz Mountains. The resulting images showed maximum variation in saturation and intensity for

any given hue of an alluvial fan surface. Decorrelation images derived from bands 1, 5 and 7 and displayed as blue, green and red, respectively, generated the best image for discriminating between different fan surfaces (Plate 1).

Images were also processed using the hue-saturation-intensity transformation which numerically describes color in the image domain using spherical coordinates. With this transformation, the original data are transformed to a spherical coordinate system whose polar angle, radial axis and longitudinal axis represent intensity, saturation and hue, respectively. The advantage of this method is that before retransformation to the original coordinate axes for display, a linear stretch can be applied to the band representing saturation. This procedure has the effect of greatly enhancing the subtle variation of a particular hue. Normal color composites of bands 1, 2 and 3 and false color composites of bands 1, 4 and 7 were best for lithologic discrimination. Even though the hue-saturation-intensity transformation is a valuable aid for lithologic discrimination, the approach proved to be of limited utility because of the spatial resolution of TM data. The subtle variations which could be enhanced were commonly features whose variation in hue was on a scale smaller than the resolution provided by the TM sensors. Although the hue-saturation-intensity transformation may represent an over-enhancement at the present time, it may be more useful with the increased spectral and spatial resolution of future sensors such as the Airborne Visible Infrared Imaging Spectrometer.

To enhance structural information, TM and SPOT images were processed using various filtering operations. These operations fall into the general class of high-pass convolution filters in which an n x n box of non-unity weights is passed over the image, pixel by pixel, to exaggerate the local data number contrast. The size of the box determines the relative spatial frequencies that are enhanced; a small box (i.e., 3 x 3) will boost very high frequencies, a larger box will boost lower frequencies.

Convolution box-car filtering was applied using two different filter sizes: 1) small filters of 5 x 5 or 7 x 7 boxes for high frequency enhancement and 2) large filters of 31 x 31 boxes to suppress gross brightness variations due to albedo differences across the scene. Commonly, the imagery contained areas

of very dark bedrock and very bright alluvial fans and playas. The large box filters suppressed the gross albedo differences and produced images where the overall contrast of the entire scene was more or less uniform. This allowed details to be displayed in both types of albedo regions without destroying the relative, local contrast variations.

The second type of convolution filtering used were Laplacian filters. These are also box-car filters, but the weight matrix has values other than unity. The effect of applying these filters to an image is to exaggerate the contrast differences by computing the local first derivative or gradient. The advantage of Laplacian filters over standard, box-car filters is that artifacts introduced into the data by the filter are reduced. Such artifacts are referred to as "ringing" and appear as bright halos where severe brightness gradients occur at a fine scale.

The analysis of processed TM data proved invaluable in the acquisition of new geologic information relevant to this study; in part, because the large TM scenes provided a synoptic view of the area. The TM images made possible the detection of large-scale lineaments in addition to lithologic and structural discontinuities that were difficult or impossible to observe on the ground. The images also proved to be critically important for studying Quaternary sedimentation and tectonism. Distal portions of alluvial fans, offset 25-30 km laterally along the southern Death Valley fault zone, were detected from the imagery because the fan surfaces have distinctive hues which differ from the hues of the adjacent source areas. By matching the particular combination of clast types on these fan surfaces with surrounding bedrock types, it was determined that the alluvial fans upon which the clasts were deposited have been offset several kilometers from their source rocks to the northwest.

The synoptic view provided by the imagery was also useful for preliminary reconnaissance mapping preceding geologic fieldwork. Careful analysis of the imagery identified important target areas for ground investigations thereby significantly improving the efficiency of those efforts. This pre-selection procedure was especially beneficial for dealing with this vast and remote region. The imagery also played a major role in extending and improving the

detail and accuracy of existing geologic maps some of which will be published by the U.S. Geological Survey.

RESULTS AND FINDINGS

Geological investigations focused on seven areas: 1) Noble Hills, 2) Avawatz Mountains, 3) Kingston Wash, 4) Soda Mountains, 5) Soda Lake, 6) Bristol Mountains and 7) Ivanpah Valley (Figures 1 and 2).

NOBLE HILLS

The Noble Hills extend 14 km northwestward from the northwest part of the Avawatz Mountains (Figure 2). They rise approximately 310 m above the floor of Death Valley. Sub-parallel branches of the southern Death Valley fault zone bound the hills and lie within them (Figure 3). En echelon branches of the fault zone continue 3 km farther northwest of the Noble Hills on the floor of Death Valley. The branches die out or are buried by alluvial fans extending eastward into Death Valley from the Owlshead Mountains.

The general geologic features of the Noble Hills were originally described by Noble and Wright (1954). Troxel (unpublished data) mapped the hills in the mid-1960's and Brady (1986) refined Troxel's data. Butler (1984) supplemented part of Troxel's map northwest of the Noble Hills on the floor of Death Valley. New data on the Noble Hills was acquired in the course of this project using processed imagery.

The rocks in the Noble Hills consist mainly of fanglomerate and fine-grained, basinal, clastic sediments with interbedded halite, gypsum, limestone, tuff and celestite. The strata range in age from Pliocene or latest Miocene to Holocene.

From the Avawatz Mountains northwest to the point where Denning Springs Wash cuts through the hills, the sequence of strata is: 1) coarse Plio-Pleistocene fanglomerate derived from the Avawatz Mountains, 2) coarse-to-fine-grained basin sediments of probable late Miocene age and 3) very coarse, Plio-Pleistocene fanglomerate composed nearly entirely of quartz monzonite

derived from the Owlshead Mountains. Right-lateral, strike-slip faults separate each rock unit and additional faults cut the basin sediments.

The southwestern fanglomerate unit dips towards the southwest and is locally folded. The central unit of basin sediments is broadly folded into a northwest-plunging anticline. The northwestern fanglomerate unit dips moderately-to-steeply northeast and is bounded on the southwest and northeast by strike-slip faults. Between most of the primary strike-slip faults are lesser, sub-parallel faults that form an anastomosing pattern.

Several stream channels that pass through the Noble Hills, originate in the Avawatz Mountains and contain gravel deposits genetically related to alluvial fan deposits on the northern flank of the Avawatz Mountains. Because several of the gravel deposits overlie or are cut by branches of the southern Death Valley fault zone, the fault traces can be assigned to a relative-age classification. In this way, the image processing was used to correlate fan units of similar age and morphology throughout the Noble Hills and along the entire front of the Avawatz Mountains.

As it does in the Confidence Hills 20 km north of the Noble Hills, the age of faulting on branches of the southern Death Valley fault zone in the vicinity of the Avawatz Mountains decreases from southwest to northeast (Troxel, 1970). For example, the southwesternmost and oldest fault branch in the Noble Hills juxtaposes fanglomerate against basin sediments. This branch and surrounding strata have been folded by movement on younger faults farther northeast in the Noble Hills. The most northeasterly fault branch, at the mouth of Denning Spring Wash in the Noble Hills, is overlain by a Quaternary fanglomerate unit (Figure 3). About 3 km northwest of the wash, this same fanglomerate unit is cut by fault branches that extend northward onto the floor of Death Valley. The youngest faulting and related folding has occurred on northeastern branches along the valley floor. Topographic relief along these faults is rarely more than a few meters. Butler *et al.* (1988) have shown that the Amargosa River channel is responding to Holocene faulting on the valley floor north of the Noble Hills.

AVAWATZ MOUNTAINS

Investigations in the Avawatz Mountains focussed on four main topics: 1) fracture measurements along the Garlock fault zone, 2) sedimentology and stratigraphy of the Owl Hole Spring formation between the Avawatz and Owlshead Mountains, 3) stratigraphy and morphology of Quaternary alluvial fans on the north and east side of the Avawatz Mountains and 4) bedrock mapping using TM and TIMS imagery within restricted areas of the Avawatz Mountains in the Fort Irwin Military Reservation.

Fracture Measurements

Fracture measurements were made at two areas in the Avawatz Mountains in an attempt to characterize the fracture pattern along the Garlock fault zone. The purpose of these measurements was to provide a frame of reference for similar measurements made in Kingston Wash along the hypothesized eastern continuation of the Garlock fault. One of the areas studied in the Avawatz Mountains was the metavolcanic bedrock located along the Garlock fault; the other was the basement "diorite" between the Mule Spring fault and southern branches of the Garlock fault (Figure 3). The data were analyzed for preferred orientation using a computer and a stereonet contouring program.

The first site, along the Garlock fault, contains two primary fracture populations: 1) a north-northeast striking population of fractures and shears that dip steeply northwest or northeast and 2) a very intense, penetrative shear foliation that strikes due east and dips an average of 40° S. At the second site, fractures in the basement diorite mainly strike east and dip moderately to vertically. Although there are minor differences in fracture orientations at the two sites, most of the fractures at both sites have a marked east-striking preferred orientation. Thus, where measured, the Garlock fault zone in the Avawatz Mountains is characterized by a pronounced east-striking fracture foliation (Figure 4A).

Figure 4. Contoured lower-hemisphere stereoplot of poles to major joints and fractures. Pattern in B and C are notably dissimilar to that in A. A: Pattern of fractures along Garlock fault zone. The strike is mainly east-northeast and the dip is steep to the north. B: Pattern of fractures for a location in the Salt Spring Hills south of the eastern extension of the Garlock fault zone . Pattern shows two populations of steep to moderately dipping, intersecting fractures: one population is striking north-northeast and the other is striking north-northwest. C: Pattern of fractures for a location in the northern Silurian Hills north of the eastern extension of the Garlock fault . Pattern shows mainly near-vertical fractures striking north.

GARLOCK FZ
AVAWATZ MTS

A.

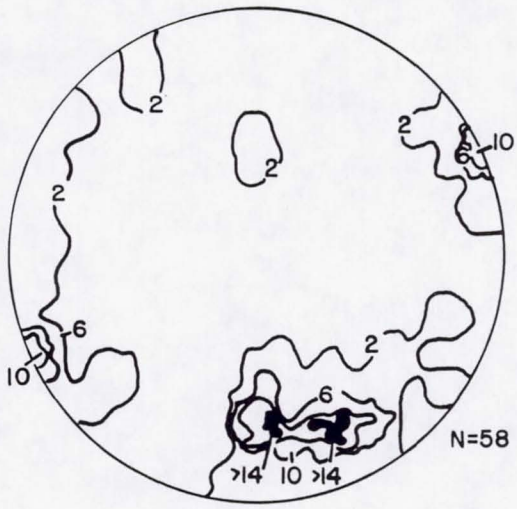

SOUTHERN
SOUTHERN SALT
SPRING HILLS

B.

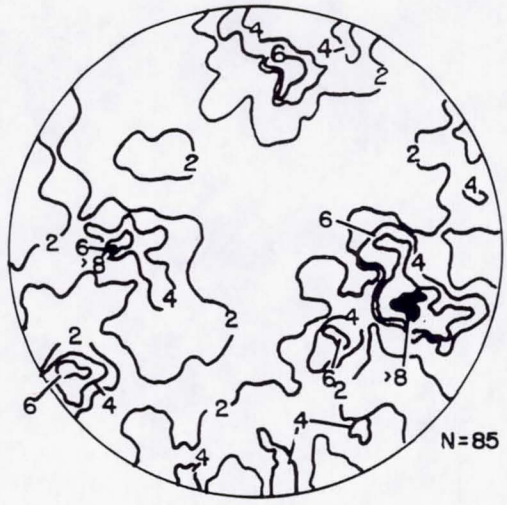

NORTHERN
SILURIAN HILLS

C.

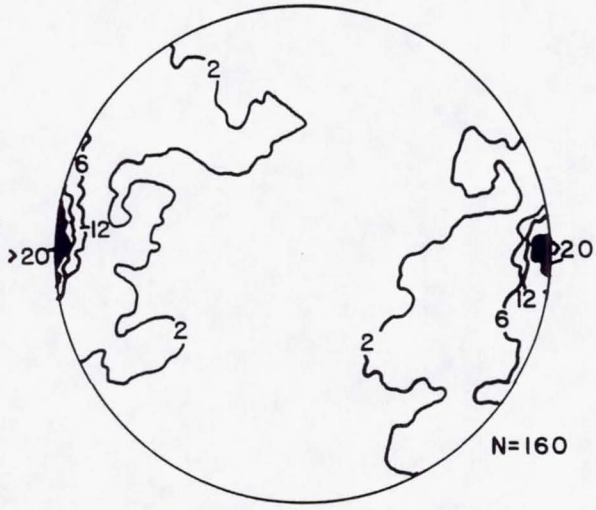

Significance of the Owl Hole Spring Formation

The Owl Hole Spring formation (new name) is an important unit in the study area because it constrains the amount and timing of offset that has occurred on the eastern traces of the Garlock fault zone. The Owl Hole Spring formation is a sequence of Neogene continental strata that was deposited in a triangular-shaped basin between the Avawatz and Owlshead Mountains (Figure 3).

The formation has two members (Figure 5). The lower member contains claystone, sandstone, celestite-bearing limestone, gypsum, halite, bedded manganese, granule-to-pebble conglomerate and breccia, and a tuff that has a radiometric age of 6.31 ± 0.21 Ma (Appendix I). These strata are interpreted to represent deposition in a paleoenvironment that shifted vertically from lake to playa to the distal fluvial fringe of an alluvial fan. The upper member consists of pebble-to-boulder conglomerate that represents a prograding alluvial fan complex.

The composition of clasts changes upward through the unit (Appendix II). The lower member contains alternating conglomerate beds whose clasts were derived mainly from two distinctive sources: 1) metavolcanic rocks similar to those exposed in the Avawatz Mountains and 2) Tertiary volcanic and Mesozoic granitic rocks such as those that make up most of the Owlshead Mountains. Rarely are these two lithologic associations mixed in the same bed, but rather they appear in discreet horizons. Metavolcanic clasts occur in volumetric proportions approximately equal to the combined volume of volcanic and granitic clasts. Clasts in the upper member are nearly entirely derived from a metavolcanic source. The change in clast composition occurs rather abruptly at the boundary between the lower and upper members.

The Owl Hole Spring formation is interpreted to have been deposited in a lacustrine basin that lay between the Avawatz and Owlshead Mountains and that was filled by alluvial fans prograding from the adjacent ranges. As the Owl Hole Spring formation contains sediment derived from both ranges and is essentially in place, the total lateral offset on the Garlock fault between the

Figure 5. Generalized stratigraphic section of the Owl Hole Spring formation showing two members. M= silt, S= sand, P= pebble, C= cobble, B= boulder.

OWL HOLE SPRING FORMATION

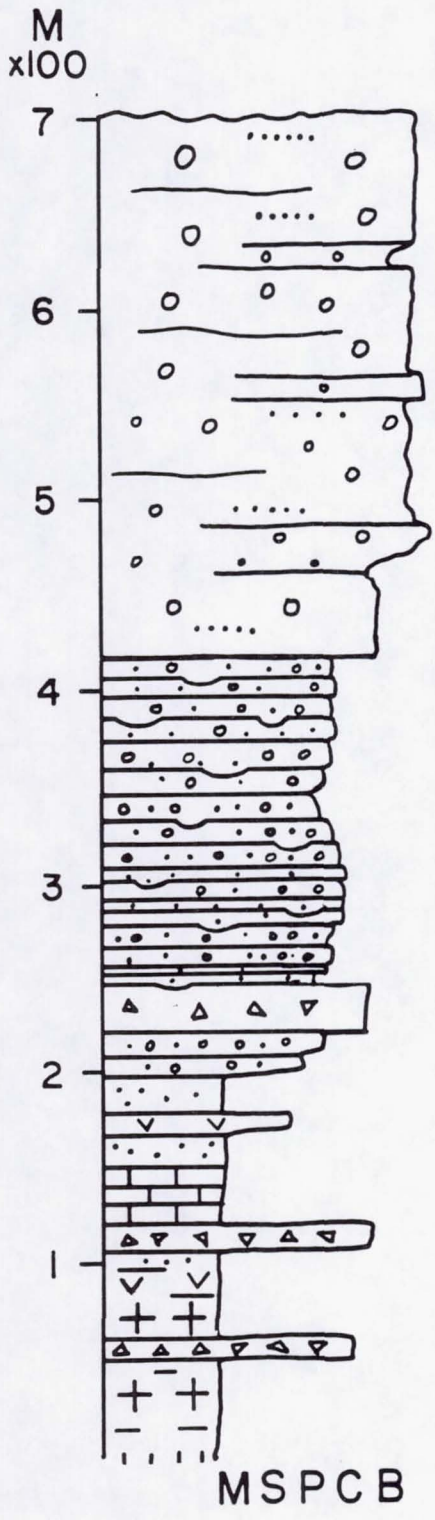

UPPER CONGLOMERATE MEMBER

LOWER EVAPORITE-CARBONATE-CLASTIC MEMBER

Avawatz and Owlshead Mountains can have been no more that a few kilometers since the Owl Hole Spring formation was deposited about 6.3 Ma. This interpretation greatly constrains models for the amount and timing of offset on the Garlock fault.

Quaternary Alluvial Fans

Three Quaternary alluvial fans along the northern flank of the Avawatz Mountains were studied in detail. They are, from west to east, the Sheep Creek, Anvil Canyon and Avawatz Peak alluvial fans (Figure 6). Because of the low relief and very low slope of alluvial surfaces, alluvial fans are ideally suited for remote sensing. Remotely-sensed data of alluvium are commonly better indicators of local bedrock geology than the bedrock itself because the bedrock is usually located in mountainous areas of high relief and steep slopes. Thus, spectral information is obscured by slope-related albedo effects, by spatial variability of vegetation, and by staining from chemical weathering processes. In contrast, active transport on recent fan surfaces and along modern stream channels delivers fresh unweathered material to the relatively flat-lying surfaces and the uniformly sparse vegetation present on alluvial surfaces does not interfere with the spectral response of surface lithologies (Shipman and Adams, 1987).

However, remote-sensing of alluvial fans provides only information about the surface of the fans, whereas alluvial fan deposits, because they are 3-dimensional, must be investigated in the field. Since an alluvial surface does not necessarily coincide with the original surface of a deposit, the distinction between alluvial fan deposits and their overlying surfaces will be kept clear in this discussion.

Satellite imagery of the northern flank of the Avawatz Mountains revealed two uplifted fanglomerate units within the mountain range and a younger, uplifted and tilted alluvial fan deposit north of the mountain-front (Plate 1). The thickest and most elevated fanglomerate unit (QPf1 on Figure 7) is about 50 m thick. It is well-exposed along the Mule Spring fault and is probably the oldest alluvial deposit in the Sheep Creek Wash canyon. Near the mouth of the Sheep Creek canyon, the younger uplifted fanglomerate unit (QPf2 on

Figure 6. Interpretive map of Plate 1 showing three major alluvial fans and the intersection of the Garlock and Death Valley fault zones along the northern Avawatz Mountains. Heavy lines are fault traces, thin lines are roads and rivers, dashed lines are alluvial fan boundaries and dotted lines are fan surface boundaries.

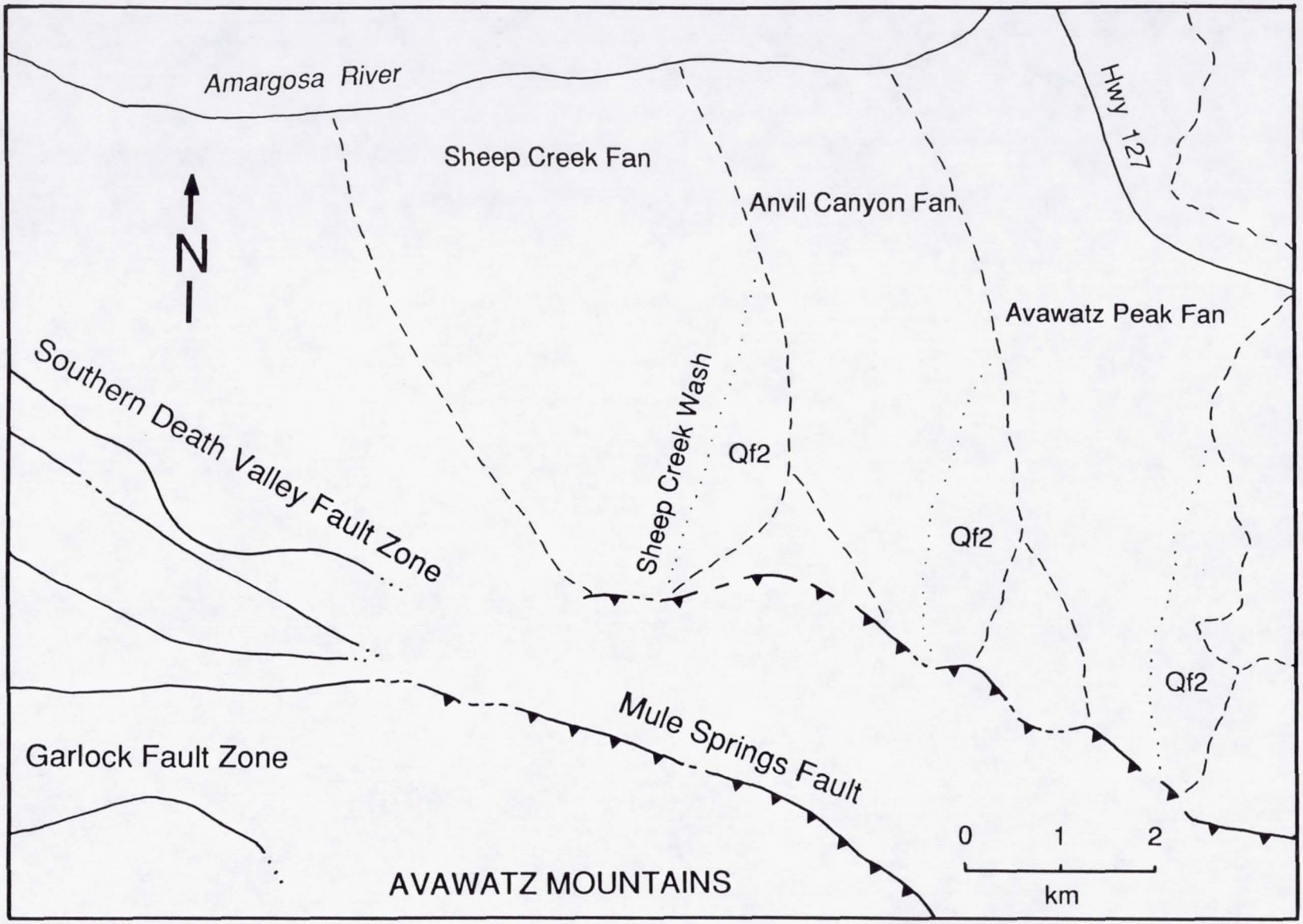
Amargosa River
Sheep Creek Fan
Anvil Canyon Fan
Hwy 127
N
Avawatz Peak Fan
Southern Death Valley Fault Zone
Sheep Creek Wash
Qf2
Qf2
Qf2
Mule Springs Fault
Garlock Fault Zone
0
1
2
km
AVAWATZ MOUNTAINS

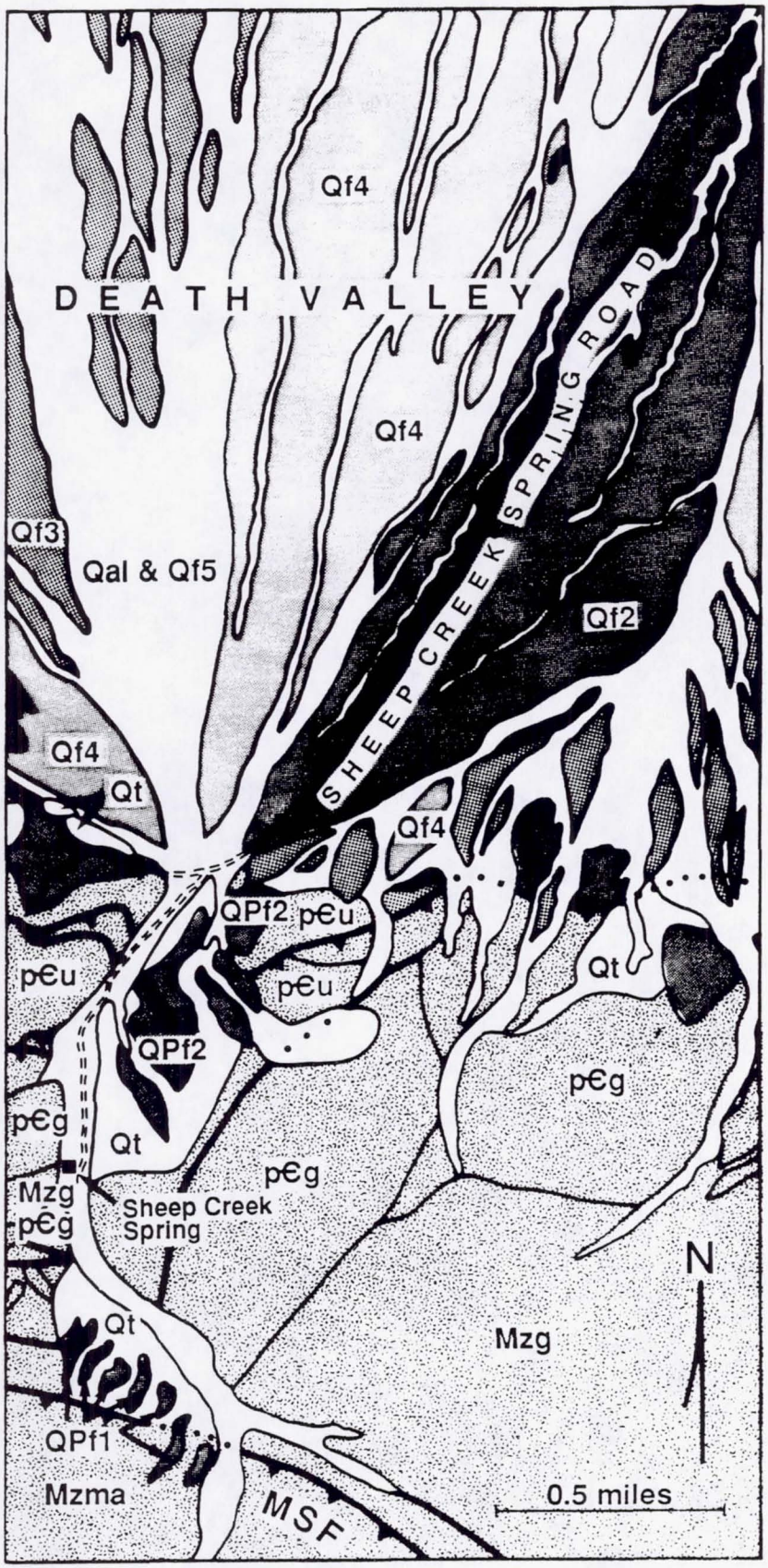
Qf4
DEATH VALLEY
Qf4
SHEEP CREEK SPRING ROAD
Qf3
Qal & Qf5
Qf2
Qf4
Qt
Qf4
QPf2
pЄu
pЄu
pЄu
Qt
QPf2
pЄg
pЄg
Qt
pЄg
Mzg
pЄg
Sheep Creek
Spring
N
Qt
Mzg
QPf1
Mzma
MSF
0.5 miles

Figure 7. Geologic map of lower Sheep Creek canyon and proximal alluvial fan region. MSF= Mule Spring fault, PCg= Precambrian gneiss, PCu= Precambrian undifferentiated sedimentary rocks, Mzma= Mesozoic Avawatz monzodiorite, Mzg=Mesozoic granitic rocks, QPf1= older uplifted fanglomerate, QPf2= younger uplifted fanglomerate, Qt= Quaternary talus, Qf2 through Qf5= Quaternary fan surfaces in order of decreasing age, Qal= modern stream channel deposits. Bedrock geology from Troxel and Butler (1979).

Figure 7) is only about 12 m thick. The uplifted and tilted fan deposit (Qf2 on Figure 7) is at least 6 m thick and is the oldest deposit north of the mountain-front (Clayton, 1988).

Four diachronous alluvial fan surfaces were identified using the imagery. Relative-age assignments for the four surfaces were made using the principles of superposition and the unique spectral properties of the different surfaces (ie. hue, intensity, etc.). For example, the hue of fresh material in the main feeder channel of an alluvial fan matched the hue of the youngest surface on that fan. The fan surfaces were seen on the imagery to overlap and partially cover older fan surfaces. In many cases, specific rock types could be traced directly to their respective bedrock sources because they had similar hues, although on the imagery the fan gravels appeared brighter than their source rocks. The lower intensity of reflected light from the source rocks is attributed to slope-related albedo effects and chemical weathering on their surfaces in contrast to the unweathered surface of the fresh alluvium.

The spectral properties of older fan surfaces are very different from those of younger surfaces. The unique spectral signatures are caused by differences in topography, particle size and the amount of desert varnish developed on the fan surfaces (Kahle and Goetz, 1983). An older, smooth surface with well-developed desert pavement reflects light more effectively than a younger surface with irregular bar-and-channel topography. Large, bouldery bars scatter reflected light more than smooth desert pavement, sandy channel bottoms or fine-grained distal-fan deposits. The presence of desert rock varnish also affects the hue and intensity of the light reflected from a surface. Even though the development of rock varnish tends to smooth or polish the exposed sides of gravel clasts, the dark hue of the varnish increases the overall absorption of reflected light across the visible and near infrared portion of the electromagnetic spectrum. Not only are the absorption features of the surface spectra greatly smoothed by the rock varnish, but the overall intensity of light reflected from a varnished surface is significantly decreased (Shipman and Adams, 1987) This decrease in reflection arises from the differences in mineralogy and from the chemistry of the darkly colored rock varnish.

Based on the imagery, the Avawatz Peak alluvial fan, located near the northeast corner of the Avawatz Mountains, is the largest of the three adjacent fans, yet its drainage basin is smaller than those of the other fans (Figure 6, Plate 1). This drainage basin also possesses the greatest relief of the three basins, therefore the greater volume of the drainage basin accounts for the large areal extent of the Avawatz Peak alluvial fan. These attributes imply that this fan developed where uplift is greatest, and consequently erosion is deepest, in the Avawatz Mountains.

The satellite imagery clearly shows that the distal ends (fan aprons) of the Sheep Creek and Anvil Canyon alluvial fans are truncated by the Amargosa River (Plate 1). Undisturbed deposition of alluvium should produce cone-shaped alluvial fans having lobate, distal-fan aprons (Bull, 1968). Truncation of these distal lobes may have occurred during uplift of the alluvial fans along a fault segment presently buried beneath the alluvium. Similarly, a tributary of the Amargosa River has entrenched the distal-end of the Avawatz Peak alluvial fan. Small, secondary fans have developed below the mouths of uplifted distributaries suggesting that the alluvial fan has been uplifted during late-Quaternary time. Truncated fan aprons associated with secondary-fan development indicate tectonically controlled changes in base-level (Bull, 1978).

The uplifted fanglomerate units and the alluvial fan surfaces were examined in the field to determine their relative-ages. Relative-age assignments were based on topography, the degree of development of desert pavement and rock varnish, the depth and width of channel incisions and the relative elevation of the fan's surface. Clast counts were employed to determine if there were lithologic trends in the fan surfaces and deposits.

Clast counts provided information about the erosional history of the Sheep Creek drainage basin. Modal abundances of clast types were determined for the various surfaces and their underlying deposits. Each count included two hundred clasts from a surface area of approximately one square meter. Along channel-cut banks where clasts from fan deposits could be counted, counts were performed at three places: 1) the upper surface, 2) near the channel

bottom and 3) at a midway position. The clasts counted ranged in size from 1 cm to about 30 cm.

Because clasts of Avawatz quartz monzodiorite are ubiquitous in the uplifted fanglomerate units and all of the alluvial fans, it was more useful to look at trends in clasts derived from the metasedimentary roof pendants and from Tertiary volcanic rocks which at one time probably flanked or were atop the monzodiorite. Clast counts from the younger, uplifted fanglomerate unit (QPf2), adjacent to the Mule Spring fault, showed that the modal abundance of Tertiary volcanic clasts in the lower strata (9-12%) is greater than that of the upper strata (3.5%). The older uplifted fanglomerate contains Tertiary volcanic clasts only in its lower strata (6.5%). The increase in the modal abundance of Tertiary volcanic clasts in the younger uplifted fanglomerate may be partially attributed to deposition and erosion of pre-existing alluvial deposits. A closer examination of the volcanic clasts may better constrain the erosional history of the Avawatz Mountains.

The modal abundances of metasedimentary and volcanic clasts from the younger, uplifted fanglomerate unit (QPf2) and the Qf2 alluvial fan-deposit display very similar trends. This similarity suggests that these two units may be the same and that during late-Pleistocene time, the proximal portion of the alluvial fan, now part of the mountain range, was uplifted about 20 m. Based on calibrated rock varnish cation-ratio curves, the absolute age of the Qf2 fan surface is tentatively estimated to be 40,000 years. If this age is correct, uplift of the rocks in lower Sheep Creek canyon has proceeded at an average rate of 0.5 mm per year.

The younger, uplifted fanglomerate unit along the eastern side of lower Sheep Creek canyon primarily contains clasts from the Avawatz monzodiorite and is virtually devoid of gneiss. The surface of this fanglomerate however, is covered with a layer of gneissic detritus which has eroded from uplifted gneissic bedrock. Because the fanglomerate is deposited over bedrock gneiss and the gneissic detritus exists only at the surface of this fanglomerate unit, it is assumed that the bedrock gneiss was uplifted and exhumed in the lower Sheep Creek canyon sometime during mid- to late-Pleistocene time.

The depositional pattern of the alluvial fan surfaces, revealed on the imagery, indicates that the orientation of the depositional slope has shifted through time. The direction of deep channel incisions on the older fan surfaces is northeast. The direction of channel inception on the older surfaces is northwest. The younger fan surfaces also have a northwest-directed depositional slope which has caused the sediment from each alluvial fan to overlap the adjacent fan to the west (Plate 1). This pattern of alluviation implies that the bedrock underlying the alluvial fan deposits has tilted to the northwest during Quaternary time.

Although fan surfaces undergo episodes of erosion and deposition, they are regions of net deposition. The fan strata in and adjacent to the Avawatz Mountains consist mainly of debris flow and sheet flood deposits with subordinate channel and sieve deposits. The general upward-fining trend in clast size observed in the deposits suggests that during the Holocene there has been a decline in stream competence and therefore sediment delivery rate to the alluvial fans.

The oldest, stable fan surfaces along the north flank of the Avawatz Mountains are the uplifted and tilted fan surfaces designated as Qf2 (Figure 7). These surfaces are characterized by tightly interlocking desert pavement with dark, brownish-to-black rock varnish. The Qf2 surface is more deeply incised than other surfaces. Along the eastern flank of the Avawatz Mountains, Brady (1986) mapped a veneer of severely eroded alluvial material which he designated "Qf1." The greater tilt of the Qf1 surface relative to the Qf2 surface along the northern flank may indicate that uplift of the Avawatz Mountains began near the southeast corner of the mountain range. The Qf1 surface on the eastern flank dip 15° east, whereas the Qf2 surface on the northern flank dips 6° north.

Tilted fan surfaces on the Sheep Creek alluvial fan, previously mapped by Brady (1986) as Qf2, are now considered to be a somewhat younger exhumed surface herein designated Qf3 (Figure 7). The different age for this surface was first deduced from processed imagery which consistently showed that this surface was a slightly lighter shade than Qf2 surfaces elsewhere on the fan (Plate 2). Subsequent field investigations have supported the assignment of a

younger age for this surface: the Qf2 surface is situated higher on the alluvial fan than the Qf3 surface, the Qf2 surface possesses better developed desert pavement and darker rock varnish than the Qf3 surface and channel incisions are deeper in the Qf2 fan surface than they are where this lighter colored Qf3 surface is present.

Data from surface clast counts and soil descriptions from two test pits excavated on each surface also support the age difference. Red granite clasts, common to both of these surfaces, are more fragmented on the Qf3 surface, suggesting that the clasts may have been reworked from pre-existing fan deposits and redeposited downslope. Clasts of monzodiorite buried below the Qf2 surface are almost completely decomposed, while diorite clasts buried below the Qf3 surface are still intact. Soil structure and color are slightly better developed beneath the Qf2 surface than beneath Qf3. Qf2 soil possesses a thicker A horizon than Qf3 soil and a better developed, darker red B_K horizon containing slightly hard, weak-to-medium, angular blocky soil peds. In contrast, the Qf3 soil, has an incipient B_K horizon that is not as red and consists mainly of loose, sandy soil with minor soft, weak, angular blocky soil peds. These data suggest that the Qf2 surface is older than the Qf3 surface and that the Qf2 surface has remained stable for a longer period of time.

The Qf4 surface is easily distinguished from all older surfaces by its lack of rock varnish and desert pavement and by the fact that it is topographically lower than older deposits. The Qf4 surface has a cobble-to-boulder, bar-and-channel topography and is deposited from a northwesterly flow. The only surface younger than Qf4 overlies a coarse-grained, sandy, distal-fan deposit (Qf5). The youngest surfaces on the fan overlie gravelly, terrace deposits and modern stream channel deposits (Qal) which are inset into all older deposits.

Offsets in stream channels, bedrock, and uplifted fan surfaces detected on the imagery were used to determine the sense of fault offset. Left-lateral offset was detected on the Quaternary feeder channels of fans along the Garlock fault zone and right-lateral oblique offset was detected on channels of fans along the east flank of the Avawatz Mountains. Because slickenlines resulting from recent tectonism along the east flank of the Avawatz Mountains are nearly

vertical, implying near-vertical reverse-slip (Brady, 1986), the right-lateral offset observed on stream channels probably formed before the reverse-slip motion occurred. The imagery also revealed right-lateral offset in the layered strata of the Avawatz Formation on the south side of the range, and what are apparently "tear" faults within the crystalline core. These tear faults appear to have divided the crystalline mass into smaller structural blocks.

There is an abrupt change in the size and shape of the Sheep Creek canyon at the point where the Mule Spring fault crosses Sheep Creek Wash. North of this fault, where the uplifted fanglomerate is located, the canyon is shallow and wide. South of the fault, within the Avawatz monzodioritic block, the canyon is narrow, V-shaped and deep and has nearly 1000 m of relief. This contrast is undoubtedly the result of uplift of the Avawatz Mountains along the Mule Spring fault.

Geomorphic expressions of neotectonic activity were observed in lower Sheep Creek canyon. Between the mountain-front and the Mule Spring fault, Precambrian gneiss underlies the uplifted fanglomerates. Near the canyon floor, small, vertical drainage channels are cut into the face of the weathered gneiss. Two meters above the canyon floor, these small channels abruptly become wider and deeper indicating that above this abrupt change, the bedrock has been exposed to surfacial weathering for a longer period of time. These erosional features therefore, suggest that the most recent tectonism of the lower canyon block resulted in about 2 m of vertical displacement.

The imagery also provided information about the tectonic activity that affected the alluvial fans. For example, a continuous fan surface that has been cut by Quaternary faulting was detected at the northeast corner of the Avawatz Mountains (Plate 3). The partially obliterated portion of the semi-circular shaped scarp was nearly impossible to delineate without the imagery. The arcuate shape of the trace suggests that the southwest side of the relict fan surface was uplifted along a low-angle thrust fault. In addition, a slight rotation of the uplifted surface towards the horizontal implies that the fault surface flattens westward. This fault may be a dip-slip splay within the Death Valley fault zone.

What is apparently the same fault is exposed in Sheep Creek canyon along the northern mountain-front (unnamed fault on Figure 8). There, the fault appears to dip more steeply to the south suggesting that the fault flattens eastward from Sheep Creek canyon. The idea that this range-bounding fault shallows and flattens with depth is also supported by a low-angle fault trace in the uplifted gneiss bedrock of lower Sheep Creek canyon.

In the lower Sheep Creek canyon, several faults oriented nearly perpendicular to the canyon, are thought to be splays within the southern Death Valley fault zone (Troxel and Butler, 1979). These anastomosing traces have been truncated and overidden by the Avawatz monzodiorite which was uplifted along the left-lateral, oblique-reverse Mule Spring fault. From the presence of abundant alluvium in lower Sheep Creek canyon, this portion of the southern Death Valley fault zone probably occupied the margin of a depositional basin. Because the fault zone now lies exposed within the mountain range, a northward enlargement of the range is inferred. Thus, the uplifted fanglomerates record the northward migration of the mountain-front.

Geologic Mapping with TM and TIMS Imagery

Much of the southwestern Avawatz Mountains is within the Fort Irwin Army Training Center and, with few exceptions, is off-limits (Figure 2). The area around Leach Lake is particularly hazardous because it is within an air-to-ground gunnery range that abounds with undetonated ordnance. Unfortunately, several relationships critical to determining the age and offset on traces of the Garlock fault are exposed here. Fortunately, the TM and TIMS imagery covered this area in considerable detail and initial geologic work along the borders of the restricted area had been completed. Thus, the geological mapping could be extended into the critical area by integrating the "ground truth" with the imagery, which resulted in good-quality, "second order" geological coverage. This additional information has been added to Brady's (1986) 1:24,000 geologic map of the Avawatz Mountiains, which is proposed for publication as a colored map sheet by the U.S. Geological Survey.

Figure 8. Generalized cross-section of the lower canyon and alluvial fan of Sheep Creek in the northern Avawatz Mountains. The Mule Spring fault (MSF) at the head of the lower canyon forms the boundary between Mesozoic intrusive rocks (Mzma) and Precambrian rocks (PCg= gneiss, CS fm= Crystal Spring Fm, and KP fm= Kingston Peak Fm) that are covered by Plio-Pleistocene alluvial fan deposits (QPf1, QPf2). Fault segments of the Death Valley fault zone are exposed in the lower canyon and perhaps lie buried beneath the Quaternary alluvial fan deposits (Qf2, Qf3). Solid circles indicate well-developed rock varnish; open circles represent fresh or unweathered detritus.

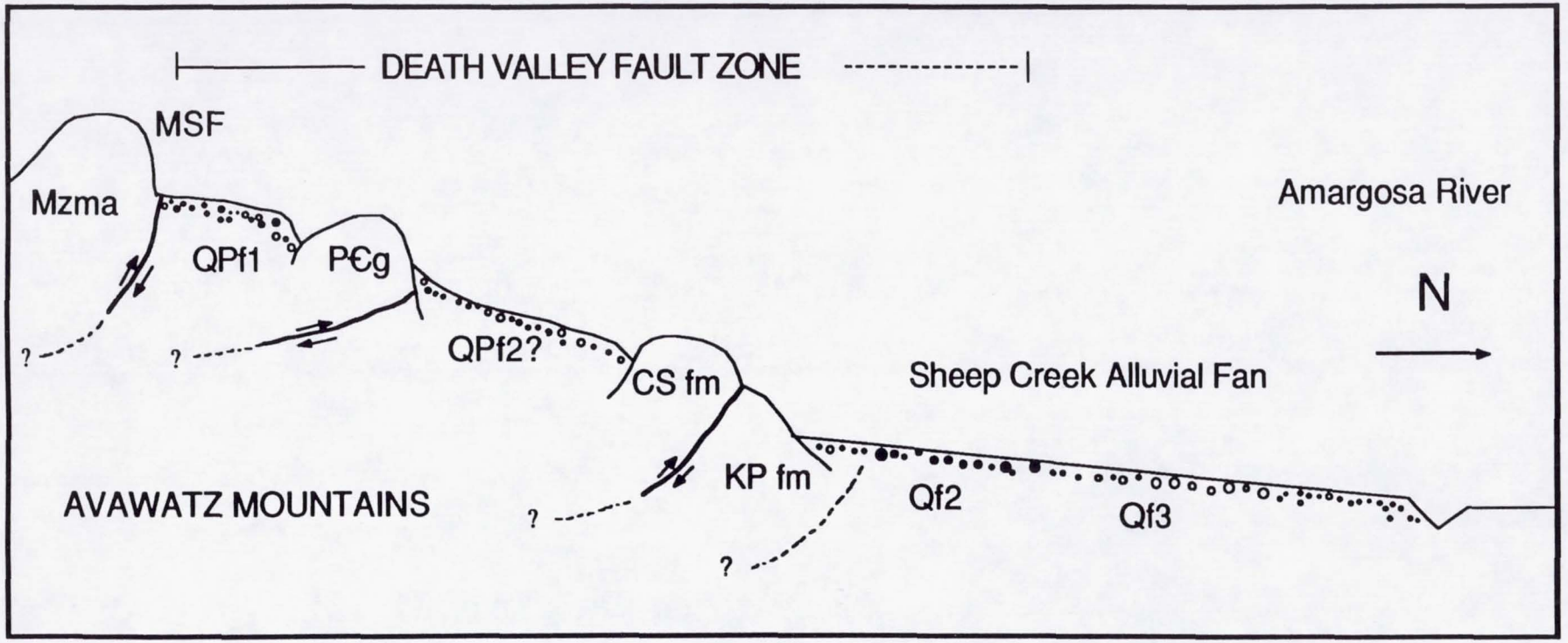
DEATH VALLEY FAULT ZONE
MSF
Mzma
QPf1
P€g
QPf2?
CS fm
KP fm
Qf2
Qf3
Amargosa River
N
Sheep Creek Alluvial Fan
AVAWATZ MOUNTAINS
?
?
?
?

Another important tectonic feature of the southern Avawatz Mountains inside Fort Irwin was illuminated by the imagery. Davis and Burchfiel (1973) identified a low-angle fault between the Avawatz and Granite Mountains (referred to herein as the Drinkwater Lake fault) as the southern portion of the Layton Wells thrust that has been offset by movement on the Garlock fault. The Layton Wells fault is a Jurassic, east-vergent thrust fault exposed in the Slate Range (Figure 3). Although access to the Drinkwater Lake fault is restricted, it is well-depicted on the imagery. The spectral characteristics of the klippe are unlike those of rocks in the Slate Range and are virtually identical to those of the monzodiorite of the Avawatz Mountains. This suggests that the rock in the upper plate of the Drinkwater Lake fault was derived from the Avawatz terrane. Therefore, rather than being an east-directed, low-angle, thrust fault, similar to the Layton Wells thrust fault, the Drinkwater Lake fault transported rocks from east to west, opposite the sense of transport along Jurassic thrust faults in the region, but consistent with the transport direction of Tertiary, low-angle extension faults. Therefore, based on the imagery and on limited field work, our interpretation is that the Drinkwater Lake fault is a west-vergemt, Tertiary normal fault rather than a Jurassic thrust fault.

KINGSTON WASH

Kingston Wash lies east of the Avawatz Mountains and north of the Silurian Hills (Figure 2). Examination of the Kingston Wash area was critical to this project in order to study the hypothesised "eastern extension of the Garlock fault."

According to Davis and Burchfiel (1973) and Plescia and Henyey (1982), the Garlock fault zone continues east of the Avawatz Mountains along the the southern margin of Kingston Wash, passing through a 0.5 km-wide gap, between the southern Salt Spring Hills and the northern Silurian Hills. According to these authors, the left-lateral offset on the Garlock fault is distributed along its entire length and therefore, there should be about 64 km of offset between the southernmost Salt Spring Hills and the northern Silurian Hills.

Plescia and Henyey (1982) interpreted contoured magnetic data and, to a lesser extent, gravity data as indicative of the existence of a geophysical anomaly along the southern margin of Kingston Wash. They proposed that the "eastern extension of the Garlock fault" lies between the Salt Spring and Silurian Hills separating a geophysically "smooth" terrane to the north from a geophysically "complicated" terrane to the south.

The processed images show no evidence for left-lateral displacements of Quaternary deposits east of the intersection of the two fault zones in the Kingston Wash area. In contrast, west of the intersection, imagery of the north flank of the Avawatz Mountains revealed a pronounced change in the elevation on opposite sides of the Garlock fault and numerous left-lateral fault scarps in Quaternary deposits.

The area of Kingston Wash between the Silurian Hills and the Valjean Hills, east of the Salt Spring Hills, and along the proposed eastern extension of the Garlock fault was also examined in detail (Plate 4). The TM image depicted is a color composite of bands 4, 5 and 7, processed using decorrelation stretching, as described in an earlier section. Black-and-white single band images were also examined and interpreted (images not shown here), after application of high-pass filtering to enhance spatial detail.

No evidence for an east-trending fault exists in the area traversed by Kingston Wash, either in the Quaternary alluvium, or in older rocks. On the interpretive map (Figure 9), unit 4 (oldest alluvial unit) is exposed across Kingston Wash. Bedding attitudes are identical, with moderate dips and strike to the north. Indicated deformation consists of tilting and/or folding of these young sediments along north-south axes; expected "Garlock" east-west structural deformation/shear zones/faulting is completely absent in this region. Older Tertiary sediments (unit T on Figure 9) are similarly tilted and folded, with generally north and northeast strikes. Outcrops of individual units can be traced continuously across Kingston Wash, with no evidence of tectonic disruption. The same units can be mapped based on image colors across the wash without offset or other east-west disruptions. These Tertiary sediments are estimated to be of Pliocene and/or Miocene age (Hewett, 1956); therefore a continuation of the Garlock fault in this area would have to be older than the

Figure 9. Interpretive map of Plate 4 showing continuous traces of Tertiary and Quaternary alluvial units across Kingston Wash.

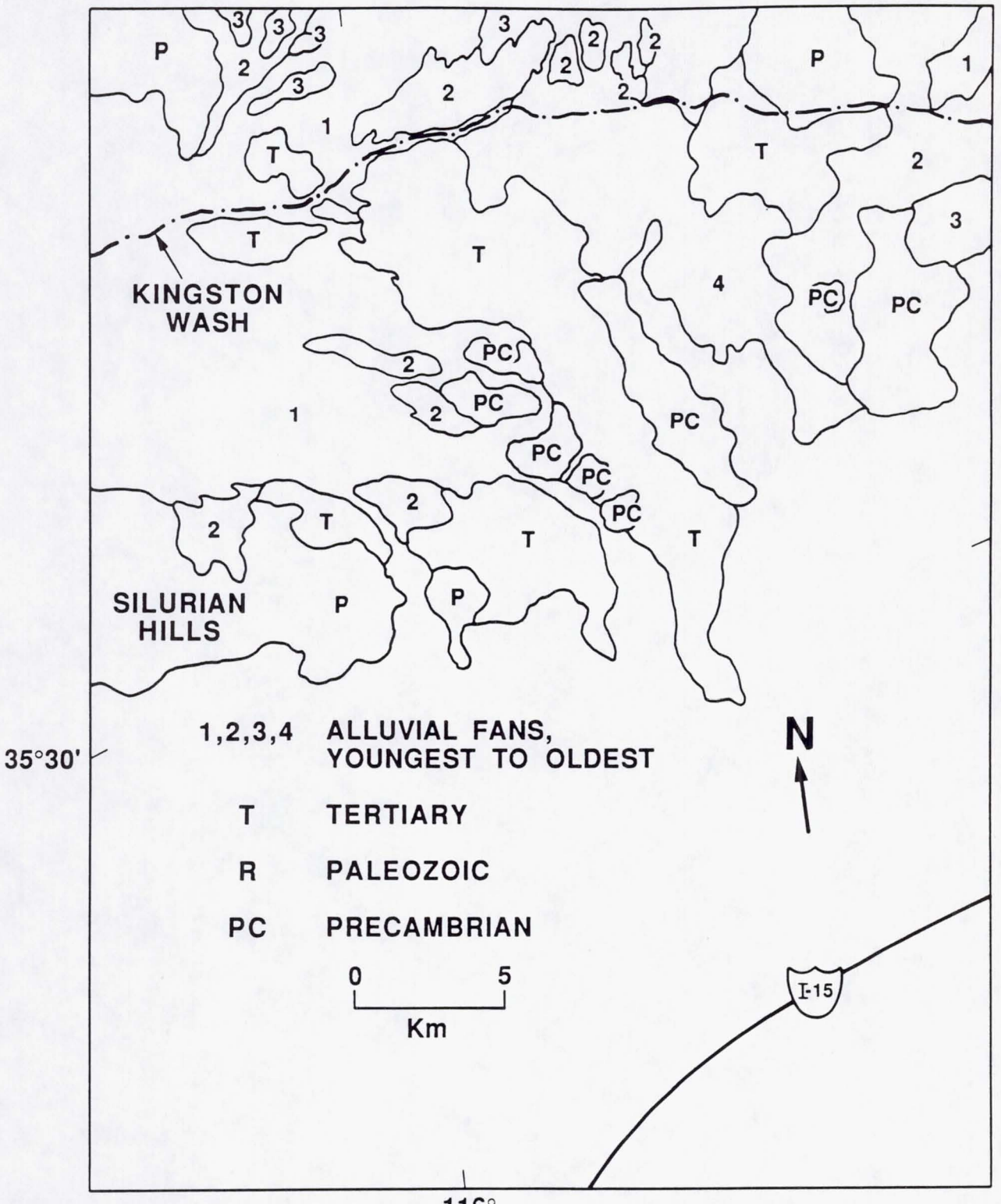
KINGSTON WASH
SILURIAN HILLS
1,2,3,4 ALLUVIAL FANS, YOUNGEST TO OLDEST
T TERTIARY
R PALEOZOIC
PC PRECAMBRIAN
0 5
Km
N
I-15
35°30'
116°

sediments, which is negated by age relationships west of the Avawatz Mountains and along the north flank of the range.

Since there is no surficial evidence for the "eastern extension of the Garlock fault", the surrounding rocks were examined for evidence of a shear fabric in bedrock that could indicate the presence of the fault. Efforts were concentrated on rocks in the southern Salt Spring and the northern Silurian Hills which form the 0.5 km-wide gap through which the proposed "eastern extension of the Garlock fault" passes. Field investigation were based on two assumptions: 1) the amount of offset proposed to exist on the "eastern extension of the Garlock fault" (approx. 64 km) is sufficient to impart a significant shear fabric onto the rocks through which it passes and 2) the fabric along the "eastern extension of the Garlock fault zone" should resemble that along the Garlock fault zone in the Avawatz Mountains: it should have a pronounced, high-angle, east-striking foliation.

The northern Silurian Hills contain mainly Precambrian quartzite and siliciclastic rocks whose bedding dips steeply northeast. Several hundred fracture measurements were made in five localities along the northern margin of the Silurian Hills in the location of the proposed eastern extension of the Garlock fault. The contoured stereoplot of these fractures (Figure 4C) shows that the fractures strike predominantly north or northeast and dip steeply to vertically. Thus, the fractures strike nearly perpendicular to the fault, and there is no evidence for the dominant, east-striking foliation that appears along the Garlock fault in the Avawatz Mountains (Brady, 1986).

Several hundred fractures were also measured in the the southern Salt Spring Hills. Their contoured stereoplot (Figure 4B) shows a bi-modal distribution of northeast- and northwest-striking, moderately dipping fractures. This pattern is unlike that of either the Silurian Hills or of the Garlock fault zone in the Avawatz Mountains indicating that the fractures in the Silurian Hills formed in a strain domain unlike that along the Garlock fault.

The fracture patterns in the Silurian Hills and the Salt Spring Hills are inconsistent with those that would be expected for the proposed extension of the Garlock fault. This inconsistency can be explained in three ways: 1) the

eastern extension of the Garlock fault zone created asymmetric fractures at a high-angle to its strike in contrast to the east-striking fractures created throughout its length west of the Death Valley fault zone, 2) the Garlock continuation exists but does not lie between the Salt Spring Hills and the Silurian Hills, or 3) the Garlock fault terminates west of the southern Death Valley fault zone and does not continue into Kingston Wash. The latter explanation is most consistent with results from other parts of this project.

SODA MOUNTAINS

Field work in the Soda Mountains consists of two parts: 1) detailed geologic mapping and structural analysis of the Soda-Avawatz fault zone in the eastern Soda Mountains and 2) geophysical investigations of the Soda-Avawatz fault zone between the Soda and Avawatz Mountains (Figure 10).

Geological mapping at a scale of 1:24,000, and the geometric analyses of rock fracture patterns were conducted in the vicinity of the Soda-Avawatz fault. The goal of this work was to test the three outstanding hypotheses for the Soda-Avawatz fault zone. The first hypothesis is that of Davis (1977) who suggested that the Soda-Avawatz fault was the southward continuation of the Arrastre Spring fault zone exposed in the Avawatz Mountains (Figure 3). He based this interpretation on the similar pattern of branching faults, the direct alignment of the fault zones, and the fact that both fault zones separate metavolcanic terranes on the west from plutonic and Paleozoic metasedimentary rocks to the east. Using seismic refraction data, Honeycutt *et al* (1986) proposed that the Soda-Avawatz fault zone was an older, strike-slip fault system that has been overprinted by east-vergent thrusting. Grose (1959) interpreted certain structures in the eastern Soda Mountains as en echelon drag folds and concluded that the Soda-Avawatz fault zone is a right-lateral fault.

Cenozoic Stratigraphy

Four main units of Cenozoic continental strata occur within the Soda-Avaawatz fault zone (Figure 11). In order of decreasing age, these are: Tertiary alluvial fanglomerate, Tertiary alluvial sand and fine-grained

Figure 10. Generalized index map of the study area in relation to structural features examined herein. GFZ = Garlock fault zone, DVFZ = Death Valley fault zone, S-AFZ = Soda-Avawatz fault zone, SLL = Soda Lake lineaments, BMFZ = Bristol Mountains fault zone. Location of gravity and seismic studies are also indicated.

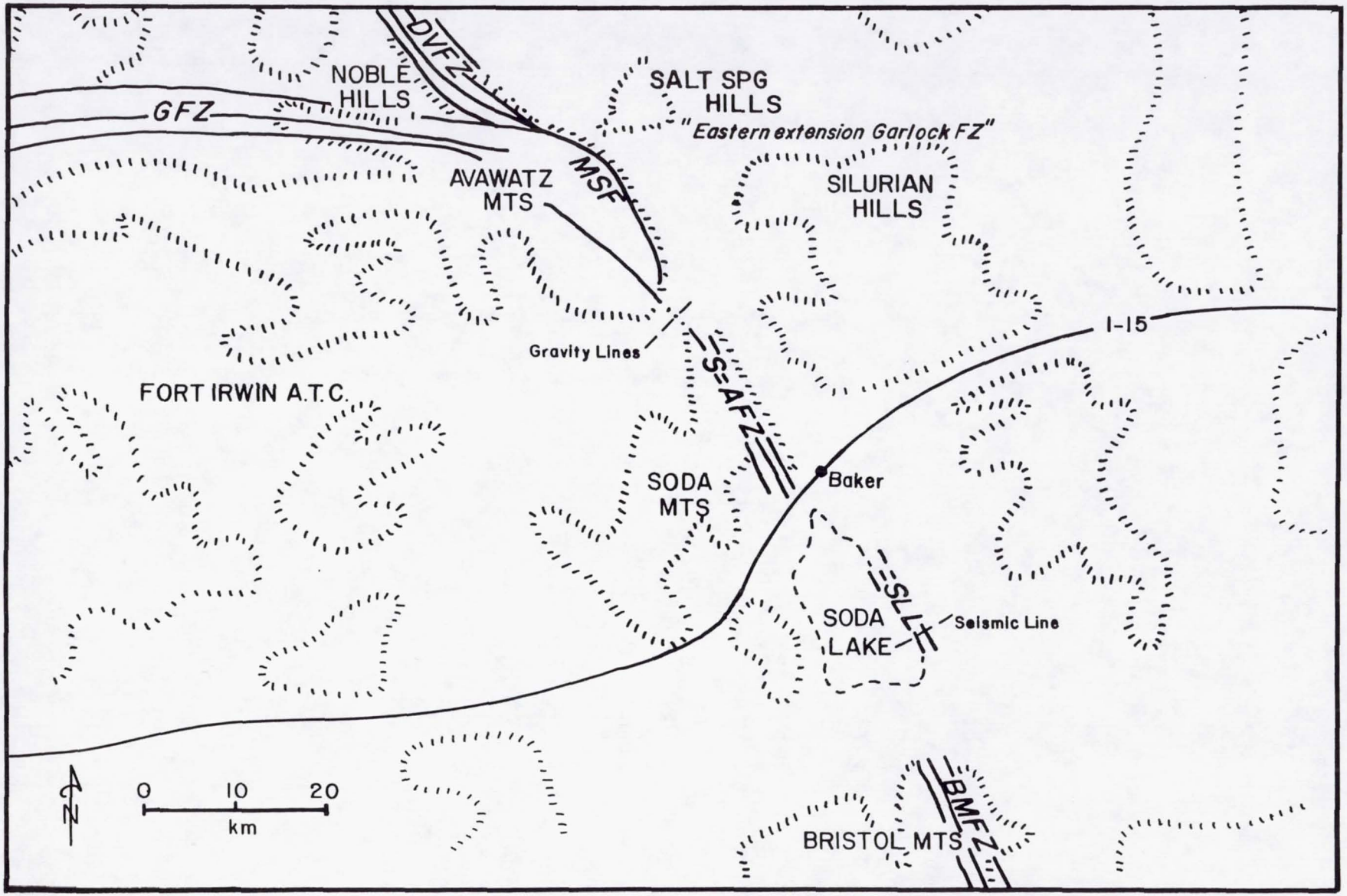
DVFZ
NOBLE HILLS
GFZ
SALT SPG HILLS
"Eastern extension Garlock FZ"
AVAWATZ MTS
MSF
SILURIAN HILLS
I-15
Gravity Lines
S-AFZ
FORT IRWIN A.T.C.
Baker
SODA MTS
SLL
SODA LAKE
Seismic Line
BMFZ
BRISTOL MTS
0 10 20
km

Figure 11. Generalized geologic map of the eastern Soda Mountains showing main branches of the Soda-Avawatz fault zone. Modified from Grose (1959) and Cregan (in prep.).

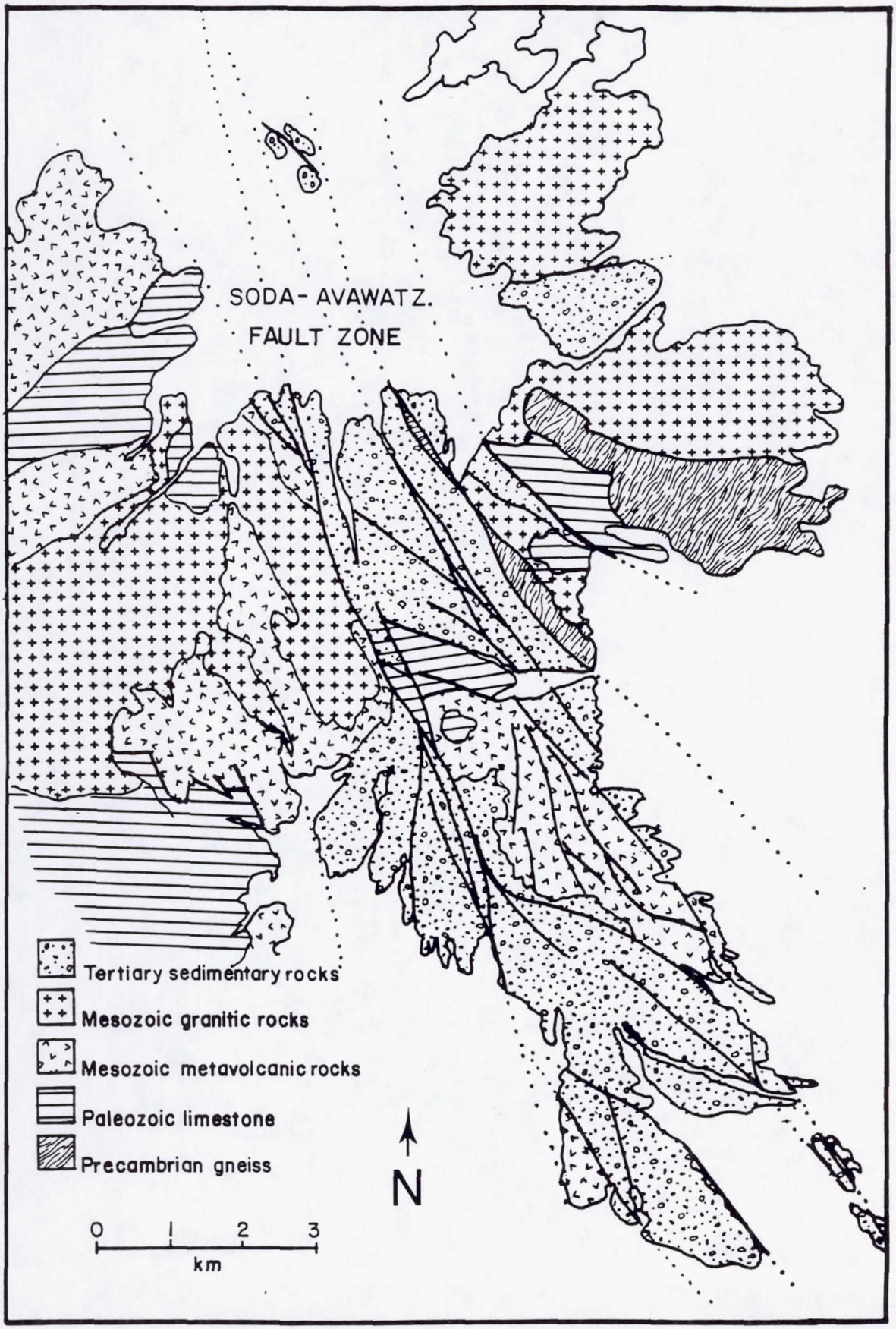
SODA - AVAWATZ.
FAULT ZONE
Tertiary sedimentary rocks
Mesozoic granitic rocks
Mesozoic metavolcanic rocks
Paleozoic limestone
Precambrian gneiss
N
0 1 2 3
km

sediments, and two gravel units of Quaternary age. The Tertiary rocks have tentatively been correlated with the second and third members of the Avawatz Formation as described by Spencer (1981).

The older Tertiary unit is boulder-to-cobble conglomerate which rests unconformably on Mesozoic metavolcanic basement rocks. In order of decreasing abundance, clast types include metavolcanic, carbonate, sandstone, and granitic rocks. Tectonically intercalated within this unit are large, fault-bounded, carbonate breccia bodies consisting of Upper Paleozoic Bird Springs Formation.

The younger Tertiary unit rests conformably above the older one in the southwestern part of the field area. All other contacts between the two are fault. The younger unit is comprised predominantly of conglomerate, sandstone, siltstone and scattered tuff layers. Clasts in the conglomerate consist of limestone, metavolcanic, granite, intermediate intrusive rock and quartzite. On the basis of shard chemistry one of the tuffs could be correlated to a tuff in Deep Sea Drilling Program (DSDP) cores. The tuff in the cores has a K-Ar age of 11.6-11.8 Ma (Appendix I).

The older Quaternary unit consists of sandy, cross-bedded, gravel-to-cobble conglomerate containing clasts of limestone, dolomite, granitic, and metavolcanic rock, and intermediate intrusives rocks. The percentages of each clast type vary considerably, depending upon locality. The unit unconformably overlies the Tertiary units and, locally, crystalline basement rocks with an angular discordance of 6-70°. Desert pavement with varying degrees of varnish development has formed on the uplifted areas of the Quaternary unit. These areas may be as much as 3-7 m above the modern channels. On the basis of soil development, a deformed 200,000 year-old fan surface developed on the unit has been tentatively correlated with the Qfo surface of Ritter (1985) in the Silver Lake area (Figure 1).

The younger Quaternary unit was mapped in reconnaissance only. It is unconsolidated-to-poorly consolidated fan gravel that was deposited in low-lying areas, outside of the currently active washes.

Cenozoic Structure

The Cenozoic structure of the eastern Soda Mountains is dominated by a group of five, approximately parallel, near vertical, through-going Tertiary faults herein designated as the western, southwest, central, east and far eastern faults. These faults have straight or slightly curved traces, they delineate separate domains having different lithologies, and they abruptly truncate the crystalline basement rocks. Structural domains between the major faults contain numerous smaller shears and one large, en echelon, anticline-syncline fold pair.

The western fault extends the length of the study area along a general strike of 330°. The dip varies from vertical to 75° E. In the north, the fault juxtaposes the older Tertiary rocks to the east against Mesozoic metavolcanic and quartz monzonite. The trace of the fault is an 8 m-wide zone of tectonically powdered rock whose western edge is bounded by a group of discontinuous, sub-parallel shears. The shears have produced at least two possible fault scarps in the older Tertiary rocks with a relative east-side-down displacement of 1-1.5 m. Although the slip cannot be determined, the straight trace of the fault, the near vertical dip and the striations, which rake 10-23°, strongly suggest that the displacements are lateral.

The southwest fault is a previously unmapped fault that strikes 338° and dips 82-86° NE. It separates the older Tertiary rocks on the east from Mesozoic metavolcanic rocks. Along the central segment of this fault, a Tertiary basin containing terrigenous, tuffaceous sediments, primarily devoid of metavolcanic detritus, is faulted against Mesozoic metavolcanic rocks. The age of displacement is considered to be Plio-Pleistocene, or perhaps even younger, based on offset soil that has developed on fan deposits of the green metavolcanic detritus. The sense of slip has not been determined; however, along the trace of the fault, stream channels on the east side of the fault are deflected southward, which is consistent with right-lateral displacement.

The central fault is a 2 m-wide shear zone that separates the older from the younger Tertiary rocks along a general trend with a strike of 336° and a dip of 86° SW. The northern part of this fault divides into at least three parallel

branches. The branches bound slivers of granite, metavolcanic rocks and limestone breccia. The straight trace of the fault and striations that rake 20-34° N strongly imply that there have been lateral displacements with a moderate vertical component along the fault.

The east fault juxtaposes granitic rocks to the east against the younger Tertiary rocks along a general strike of 337° with dips of 48-85° SW. Slickensides developed on the fault surface rake 8-35° N; chatter marks and pebble-induced grooves indicate that the displacement is right-lateral. West of the fault, attitudes in the older Tertiary rocks are deflected progressively northward towards the central fault. This suggests that the domain of the older rocks between the east and central faults has been rotated. The amount and direction of rotation is undetermined.

The far east fault consists of two, slightly diverging fault branches that bound a central block of the older Tertiary rocks. They strike 312° and 325° and their dips range from 30-80° SW. The western branch cuts deposits of the older Quaternary unit which indicates that the latest deformation is of a Quaternary age. The sense of slip for either branch has not been determined.

Four sets of minor faults exist within the Tertiary sediments. These faults fall into two major groups: high-angle faults having dips of 65-90° and low-angle faults with dips of 28-40°. Slickensides on both sets of faults show rakes of 2-38°, indicating that motion was predominantly lateral. The sense of slip was determined on 16 faults: 14 were right-lateral and 2 were left-lateral. This result is consistent with an overall right-lateral sense of displacement for the far east fault zone.

The major anticline and en echelon syncline trend about 312° and involve the Tertiary rocks. The core of the anticline is composed of metavolcanic rocks which do not appear to have been folded, suggesting that the fold shape may be the result of faulting rather than regional compression. Numerous smaller folds, trending 60-80° to the major shears, are located in the Tertiary sediments of the interior of the far east fault zone. These minor folds appear to be related to movement along adjacent shears.

The five principal faults that comprise the Soda-Avawatz fault zone have predominately strike-separation with significant evidence for movement during Pliocene- to possibly Pleistocene time. Thus the preferred interpretation is that the Soda-Avawatz fault zone is predominantly a strike-slip fault zone similar in geometry and age of youngest offset to the Death Valley fault zone. No evidence has been found to support the suggestion of Honeycutt *et al* (1986) that there has been east-directed thrusting of Tertiary age. Correlation of the Soda-Avawatz fault zone with the Arrastre Spring fault, as proposed by Davis (1977) is untenable for two reasons. First, the Arrastre Spring fault is overlain by tuff deposited on it 11-12 my ago (Spencer, unpublished data), whereas deformation along the Soda-Avawatz fault zone has occurred in Quaternary time. Second, unlike the Soda-Avawatz fault zone which shows primarily strike-slip movement, the Arrastre Spring fault shows mainly dip-slip movment with the west side down (Spencer, 1981).

TM and SPOT Imagery

TM and SPOT data interpretations support the field investigations and show the major features associated with the Soda-Avawatz fault zone. The SPOT image, corresponding TM image, and interpretation appear as Plates 5 and 6 and Figure 12.

The SPOT data were contrast enhanced, and interpreted at an original scale of 1:62,500. The TM image is a mosaic of two different acquisitions. The data were radiometrically normalized by forcing the instrument responses to conform, based on the statistics of the overlap region between the two. The TM data were further processed by decorrelation stretching of bands 4, 5 and 7, and composited to produce a false color print, also at a scale of 1:62,500.

The five faults in the eastern Soda Mountains appear as prominent, straight linear features on the SPOT image, evident also by juxtaposition of terrains with different morphologic characteristics, reflecting the differing bedrock types. At further enlargement on a CRT display monitor, topographic disruptions could be seen to affect the youngest alluvial unit (unit 1 on Figure 12), further suggesting Quaternary activity along the faults.

Figure 12. Interpretive map of Soda Mountains area made from TM and SPOT images (Plates 5 and 6). Depicted are faults inferred from images and distribution of Tertiary and Quaternary alluvial units. Bedrock units unlabeled.

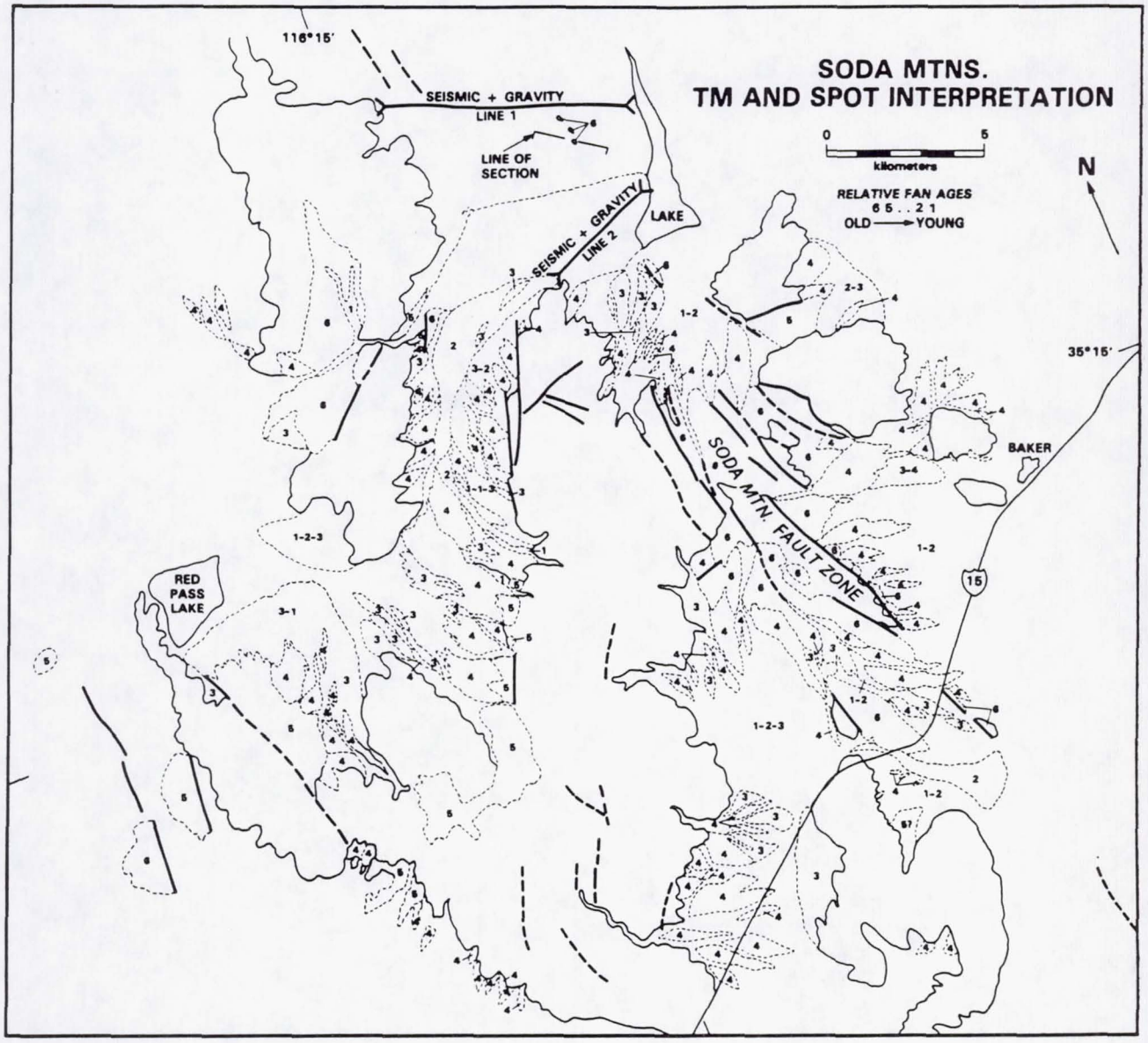

On the TM image, the fault zone is similarly expressed by linear disruptions of geomorphic features. In addition, juxtaposition of different colored units on either side of the fault is evidence of lithologic offsets. Particularly evident is the central fault, whose branches at the north end bound slivers of granite, metavolcanic rocks and limestone. These appear as elongated, yellow, red and blue slivers. Farther south along this fault, an elongate area of yellow outcrops represent metavolcanic rocks similarly bounded by the fault.

Based on geomorphic appearance, six relative age units were mapped from the TM and SPOT data (Figure 12). Unit 6 corresponds to the Tertiary alluvial sediments. The older Quaternary deposit corresponds to unit 4 and some of unit 3. Units 2 and 1 are active and very recent alluvial units. These units are mappable from their colors on the TM image, and relative drainage dissection, topographic relief, and degree of incision. Evidence of involvement of Units 6 through 4 with fault disruption, inferred from the images, is in agreement with the field data.

Geophysical Investigations

A gravity study was undertaken in the area between the Soda and the Avawatz Mountains (Figure 10) by Jon Acord at California State College, Bakersfield. The study was designed to determine if branches of the Soda-Avawatz fault zone could be traced northward beneath the alluvial cover into the Avawatz Mountains. If so, then the Soda-Avawatz fault zone could reasonably be considered to be a southern continuation of the Death Valley fault zone or the Arrastre Spring fault rather than a separate fault zone (Figure 2). The gravity study involved 285 surveyed stations along four lines between the Avawatz and Soda Mountains. The details are presented in Appendix III.

The gravity data indicates that: 1) a zone of irregular, subsurface, basement topography extends from the Soda to the Avawatz Mountains, 2) the central part of the northern projection of the Soda-Avawatz fault zone contains a tectonically (?) uplifted block between what appear to be fault strands and 3) a subsurface, linear trough between the ranges trends parallel to the Soda-

Avawatz fault zone. The axis of the trough, which represented the paleo depocenter, is not coincident with the modern depocenter. Rather, it is situated 4 km farther west and is aligned with the southern projection of the Death Valley fault zone.

One possible interpretation of the gravity data, is that the extension of the southern Death Valley fault zone may exist beneath the fanglomerate of the southern Avawatz Mountains and emerge as the Soda-Avawatz fault zone.

SODA LAKE

Soda Lake playa is situated approximately 5 km south of the town of Baker and occupies the basin between the Soda Mountains and the Old Dad Mountains (Figure 2). The southern Soda Mountains consist mainly of granitic and metavolcanic rock; the Cow Hole Mountains consist mainly of Mesozoic granitic and metavolcanic rock and lesser amounts of Paleozoic sedimentary rocks. Active sand dunes cover the southern end of the playa, separating it from the Bristol Mountains 4 km farther south.

Two pronounced lineaments that cross the east-central part of Soda Lake playa (Figure 2) were pointed out on black-and-white air photos to R. Brady by Steven Wells of the University of New Mexico-Albuquerque. Once the TM imagery was acquired, five very pronounced and three less obvious lineaments became evident along the eastern margin of the playa (Figure 10). The lineaments trend north-northwest in a zone several meters wide, each ranging from 0.5 to nearly 3 km long. For the purposes of this report, the zone is referred to as the Soda Lake lineaments.

Upon ground inspection, the Soda Lake lineaments were found to consist of sub-parallel rows of fresh-water phreatophyte plants, mainly mesquite. Coppice dunes have formed around the mesquite, accentuating the relief of the lineaments. Mesquite bushes are salt-intolerant. Here, their growth is conspicuous because they are in a highly soda-saline area of the playa and are surrounded by salt-tolerant and salt-loving plants such as pickleweed and salt grass.

On the basis of unpublished hydrological data, it is certain that the regional groundwater gradient slopes toward Soda Lake from the east. Water from wells in the alluvial fans just east of Soda Lake is notably sweet and of potable quality while the water beneath Soda Lake is too saline for use. The botanical lineaments appear to have formed above narrow, planar, vertical groundwater barriers of high permeability that are intercepting the groundwater on the east side of the lake, and causing it to flow upward to the surface through the overlying salt- and soda-bearing playa deposits. The most likely interpretation of the barriers is that they are north-northwest striking, high-angle faults. Because the lineaments lie directly in the southward projection of the Soda-Avawatz fault zone, it is probable that the lineaments are traces of the Soda-Avawatz fault zone.

In order to test the hypothesis that the Soda Lake lineaments represent the southern continuation of the Soda-Avawatz fault zone, gravity, magnetic and seismic studies were undertaken across the lineaments and into Soda Lake (Figure 10). The work was done in collaboration with R. Negrini and students from California State University, Bakersfield. This study is included as Appendix IV.

Taken together, the seismic and gravity data indicate that a subsurface zone (Layer 2) with significant velocity and density differences exists in the vicinity of the lineaments. This layer is located at a depth of 7-15 m beneath a homogeneous surficial layer (Layer 1). Furthermore, the boundary between Layer 1 and Layer 2 is an irregular surface that is not at constant depth below the surface. While the boundaries of the individual "blocks" within Layer 2 do not align precisely with the individual lineaments, the overall boundary of Layer 2 correlates geometrically with the zone of lineaments. West of the lineaments, out in the lakebed, the subsurface is considerably more uniform geophysically than it is near the lineaments, and the Layer 1/Layer 2 interface is smoother.

Based on these relationships, we conclude that the geophysical data are consistent with the interpretation that the Soda Lake lineaments are northwest-striking, high-angle faults. Because the groundwater flow reaches the surface, it is likely that the zone of high permeability, corresponding to the

faults, is also near the surface. If the lineaments are faults, these faults have probably moved during Quaternary time.

At the southeastern end of Soda Lake, several isolated outcrops of conglomerate, each several tens of meters square, protrude through a dune sand (Figure 13) These features were also pointed out to Brady by Steven Wells. The outcrops are approximately 7 km southeast of, and in direct alignment with, the Soda Lake lineaments. The two most likely interpretations of these conglomerates are that: 1) they are remnants of high-standing, relict gravel bars from ancient Soda Lake or 2) they are older gravel deposits that have been uplifted (or folded) along sub-parallel faults.

The gravel bars of ancient Soda Lake are probably not Quaternary in age because: 1) their position is not coincident with other known shoreline features, 2) the clasts are moderately sorted and sub-angular to sub-rounded rather than being well-rounded and well-sorted as are clasts in other Quaternary bars of Soda Lake (Wells *et. al.*, 1984) and 3) the conglomerates lack the southward, back-dipping imbrication characteristic of other beach bars of Soda Lake.

Most likely, the conglomerates are distal portions of older Quaternary or late-Tertiary alluvial fan strata. Their presence indicates that the structures responsible for the Soda Lake lineaments may continue beyond the southeastern margin of Soda Lake. Unfortunately, sand dunes obscure all other deposits in the area. Because the outcrops are topographically higher than the surrounding dunes, the conglomerate may have been uplifted during Quaternary (Holocene?) time.

NORTHERN BRISTOL MOUNTAINS

The northern Bristol Mountains (Figure 13) are the southernmost area examined in this project. The only previous mapping of the area is the reconnaissance work of Basset and Kupfer (1964). The mountains lie at the south edge of Soda Lake, and are accessible only with great difficulty by four-wheel drive along dry washes. The northern Bristol Mountains are composed mainly of Mesozoic granitic rock and minor amounts of Precambrian (?)

Figure 13. Index map of the northern Bristol Mountains showing major faults and locations of Tertiary sedimentary sequences discussed in text. Numerals refer to measured sections and cobble counts presented in Appendices V and VI.

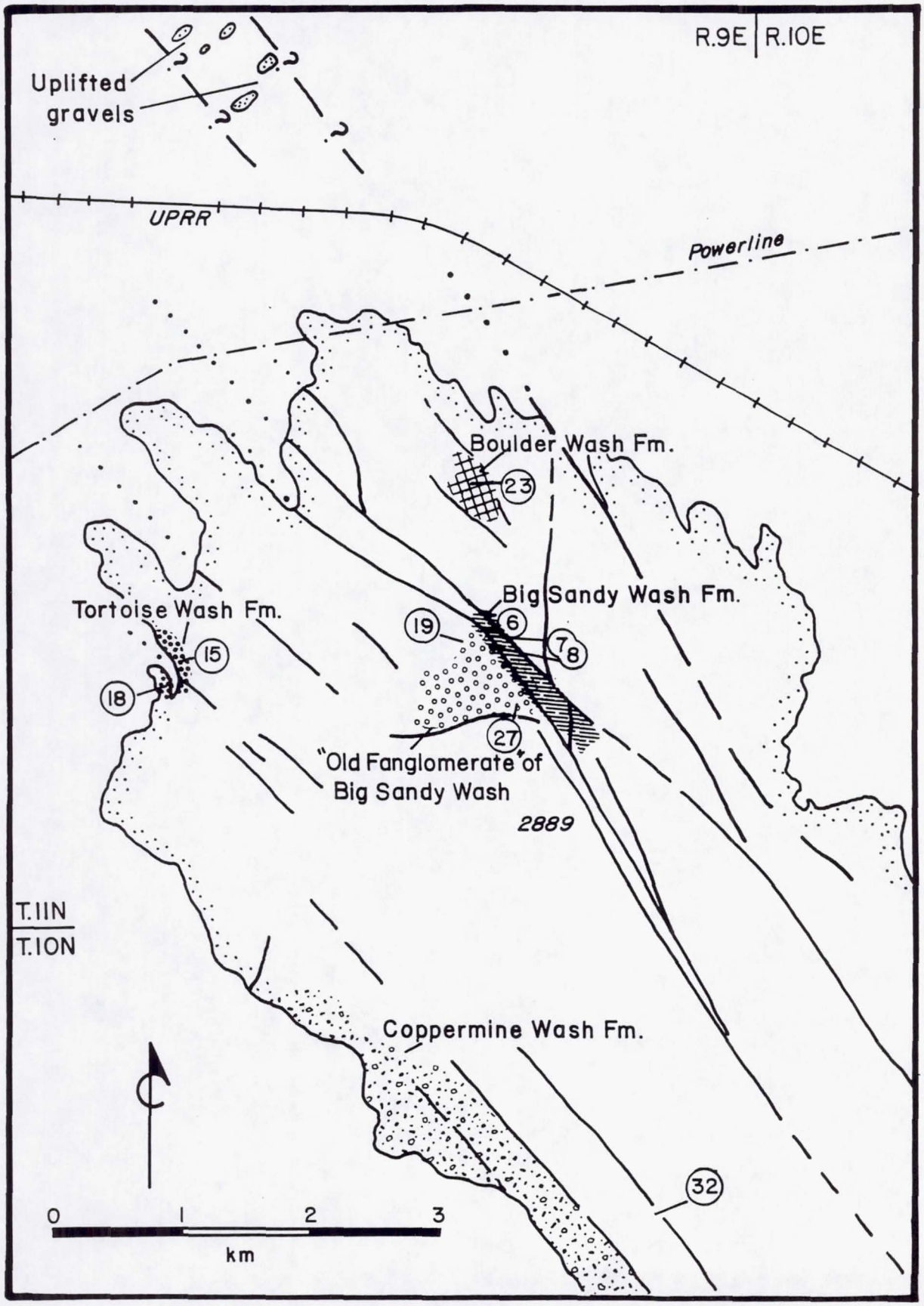
R.9E | R.10E
Uplifted gravels
UPRR
Powerline
Boulder Wash Fm.
23
Big Sandy Wash Fm.
Tortoise Wash Fm.
19
6
7
8
15
18
27
"Old Fanglomerate of Big Sandy Wash
2889
T.11N
T.10N
Coppermine Wash Fm.
32
0
1
2
3
km

gneiss on the western margin. The range is flanked on the west by thick deposits of conglomerate and is partly buried by Quaternary and Holocene sand dunes. Field mapping associated with this project disclosed the existence of four, previously-unrecognized, syntectonic Tertiary sedimenatry sequences referred to herein as: 1) the Big Sandy Wash sequence, 2) the Tortoise Wash formation, 3) the Boulder Wash formation and 4) the Coppermine Wash formation. These sequences record the evolution of a system of northwest-striking faults that are tentatively correlated with the Soda-Avawatz fault zone.

Big Sandy Wash Sequence

The Big Sandy Wash sequence (Figure 13) is a wedge-shaped section that lies in the north-central part of the Bristol Mountains nearly 350 m above the floor of Soda Lake. The sequence contains two units: 1) the Big Sandy Wash formation, and 2) the old fanglomerate of Big Sandy Wash. Both of these units are severely deformed and faulted.

The Big Sandy Wash formation is at least 23 m thick and is composed, in decreasing order of abundance, of granitic-derived conglomerate, metavolcanic-derived conglomerate, arkosic sandstone, sandy siltstone, basalt and lapilli tuff (Figure 14). The bottom of the unit is not exposed although it is believed to be in depositional contact with bedrock granite. The basalt yielded a K-Ar age of 27 $\pm$ 0.6 my on feldspar and the rhyolite tuff closely overlying the basalt yielded a concordant K-Ar age of 26.0 $\pm$ 0.6 my and 26.7 $\pm$ 0.6 my on biotite and hornblende (Appendix I). The sequence is interpreted to represent deposition in a distal braided stream environment of low gradient. This setting may have been marginal to a lake, or it may have contained significant overbank facies.

The Big Sandy Wash formation is in fault contact with, and is structurally overlain by, the old fanglomerate of Big Sandy Wash. The older fanglomerate is over 207 m thick and consists of cobble conglomerate, thinning and fining upward to the south into medium- to coarse-grained sandstone and sandy siltstone. The average clast composition is 78% granitic, 20% Tertiary

Figure 14. Measured section through the Big Sandy Wash sequence, north-central Bristol Mountains.

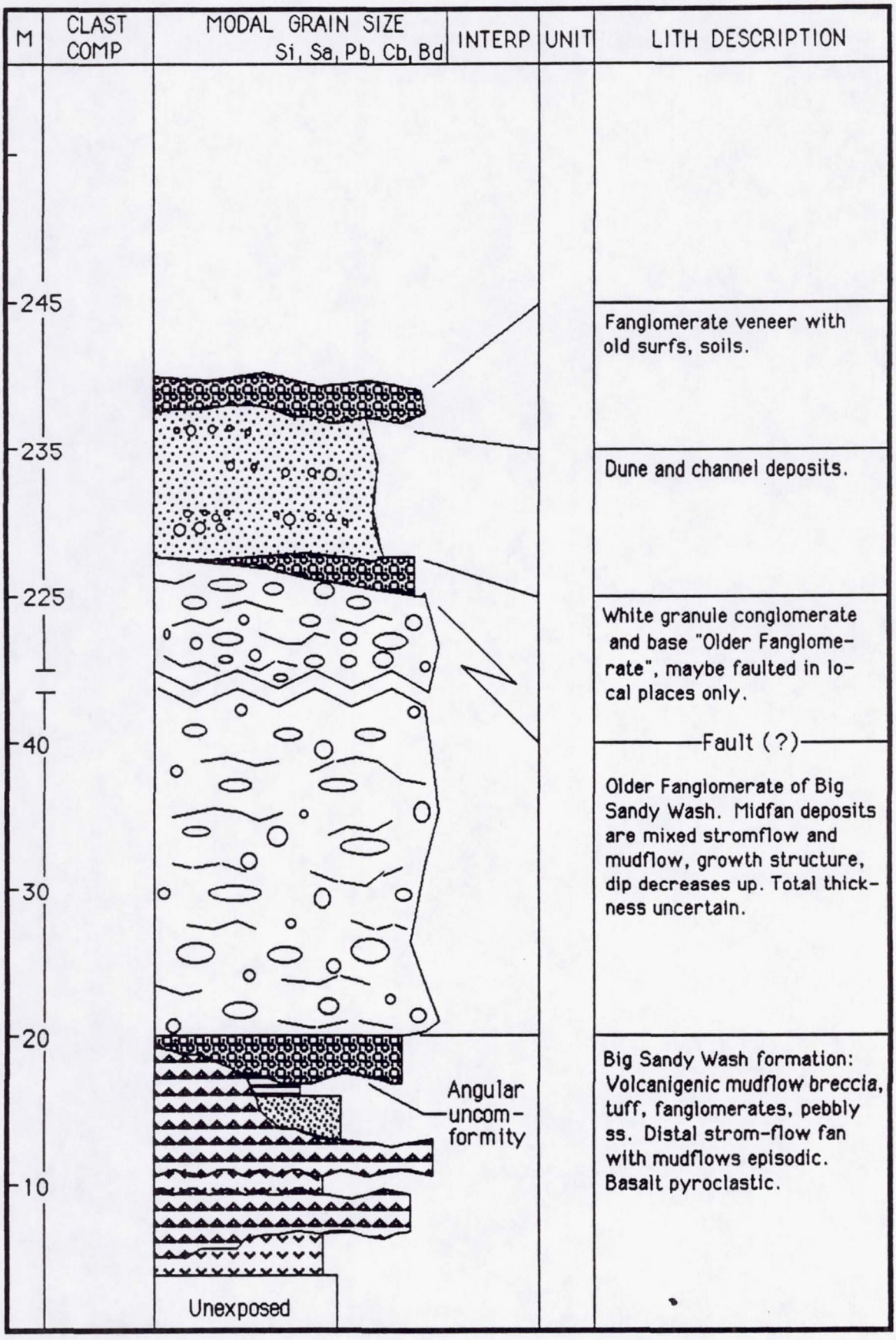
M
CLAST COMP
MODAL GRAIN SIZE Si, Sa, Pb, Cb, Bd
INTERP
UNIT
LITH DESCRIPTION
245
235
225
40
30
20
10
Fanglomerate veneer with old surfs, soils.
Dune and channel deposits.
White granule conglomerate and base "Older Fanglomerate", maybe faulted in local places only.
Fault (?)
Older Fanglomerate of Big Sandy Wash. Midfan deposits are mixed stromflow and mudflow, growth structure, dip decreases up. Total thickness uncertain.
Angular uncom-formity
Big Sandy Wash formation: Volcanigenic mudflow breccia, tuff, fanglomerates, pebbly ss. Distal strom-flow fan with mudflows episodic. Basalt pyroclastic.
Unexposed

volcanic, and 2% gneiss, quartzite, marble and dike rock (Appendix VI). It was not possible to obtain paleocurrent directions.

The older fanglomerate of Big Sandy Wash is a retrograding alluvial fan deposit that grades vertically from fluvial-dominated, mid-fan to outer-fan fringe or braided fluvial deposits. The contact between the Big Sandy Wash formation and the older fanglomerate is exposed only at one small locality. There, it is a low-angle fault that places the older fanglomerate over the Big Sandy Wash formation. Because the older fanglomerate has such a large areal extent for an intermontane basin deposit, it is believed that it is underlain only in part by the Big Sandy Wash formation and that it largely overlies granitic basement rocks.

Alluvial fan deposits collectively referred to herein as the "cap gravels" unconformably overlie the Big Sandy Wash sequence and the bounding bedrock. The cap gravels include deposits of several, discreet ages that have cut into the older units to depths of 7 m. Minor angular discordances exist between the individual deposits, but it is not known if they represent tilting or scour and fill. The cap gravels are composed nearly entirely of green and pink granite clasts that were presumably derived from the bedrock sources on either side of the basin. In this way, the provenance of the cap gravels differs from that of the older fanglomerate of Big Sandy Wash and the Big Sandy Wash formation which both contain clasts derived from sources which are not now exposed in the area.

Recent deposition has occurred in channels that have cut to depths of 9 m into the "cap gravels", thereby causing the upper surface of the "cap gravels" to be abandoned as a surface of deposition. The upper surface has low bar-and-swale microtopography, and sheetflow deposits are common. Most of the relief is due to single clasts. Desert varnish is dense, and the undersides of clasts are reddened to 2.5YR 5/6 (Munsell).

Soil has formed across the "cap gravels" (Figure 15). Steven Wells examined the soil and suggested that the soil was quite certainly Late Pleistocene in age and strikingly similar to the "Qf1" soil of Ritter (1985) in the Silver Lake area 40 km to the north. This tentative correlation was based

Figure 15. Schematic description of Pleistocene (?) soil formed on cap gravels at location 27 of figure 13.

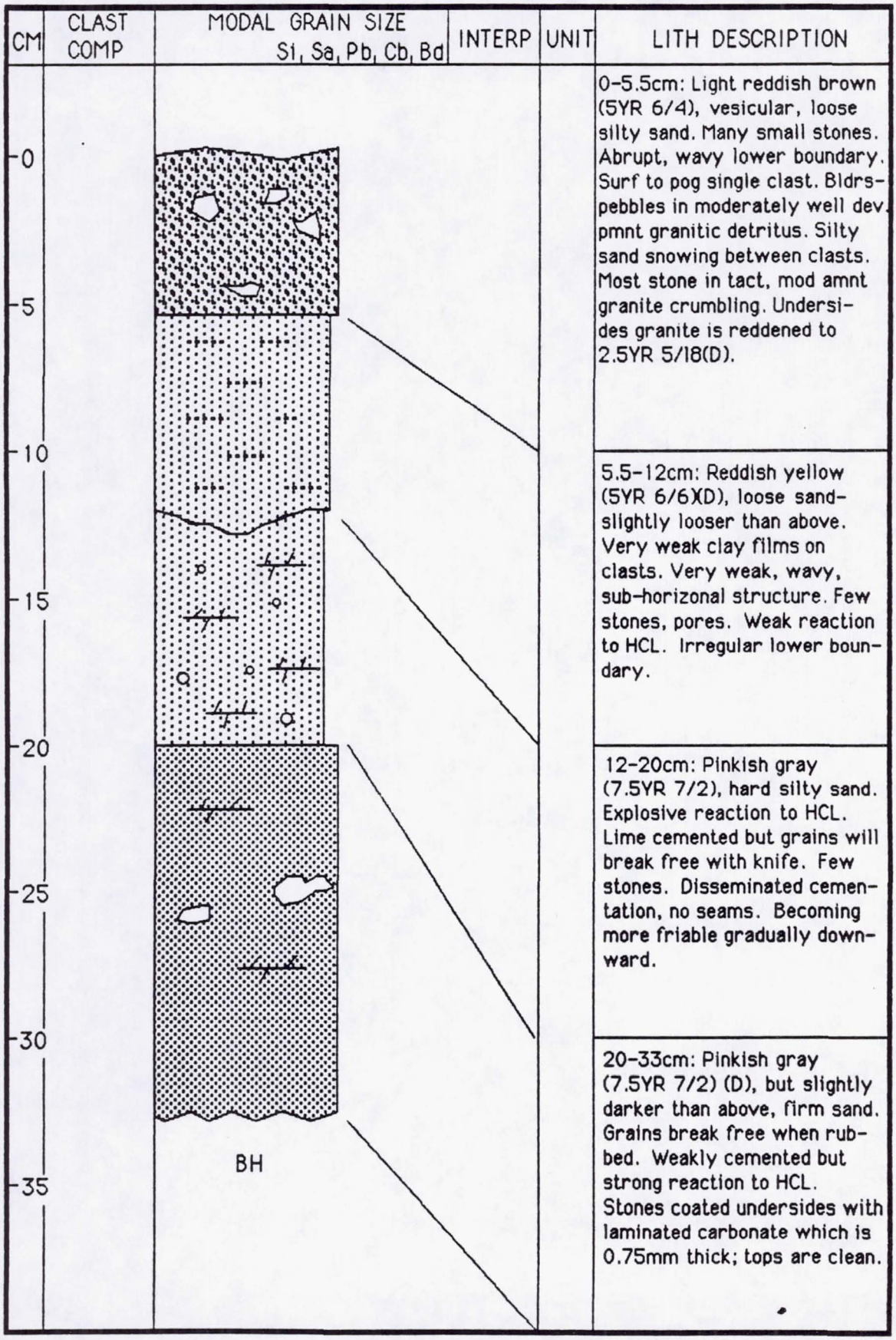
CM
CLAST COMP
MODAL GRAIN SIZE
Si, Sa, Pb, Cb, Bd
INTERP
UNIT
LITH DESCRIPTION
0
5
10
15
20
25
30
35
BH
0-5.5cm: Light reddish brown (5YR 6/4), vesicular, loose silty sand. Many small stones. Abrupt, wavy lower boundary. Surf to pog single clast. Bldrs-pebbles in moderately well dev. pmnt granitic detritus. Silty sand snowing between clasts. Most stone in tact, mod amnt granite crumbling. Undersides granite is reddened to 2.5YR 5/18(D).
5.5-12cm: Reddish yellow (5YR 6/6XD), loose sand-slightly looser than above. Very weak clay films on clasts. Very weak, wavy, sub-horizonal structure. Few stones, pores. Weak reaction to HCL. Irregular lower boundary.
12-20cm: Pinkish gray (7.5YR 7/2), hard silty sand. Explosive reaction to HCL. Lime cemented but grains will break free with knife. Few stones. Disseminated cementation, no seams. Becoming more friable gradually downward.
20-33cm: Pinkish gray (7.5YR 7/2) (D), but slightly darker than above, firm sand. Grains break free when rubbed. Weakly cemented but strong reaction to HCL. Stones coated undersides with laminated carbonate which is 0.75mm thick; tops are clean.

on: 1) the extent of a well-developed petrocalcic horizon, 2) the presence of a strong cambic B horizon and the degree of rubification of the undersides of clasts, 3) the degree of desert varnish, 4) the reduction of bar-and-swale micro-topography and 5) the similarity in clast composition to the alluvial fans in the Silver Lake area.

The Big Sandy Wash sequence is flanked by faults (Figure 13). The eastern boundary is a zone of sub-parallel, north-northwest striking, vertical faults that place the Tertiary units against very highly sheared, pink granitic rock. The fault zone varies from several discreet, well-defined faults, to a diffuse mass of sheared and mineralized rock nearly 45 m across in which the granitic protolith is all but indistinguishable. One kilometer northwest of the Big Sandy Wash sequence, the faults juxtapose the pink granitic rock on the east, against highly chloritic-altered green granitic rock. The fault zone is as wide as the wash, averaging 30-50 m, and contains phacoids of both wall rock types in various stages of tectonic disintegration. Statistical analyses of slickenline orientations suggest that the dominant shear sense is lateral.

The fault zone extends southeastward forming the northeastern edge of the Big Sandy Wash sequence. Within 50 m of the fault zone, strata of the sequence are complexly cut by minor high- and low-angle faults and are broadly to tightly folded. In several places, fault-bounded slabs of granitic bedrock are tectonically intersheaved with strata of the Big Sandy Wash formation and with the older fanglomerate of Big Sandy Wash. The separation on the minor faults appears to be limited to a few tens of meters.

The sense and amount of offset across the fault zone on the east side of the Big Sandy Wash sequence is uncertain. However, it appears to be a lateral fault because the fault trace is straight and the fault plane is essentially vertical over at least 10 km of exposure. The offset is probably greater than 4 km because two dissimilar rock masses, the green granitic rock and the pink granitic rock, are juxtaposed over that distance. The age of the youngest movement on branches of the Sandy Wash fault zone is most likely younger than late Pleistocene.

Tortoise Wash Formation

The Tortoise Wash sequence (new name) is exposed intermittently over an area of approximately 1 sq km in the northwestern part of the northern Bristol Mountains (Figure 13). The section is exposed only along the margins of modern stream channels. The section is at least 132 m thick, but neither the base nor the top is exposed (Figure 16). At the base of the exposed sequence are gray to white, arkosic, sandstone and granule conglomerate that are interpreted to be braided fluvial channel and bar deposits. These grade up into tuffaceous sandstone and tuff and limy sandstone and sandy limestone, interpreted to be a shallow lacustrine facies. At the top are basaltic agglomerate and basalt flows overlying basal pyroclastic or auto-breccia flow deposits. The basalt appears to have been derived locally because it contains inclusions of granite that resemble the bedrock of the Bristol Mountains.

Overall, the Tortoise Wash sequence probably is transitional from a shallow braided river to a marginal lacustrine depositional environment followed by infilling by basalt flows. Most of the sediment was eroded from granitic parent rock and was probably locally derived. Most likely, the lake (pond) was dry at the time the basalt erupted. Although the basal breccia of the basalt could have been formed by quenching in water, neither glass nor pillows are evident. Furthermore, zeolite alteration commonly associated with sub-aqueous eruptions is absent.

The Tortoise Wash sequence is strongly tilted from 40-80° SE. It does not appear to be folded internally, but it may contain folds whose wavelengths are longer than the measured section. The Tortoise Wash sequence is tentatively correlated with the Big Sandy Wash formation on the basis of similar stratigraphy, petrology and radiometric ages.

Boulder Wash Sequence

The Boulder Wash sequence underlies an area of approximately 1000 sq m in the northern part of the Bristol Mountains, 1 km north of the Big Sandy Wash sequence (Figure 13). The sequence fills a steep-sided, trapezoidal-

Figure 16. Measured section through the Tortoise Wash formation, northwestern Bristol Mountains.

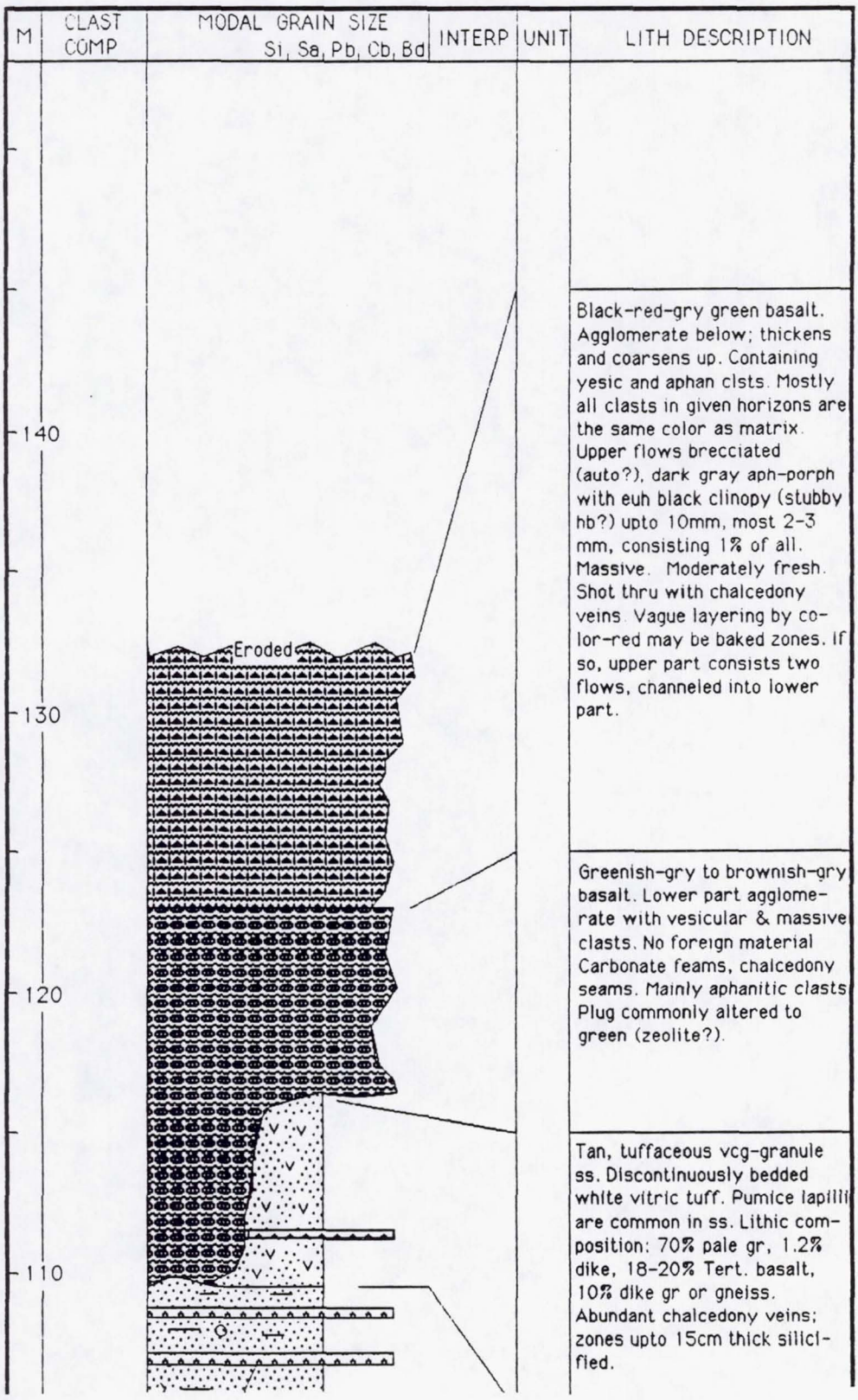
M
CLAST COMP
MODAL GRAIN SIZE
Si, Sa, Pb, Cb, Bd
INTERP
UNIT
LITH DESCRIPTION
140
130
120
110
Eroded
Black-red-gry green basalt. Agglomerate below; thickens and coarsens up. Containing yesic and aphan clsts. Mostly all clasts in given horizons are the same color as matrix. Upper flows brecciated (auto?), dark gray aph-porph with euh black clinopy (stubby hb?) upto 10mm, most 2-3 mm, consisting 1% of all. Massive. Moderately fresh. Shot thru with chalcedony veins. Vague layering by color-red may be baked zones. If so, upper part consists two flows, channeled into lower part.
Greenish-gry to brownish-gry basalt. Lower part agglomerate with vesicular & massive clasts. No foreign material Carbonate feams, chalcedony seams. Mainly aphanitic clasts Plug commonly altered to green (zeolite?).
Tan, tuffaceous vcg-granule ss. Discontinuously bedded white vitric tuff. Pumice lapilli are common in ss. Lithic composition: 70% pale gr, 1.2% dike, 18-20% Tert. basalt, 10% dike gr or gneiss. Abundant chalcedony veins; zones upto 15cm thick silicified.

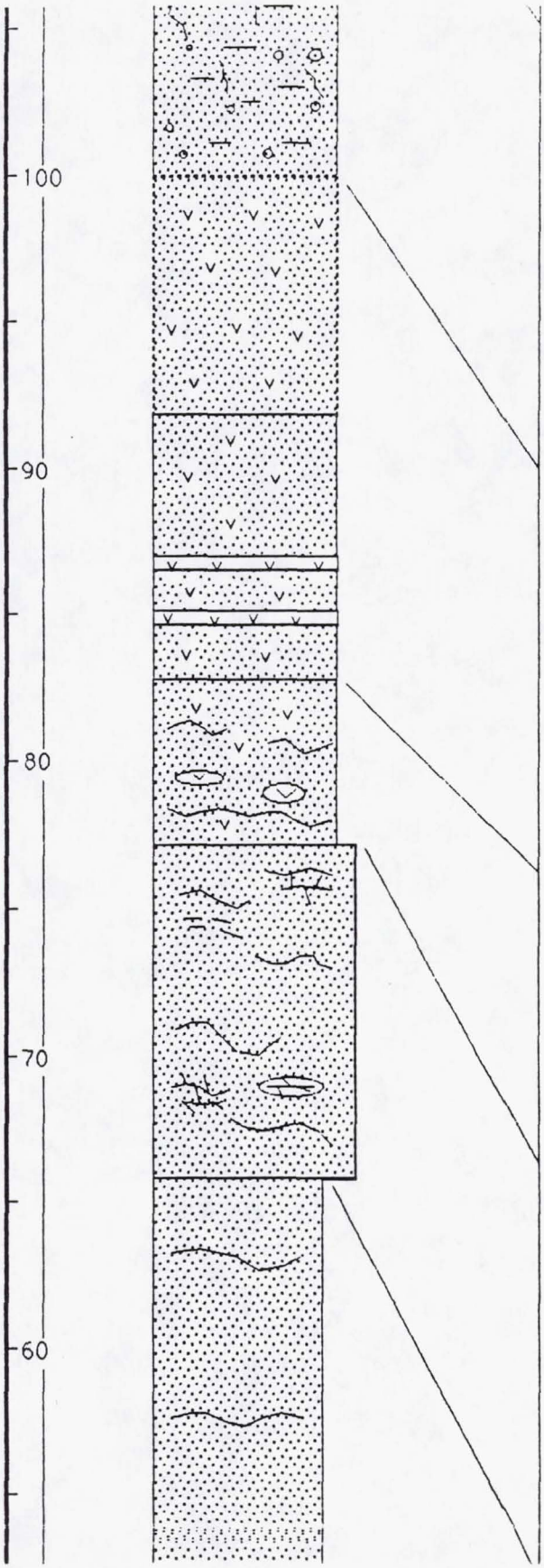

Tan-yellowish brown, pebbly-granule clayey ss. Mass beds 20-30cm thick, crudely bedded. Very poor sorted. Clasts are pale granitic. Shot thru with chalcedony veins, seams. In places muddy matrix stained pink. Near top is 2 green-gry basalt agglomerate beds 9-12 cm thick. Clasts massive to vesicular upto 5cm in diameter. Poorly indurated. Discontinuous patches white vitric tuff.

Interbedded tuffaceous ss, impore (water lain?) tuff, pore airfall tuff. Beds are well-bedded, 8-15cm thick. Nodular limest in ss. Airfall tuff; lower is about 1.4m thick. Very pore with golden biotite. Upper: separated by 70cm granule ss from lower Tan, wary. Upper part: lower tuff water-worked, limy with chalcedony seams.

Mixed clayey-limy granule ss as below, and gry, tuffaceous medium-coarse ss. Limy horizons and lenses. Bedding is highly contorted, graded with lower part. Rare cobbles of red basalt.

Tan, pebbly granule ss as below. Irregularly discontinuous, limy zones upto 12cm thick. Nodular to seamy. Clasts composition as below. Bedding is contorted. Discontinuous clayey horizons. Moderately indurated. Silica replant lime.

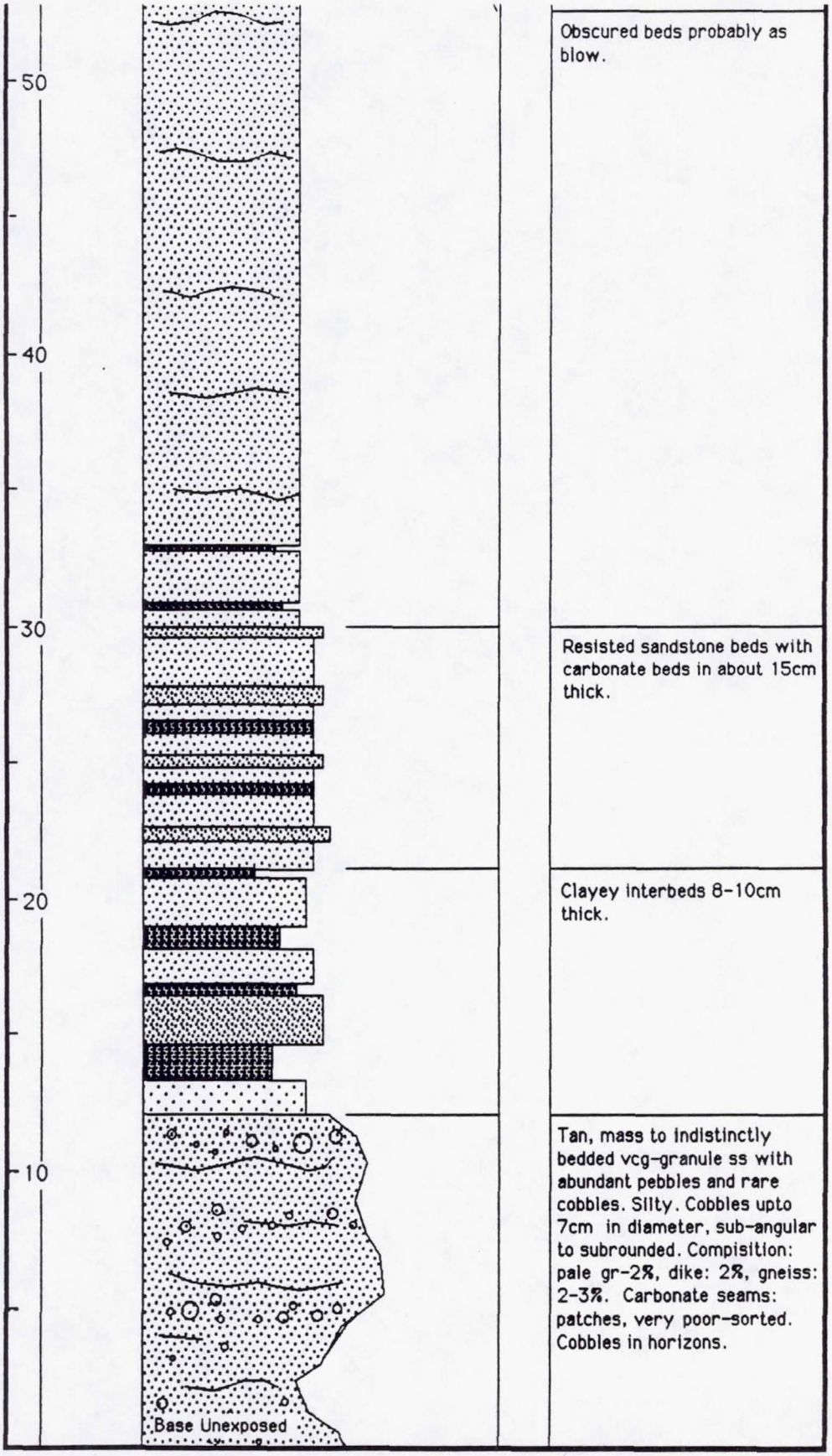
50
40
30
20
10
Base Unexposed
Obscured beds probably as blow.
Resisted sandstone beds with carbonate beds in about 15cm thick.
Clayey interbeds 8-10cm thick.
Tan, mass to indistinctly bedded vcg-granule ss with abundant pebbles and rare cobbles. Silty. Cobbles upto 7cm in diameter, sub-angular to subrounded. Compisition: pale gr-2%, dike: 2%, gneiss: 2-3%. Carbonate seams: patches, very poor-sorted. Cobbles in horizons.

shaped, northwest-trending, fault-bounded basin, approximately 460 m long by 400 m wide at the southern edge. Geometrically, the shape of the basin is similar to that of the Big Sandy Wash basin.

The Boulder Wash sequence is at least 70 m thick and the base is faulted (Figure 17). The detritus throughout the section is 99% pale granite and 1% basalt aphanite with a trace of green, phaneritic dike rock (Appendix VI). The lower 25 m of the section consists of seven thinning- and fining-upward sequences each containing a poorly graded to inversely graded, boulder-to-cobble breccia at the base. The sequences fine upward to gray, very coarse-grained-to-granule, pebbly sandstone that are marked by thin, well-defined, parallel beds. These seven sequences are interpreted to be reworked debris flow deposits of a mid-alluvial fan complex.

These deposits grade upward into pale gray, pebbly-to-granule, very coarse-grained sandstone with stringers of cobbles, one clast thick. Beds are parallel, planar and well-formed. Occasional, isolated boulders or cobbles "float" in the sandy matrix. The few channels present are shallow and broad. This section probably was deposited on the outer alluvial fan of a braided stream complex having low to intermediate slope. Discharge was most likely flashy, producing the isolated boulders as relict debris flows.

The upper half of the sequence contains two discrete deposits. The lower one is weakly bedded, granule sandstone with occasional cobble lenses. The uppermost 7 m is monolithologic cobble breccia that formed in at least two separate pulses. These units represent a change from streamflow-dominated to debris flow-dominated deposition, marking the progradation of the fan complex. The progradation appears to have been abrupt as indicated by the sharp increase in grain size. The basal contact of the Boulder Wash sequence is a pronounced buttress unconformity having at least 5 m of relief on the surrounding granitic basement rock. This contact is faulted on the west side of the sequence and is not exposed on the east side.

The age of the Boulder Wash sequence is not known, but it is tentatively assigned an early- to mid-Miocene age based on its stratigraphic similarity to dated strata of the Big Sandy Wash formation. However, because the Boulder

Figure 17. Composite measured section through the Boulder Wash formation, northeastern Bristol Mountains.

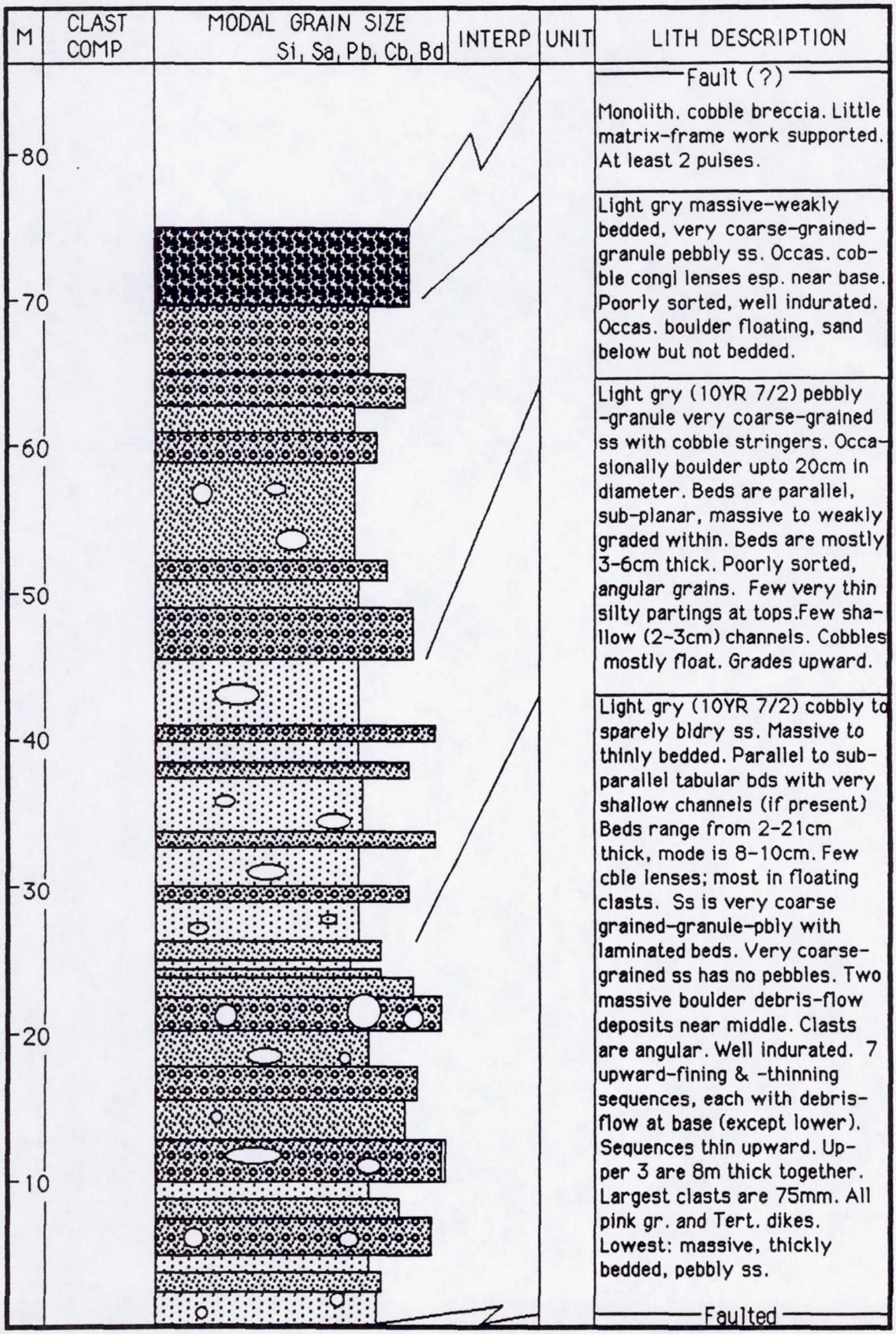
M
CLAST COMP
MODAL GRAIN SIZE
Si, Sa, Pb, Cb, Bd
INTERP
UNIT
LITH DESCRIPTION
Fault (?)
Monolith. cobble breccia. Little matrix-frame work supported. At least 2 pulses.
Light gry massive-weakly bedded, very coarse-grained-granule pebbly ss. Occas. cobble congl lenses esp. near base. Poorly sorted, well indurated. Occas. boulder floating, sand below but not bedded.
Light gry (10YR 7/2) pebbly -granule very coarse-grained ss with cobble stringers. Occasionally boulder upto 20cm in diameter. Beds are parallel, sub-planar, massive to weakly graded within. Beds are mostly 3-6cm thick. Poorly sorted, angular grains. Few very thin silty partings at tops.Few shallow (2-3cm) channels. Cobbles mostly float. Grades upward.
Light gry (10YR 7/2) cobbly to sparely bldry ss. Massive to thinly bedded. Parallel to sub-parallel tabular bds with very shallow channels (if present) Beds range from 2-21cm thick, mode is 8-10cm. Few cble lenses; most in floating clasts. Ss is very coarse grained-granule-pbly with laminated beds. Very coarse-grained ss has no pebbles. Two massive boulder debris-flow deposits near middle. Clasts are angular. Well indurated. 7 upward-fining & -thinning sequences, each with debris-flow at base (except lower). Sequences thin upward. Upper 3 are 8m thick together. Largest clasts are 75mm. All pink gr. and Tert. dikes. Lowest: massive, thickly bedded, pebbly ss.
Faulted
80
70
60
50
40
30
20
10

Wash sequence lacks volcanic detritus, it may be older than the Big Sandy Wash formation.

Overall, strata in the Boulder Wash sequence are tilted to the northeast; dips steepen from 35° in the southwest part of the sequence to 70° in the northeast. The tilting is quite clearly not a "growth feature" because the older beds (in the southwest) dip less steeply than younger ones. In the northwestern part of the sequence at the intersection of two bounding faults, bedding is vertical to overturned westward.

The Boulder Wash sequence is bounded on all three sides by north- to northwest-striking vertical faults. Two other probable faults of similar attitude are found within the sequence. The faults on the west and east sides are major elements of the through-going, regional structural grain. The minor fault bounding the south side of the sequence strikes 30° obliquely to the eastern fault, equal to the angle between the eastern and western faults. This geometry suggests that Boulder Wash basin is a pull-apart feature between the major bounding faults.

The sense of slip on the bounding faults has not been determined. Dip-slip is required in order to generate the basin and additional down-dropping must have occurred since the sedimentary in-filling. The faults have straight traces over several kilometers and are vertical. Because these characteristics are more common to strike-slip faults than to dip-slip faults, the bounding faults are most likely lateral faults.

The oldest offset on the bounding faults clearly pre-dates the basin fill which is assigned a tentative age of early- to mid-Miocene. The youngest movements that can be documented occurred on the southern fault and on one of the minor, internal faults. Here in three places Quaternary alluvial fan deposits are truncated, forming scarps 1-1.5 m high that are down to the east. The eastern fault is overlain by a fan which is not offset and which appears to be equal in age to those offset along the southern margin. The western fault appears to offset similar surfaces.

Coppermine Wash Formation

The Coppermine Wash formation (new name) was named for its prominent exposures along Coppermine Wash in the southwestern Bristol Mountains (Figure 13). The unit appears to be the thickest and most widely exposed Tertiary deposit in the northern Bristol Mountains although it was discovered during the last two days of field work in 1988 and therefore, was examined in reconnaissance only. The unit is exposed in the southwestern part of the range and covers an area of at least 3 km^2. It is at least 350 m thick: the base is faulted and the top is concealed by Holocene alluvium.

The Coppermine Wash formation is a fining- and thinning-upward sequence composed of conglomerate, breccia and sandstone. The base is a green massive, cobble breccia of quartz dioritic clasts that is in fault contact with the pink granitic rock to the east. The breccia is 24 m thick and contains clasts up to 10 cm in diameter. This unit is overlain by red, boulder to cobble conglomerate interbedded with coarse to pebbly, arkosic, sandstone. Channels are shallow, and crossbeds tend to be planar. The volume and grain size of coarse detritus decreases upward, comprising only 10-20% of the material in the upper two-thirds of the unit. The unit probably was deposited in a retrograding alluvial fan complex. The lowest (easternmost) exposures are probably inner fan colluvial deposits, perhaps formed by (tectonic?) over-steepening of the western mountain front. The upper exposures are probably fluvial-dominated, outer fan fringe deposits with minor overbank ponds. The provenance of clasts is overwhelmingly granitic, with minor gneiss. These rock types crop out to the north and east of the unit.

The age of the Coppermine Wash formation is not known. It is most likely mid-Miocene in age because it contains abundant basaltic and andesitic clasts and it has a deep red color similar to other Miocene strata in the lower Mojave area.

The Coppermine Wash formation is strongly deformed. Its northern exposures are tightly folded along the fault contact with what, in hand specimen, appears to be quartz diorite. A major fault bounds the unit on the

east, juxtaposing it against pink granitic rock. The unit overall is tilted west to southwest; it dips 85° on the east but only 25° on the west. In some places it is mildly folded internally.

Structural Synopsis of the Northern Bristol Mountains

The northern Bristol Mountains possess a marked northwest-trending topographic grain produced by sub-parallel, vertical faults, some of which extend the length of the range. Lesser-developed faults strike north and extend for one to two km. Some faults are contained entirely within the bedrock. In others, local complexities have formed fault-bounded basins that are infilled with Tertiary and Quaternary continental strata. The most pronounced of these fault zones extends the length of Big Sandy Wash forming the linear valley in the central part of the range. In several places, Quaternary fan surfaces or fan deposits are demonstrably offset by either the northwest or north-striking faults.

Neither the amount of slip nor the offset direction of the major faults has been determined because of the lack of offset geological features. However, the faults are believed to be strike-slip faults because: 1) the traces are straight for the length of their exposure throughout the range, 2) the fault planes are consistently vertical, 3) the modal rake of slickenlines is horizontal, and 4) the structural levels are similar on both sides of the faults.

It is estimated that there has been a minimum of 8 km of separation on the Big Sandy Wash fault (Figure 13). The fault separates green, chloritically altered, granitic rock on the west from unaltered, pale granitic rock on the east. Over a minimum distance of 8 km, neither rock type crops out on the opposite side of the fault. It is unlikely that the chloritic alteration developed after the faulting because the altered granitic rock is confined to the west side of the fault and nearly identical unaltered granitic rocks are found on opposite sides of the fault. Thus, the juxtaposition of the altered and unaltered rocks provides an estimate of the minimum offset although the sense of motion is uncertain.

The deformation along the fault zones appears to have been at a fairly shallow level and at a high strain rate. All of the major faults are marked by intense brecciation; in places the rock has been converted to a substance resembling fine-grained sand. Elsewhere, the fault breccia is more coarse, involving fragments up to 8 m in diameter. Nowhere is there evidence for the cataclastic flow or mylonite development that would be indicative of ductile faulting at low strain rates or under high P/T conditions.

IVANPAH VALLEY

One of the hypotheses proposed (Stewart, 1967) was that the Garlock fault has been offset right-laterally from its original eastward continuation by the southern Death Valley fault zone. If this is true, there should be some indication of the presence of an east to northeast-trending fault zone southeast of the Avawatz Mountains. Because no such zone has been reported in the literature, or shown on any map, it can be assumed that it does not have obvious expression in bedrock outcrops. The places to search for a possible offset fault are therefore in the alluvial valleys south of Kingston Wash (the location of the proposed eastward extension of the Garlock fault). Examination of the Kingman and Needles 1:250,000 geologic maps of California (Jennings, 1961; Bishop, 1963) indicates that, based on geologic criteria, the only probable candidate is Ivanpah Valley. This valley is bounded on the northwest by the Ivanpah Mountains and the Cima volcanic field, and on the southeast by the New York Mountains, Mid Hills, and Providence Mountains (Figure 18). The presence of the Garlock fault extension in this valley would require that it be offset more than 60 km in a right-lateral sense.

TM scene 40149-17441, Quadrant 1 was processed for interpretation and analysis. Channels 4, 5 and 7 were high-pass filtered using a 31 x 31 box-car filter, and were then decorrelation stretched and combined to produce a color composite, assigning blue, green and red to the three channels (Plate 7). The fault appearing on the interpretation map (Figure 18) in Ivanpah Valley was proposed by Hewett (1956), mostly based on anomalous ground water levels in wells near the town of Cima. The image shows a large north-trending dike, which has minor left-lateral offsets. There also appears to be left-lateral offset by the Clark Mountain fault, which juxtaposes granitic rocks and Paleozoic

Figure 18. Interpretation map of Plate 7 showing trace of possible offset Garlock fault running into Old Dad Mountains.

OFFSET GARLOCK FAULT: NOT IN IVANPAH VALLEY

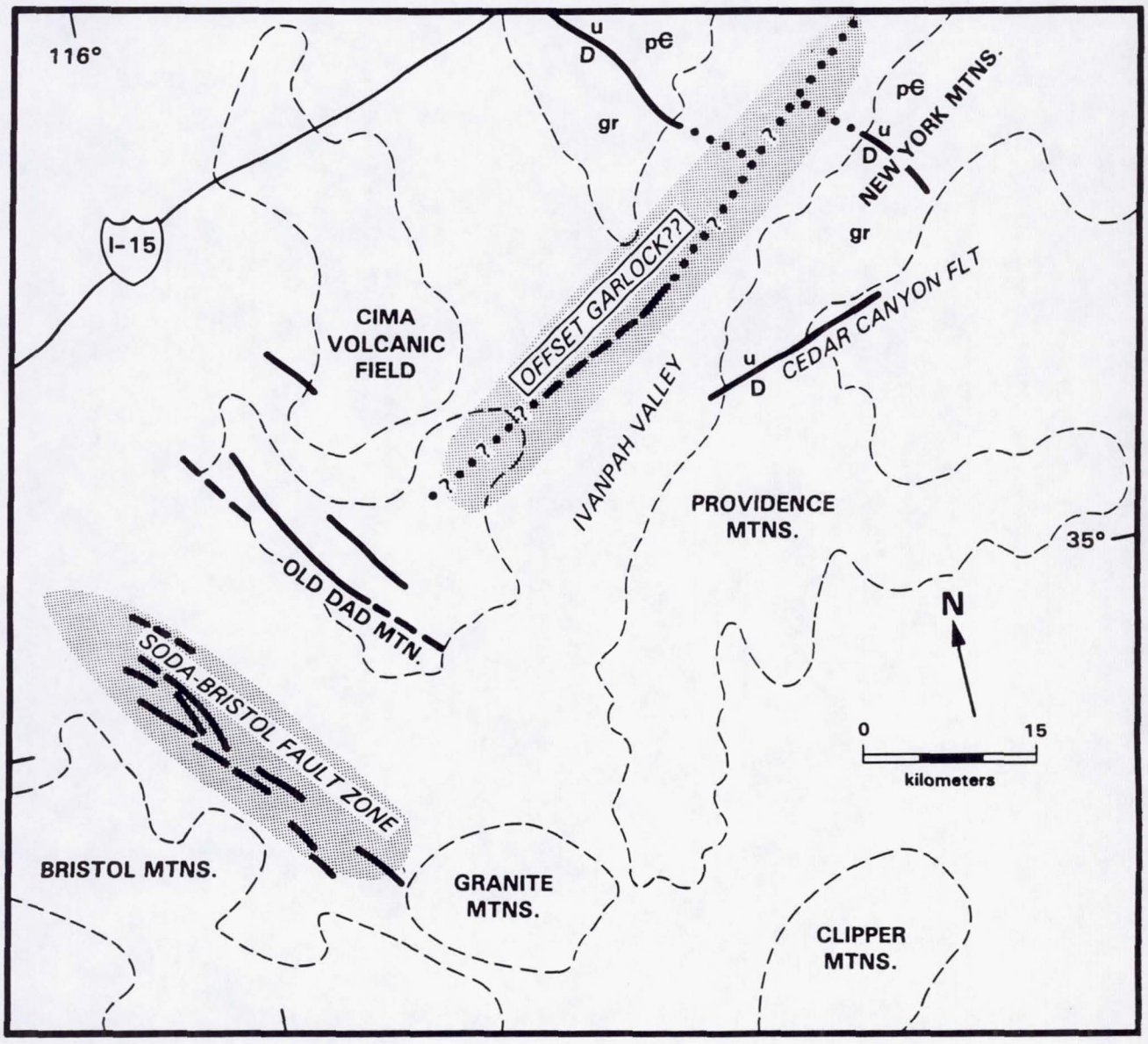

limestone on the southwest against Precambrian rocks on the northeast side. This offset is depicted on the geologic map as bending through Ivanpah Valley, connecting exposures in the Ivanpah Mountains with exposures in the New York Mountains. The lack of subsurface information, permits either explanation.

The major problem with accepting these features as evidence of an offset Garlock fault arises when considering the northeast extension of this fault from the Soda-Bristol fault zone. The fault projects directly to the middle of the Old Dad Mountains, and must go through these mountains and then through the sand-covered Devil's Playground. Examination of the TM image shows no trace of any feature following this course. The geologic map shows the northwest-trending Old Dad fault continuously transecting the range, with no offset. We therefore conclude, based on examination of TM data and published geologic maps, that it is unlikely that the Garlock fault has been offset up to 60 km. Offset greater than this amount is still possible, but was not examined.

INTERPRETATIONS

TERMINATION OF THE GARLOCK FAULT

The primary purpose of this project was to examine the kinematics of the intersection of the Garlock and Death Valley fault zones. Four hypotheses have been proposed to describe the nature of the interaction between these two active faults:

1. The southern Death Valley fault zone has less than 8 km of right-lateral offset across it and terminates in the eastern Avawatz Mountains (Davis, 1977).
2. The southern Death Valley fault zone continues several kilometers south of the Avawatz Mountains (Stewart, 1967; Troxel, 1968; Wright and Troxel, 1967; Dibblee, 1980).
3. The Garlock fault zone continues east of the Death Valley fault zone and presently lies buried beneath alluvial material of the Kingston Wash. The eastward continuation of the Garlock fault zone has been offset less than 8 kilometers to the south along the southern

continuation of the Death Valley fault zone (Davis and Burchfiel, 1973; Plescia and Henyey, 1982)

4. The Garlock fault zone terminates in the Avawatz Mountains as an east-vergent thrust fault (Hewett, 1955; Brady and Troxel, 1981).

All of the data gathered in the course of this project supports the contention that the Garlock fault zone terminates in the Avawatz Mountains against the southwestward dipping, east-vergent Mule Spring fault. This conclusion is based both on geological evidence for this hypothesis and the lack of geological evidence for other hypotheses.

One line of evidence that supports the preferred hypothesis is the continuous and unbroken surface trace of the Mule Spring fault (Figure 3). The fault bounds the Avawatz Mountains on the north and east sides of the mountain range. The relationship of the southward curving trace of this fault to the topography indicates that the fault must dip at a fairly low angle beneath the Avawatz Mountains. As the fault wraps around the mountain range, the style of deformation changes from left-lateral oblique-slip along the north flank to east-vergent reverse-slip along the east flank (Hewett, 1955; Brady and Troxel, 1981; Brady, 1986). Mesozoic intrusive rock faulted over Quaternary alluvium and the occurrence of near-vertical, dip-slip fault striations provide evidence that thrusting has occurred on the east flank. Thus, kinematic indicators and the orientation of the Mule Spring fault suggest that the Avawatz monzodiorite has been ramped up to the east along a low-angle fault surface.

Additional evidence concerning the termination of the Garlock fault zone comes from the Kingston Wash area where the proposed eastward continuation of the Garlock fault zone should be found. Neither the analysis of processed images nor measurements of fracture patterns provided any evidence for the proposed eastward continuation. However, in the western Avawatz Mountains several east-striking, splay faults, that were already well-documented in the field, could be detected from the imagery. The significance of these splay faults is that, as Freund (1971) has shown, the displacement along a fault does not have to diminish to zero at its terminus. Rather, the

motion can be absorbed by several branching segments with the same characteristics as the splay faults in the western Avawatz Mountains.

Freund (1974) has also demonstrated the geometric impossibility of two crossing conjugate faults being displaced simultaneously. He showed that the two faults must either not cross, or they must operate in sequence. As Quaternary displacement has been documented on the Death Valley and Garlock fault zones (Davis and Burchfiel, 1973; Clark, 1973; Troxel and Butler, 1979; Brady, 1986), the constraints put forth by Freund should apply to the intersection of these faults.

The behavior of faults in such a situation was studied by Hoeppener et al. (1969) in a mechanical experiment using a clay model overlying a rubber sheet that was deformed by irrotational plane strain. Non-crossing conjugate fault sets were generated in the clay model, and as deformation continued, the two sets of faults rotated in opposite directions toward the extensional axis. This pattern of behavior is very similar to the rotation toward a northwest trend that the Death Valley and the Garlock fault zones exhibit in the vicinity of their intersection.

Further evidence for the termination of the Garlock fault is indicated by the absence of an eastward-continuing, offset Garlock in the most likely area, the Ivanpah Valley. This argument is refuted by the northeast projection of possible left-lateral structures which would have to pass through the continuously exposed Old Dad Mountains and offset existing structures. No evidence for offset structures in the Old Dad Mountains, for left-lateral structures in Ivanpah Valley or for anywhere farther north, was found from interpretation of TM images and analysis of published geologic maps.

Although there is little evidence for an eastern continuation of the Garlock fault, there is strong evidence that the Death Valley fault zone continues south at least as far as the Bristol Mountains. As described above, near-vertical, strike-slip faults, having the same orientation as the Death Valley fault zone to the north, are located in the Soda and Bristol Mountains. In the playa of Soda Lake between these ranges, a lineation of springs which represents a fracture

zone, also aligns with the proposed southern continuation of the Death Valley fault zone.

All of these lines of evidence are consistent with the conclusion that the Garlock fault zone terminates in the Avawatz Mountains and the Death Valley fault zone continues south as the through-going structure.

TECTONIC IMPLICATIONS OF ALLUVIAL FANS

Alluvial fans along a mountain-front are temporary storage sites for large quantities of sediment that are en route from the mountain sources to the basins below. Tectonic events are recorded by alluvial fan deposits either as changes in the lithology of the material delivered to a fan surface, or as actual deformation of the fan deposits. The relative age and style of Quaternary tectonism that occurred along the northern Avawatz Mountains may be inferred from several features of the alluvial fans present there.

The oldest alluvial deposit that records the erosional stripping of the Avawatz Mountains is apparently the Qf1 deposit located at the southern end of the eastern mountain-front as mapped by Brady (1986). This uplifted and tilted veneer of east-dipping alluvium has been almost completely removed by erosion and re-deposited on younger fan surfaces. The age of this deposit and the amount of uplift and erosion that it has endured suggest that it is located in the vicinity of the earliest major tectonic uplift in the Avawatz Mountains. Further evidence for initial uplift having occurred here is provided by local faults. The spatial configuration of faults in this area is analogous to the configuration resulting from a pair of left-stepping, right-lateral, en echelon faults as described by Woodcock and Fischer (1986). One possibility is that the uplift was initiated by compression between the left-stepping Soda-Avawatz and Arrastre Spring faults. At the very least, the southeastern corner of the Avawatz Mountains was a topographic high prior to, or coeval with, uplift.

Uplifted fanglomerate along the northern mountain-front indicate that the rocks in the lower Sheep Creek canyon were tectonized subsequent to uplift of the Avawatz monzodioritic rock which formed the upper canyon. The uplifted

fanglomerate consists mainly of dioritic clasts, however on the surface of this fanglomerate there is a layer of gneissic gravel. The gneissic detritus has eroded from gneissic bedrock which has only recently been uplifted through its sedimentary cover in the lower canyon.

The most recent tectonism on the northern flank of the range appears to have occurred after deposition of the late-Pleistocene alluvial material (Qf2 on Figure 7) because these deposits have been slightly uplifted and tilted toward the northwest. Reverse-slip faulting apparently caused this tilt and has produced an imbricated sequence placing older Precambrian rocks over younger Precambrian rocks and Quaternary alluvium. A small component of right-slip may have accompanied this faulting, as suggested by the right-lateral bend in the Sheep Creek canyon near the mountain-front and by the slight westward tilt of the late-Pleistocene fan strata. The right-lateral offset can be explained by movement along the Death Valley fault zone. However, on the northern flank of the Avawatz Mountains, there is very little evidence for significant right-lateral offset between the fans and the mountain-front as the fan lithologies are consistent with the bedrock lithologies in the canyons directly above the fans. These observations suggest a predominant reverse dip-slip motion for the range-bounding fault segment of the northern mountain-front.

Although voluminous alluviation has clearly been associated with the Avawatz Mountains for most of the early Quaternary, the alluvial fans along the northern mountain-front are thought to be relatively thin. At mid-to-distal areas on the fans, Mesozoic granite crops out. At the granitic outcrops the thickness of the onlapping fan material diminishes to zero (Figure 6). Uplifted fanglomerate, deposited on Precambrian metasedimentary rocks and gneissic basement rock exposed in lower Sheep Creek canyon are only 12 m thick. Thus, it appears that little or no subsidence has occurred in the adjacent basin or below the alluvial fans.

The Mesozoic granite which is exposed on the Sheep Creek and Avawatz Peak alluvial fans is thought to exist below all of the alluvium along the northern mountain-front. The thin alluvial cover which indicates a lack of subsidence and the tilted, deeply entrenched, Pleistocene fan deposits suggest

that the granitic pluton underlying the alluvium may be undergoing a small but significant amount of compressional uplift as it converges on the bend in the southern Death Valley fault zone. Such a pattern of compressional uplift is in accordance with the model of Segall and Pollard (1980) for increased confining pressures in an area of an en echelon discontinuity (Figure 19).

Additional information concerning local tectonic events was inferred from the drainage system and stream channel characteristics of the alluvial fans. Headward eroding channels with debris-free channel bottoms in proximal-fan regions indicate that active downcutting is occurring (Hooke, 1967; Bull and Menges, 1977). In this case, either the base-level has been lowered or the headwaters have been uplifted. Because there has apparently been little or no subsidence of the basin or alluvial fans along the northern mountain-front, channel downcutting can be attributed to uplift of the headwaters. Following uplift, accelerated erosion in the upper canyon should take place and the resulting debris will be stored in the trunk stream until oversteepened and released to the alluvial fan or released by further tectonic uplift (Schumm, 1973). In the Avawatz Mountains, a large amount of sedimentary debris is in fact being eroded from the upper canyon walls and stored in the canyon channels. The active downcutting also implies that the uplift rate of the headwater region has been exceeding the erosional capability of overland flow. The downcutting therefore, should continue until the depositional system reaches a state of equilibrium or until the disequilibrium is rejuvenated by tectonism (Schumm, 1973).

TECTONIC IMPLICATONS OF FAULT GEOMETRY

As discussed in the section on the Quaternary alluvial fans in the northern Avawatz Mountains, each time that the proximal-fan heads were uplifted and incorporated into the mountain block, a new mountain-front formed northward from the old one, enlarging the mountain block. Either new fault segments developed to accommodate the compressional shortening, or previously existing faults accommodated the reverse-slip motion. A future episode of north-directed compression may form a new fault segment below the modern-day alluvial fans or initiate reverse-slip along a fault segment already in existence below the fans.

Figure 19. State of stress near en echelon discontinuities. Contoured stress values < -1.0 represent an increase in confining pressure. Tick marks indicate direction of minimum stress sigma-1 (from Segall and Pollard, 1980).

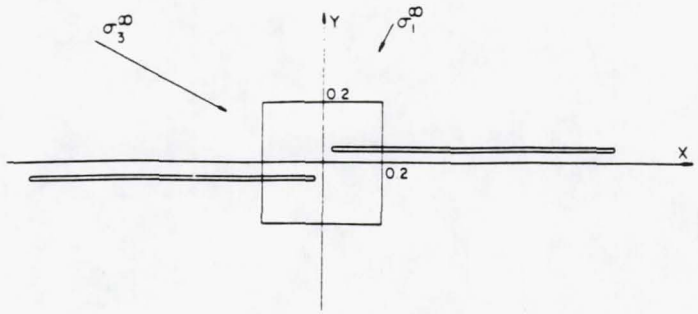
σ_3^∞
Y
σ_1^∞
0.2
X
0.2

(a)

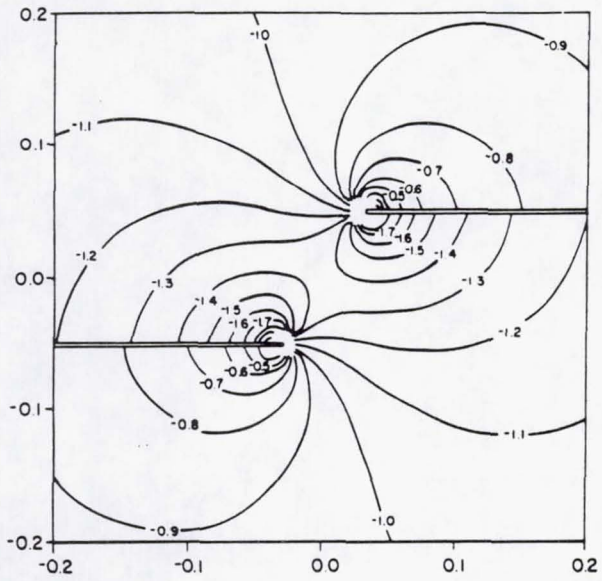
0.2
0.1
0.0
-0.1
-0.2
-0.2
-0.1
0.0
0.1
0.2

(b)

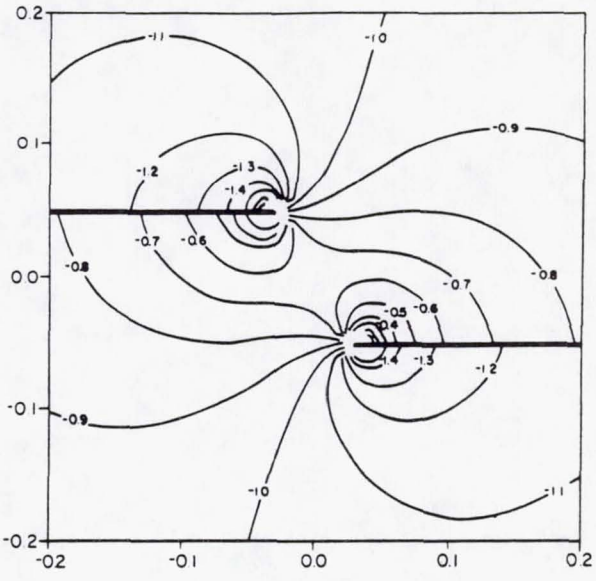
0.2
0.1
0.0
-0.1
-0.2
-0.2
-0.1
0.0
0.1
0.2

(c)

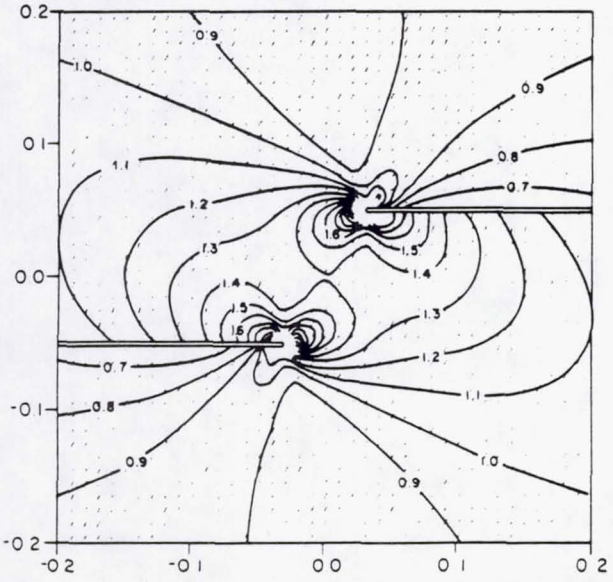
0.2
0.1
0.0
-0.1
-0.2
-0.2
-0.1
0.0
0.1
0.2

(d)

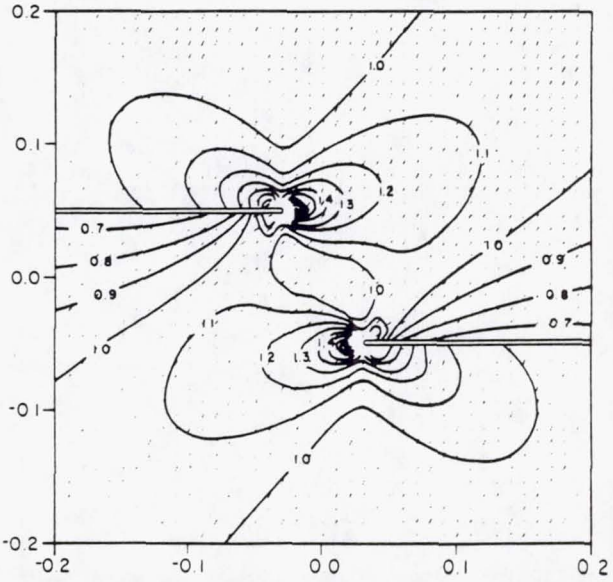
0.2
0.1
0.0
-0.1
-0.2
-0.2
-0.1
0.0
0.1
0.2

Along the Noble Hills, 6 km northwest of the Avawatz Mountains, Troxel and Butler (1979) and Brady (1986) mapped as many as six, northwest-striking branches of the southern Death Valley fault. At the Avawatz Mountains, these branches strike more westerly and continue along the northern front of the range. Troxel (1970) and Troxel and Butler (1979) documented the secular migration of these branches. The oldest fault, the westernmost branch, has the greatest separation across it. The youngest fault, the easternmost branch, has the least. This eastward stepping of the southern Death Valley fault zone is similar to the northward stepping of the uplift in the northern Avawatz Mountains, and the two phenomena are probably closely related.

Butler *et al.* (1988) suggested that migration of southern Death Valley fault zone is a response to the impingement of the Mojave province on the Basin and Range province which results in an eastward bend in the fault zone. As the bend develops in the right-lateral-slip fault system, it generates compressional stresses that are only partially accommodated by crustal shortening. Eventually new faults develop as the stress regime approaches equilibrium, as described theoretically by Freund (1974). In the future, the southern Death Valley fault zone may bypass the bend by stepping east to a position that is in alignment with the Soda-Avawatz fault zone.

A similar process may also be occurring on the San Andreas fault zone south of the "big bend." The San Jacinto and Elsinore faults, west of the San Andreas, are thought to be younger segments of the San Andreas fault zone that are developing in response to compressional stresses produced by the bend (Weldon and Humphreys, 1986).

EVOLUTION OF THE BEND IN THE DEATH VALLEY FAULT ZONE

One explanation for the bend in the Death Valley fault zone is that it was caused by west-directed extension of the Basin and Range Province along the northern side of the Garlock fault zone. However, two observations argue against this mechanism: 1) Wernicke *et al.* (1982) noted that the Spring Mountains block directly east of the intersection of the two fault zones is not

extended and 2) there is northeast-directed thrusting along the easternmost segment of the Death Valley fault zone south of the its intersection with the Garlock fault. Thus, the bend or offset in the Death Valley fault zone is more likely the result of the eastward impingement of the Mojave block south of the Garlock rather than west-directed extension in the Basin and Range province north of the intersection.

The date of the inception of movement on the southern Death Valley fault is estimated to be 14 Ma (Butler *et al.*, 1988) whereas the date of inception of the western portion of the Garlock fault zone fault is about 10 Ma (Burbank and Whistler, 1987; Golembek and Brown, 1988). If these dates are correct, then the Garlock fault would have encountered the pre-existing Death Valley fault zone sometime after 10 Ma.

These kinematic and relative-timing constraints lead to two differing kinematic models for the intersection of the Garlock and Death Valley fault zones: 1) the Death Valley fault zone was offset to the east by the Garlock fault zone producing a large, left-step in the right-lateral Death Valley fault, or 2) the Death Valley fault zone was tilted eastward by east-vergent motion of the Mojave block south of the Garlock fault zone.

Several field and experimental studies (Lensen, 1958; Sharp and Clark, 1972; Bonilla, 1979; Segall and Pollard, 1980) have addressed the question of the surface deformation associated with en echelon offset along strike-slip faults. For right-lateral faults, right steps produce pull-apart basins or rhomb grabens, whereas left steps produce local upwarps or horsts. According to the first kinematic model mentioned above, in late-Miocene or early-Pliocene time, left-lateral transport of the Mojave block along the Garlock fault produced a large, left-step in the right-lateral Death Valley fault zone in front of the Avawatz Mountains. The fault configuration that results from continued right-lateral slip along two left-stepping segments, referred to as a contractional duplex structure (Woodcock and Fischer, 1986), is very similar to the fault geometry observed in the Avawatz Mountains (Figure 20A). The minor differences in the fault geometry observed in the Avawatz Mountains can be explained by assuming that the duplex grew asymmetrically towards the north or that the southern portion of the duplex has been subsequently overridden

Figure 20. A: Line drawing showing extensional and contractional duplexing at fault offsets or restraining bends. B: Sequence of asymmetrical growth of faults at a restraining bend in plan view (from Woodcock and Fischer, 1986).

A

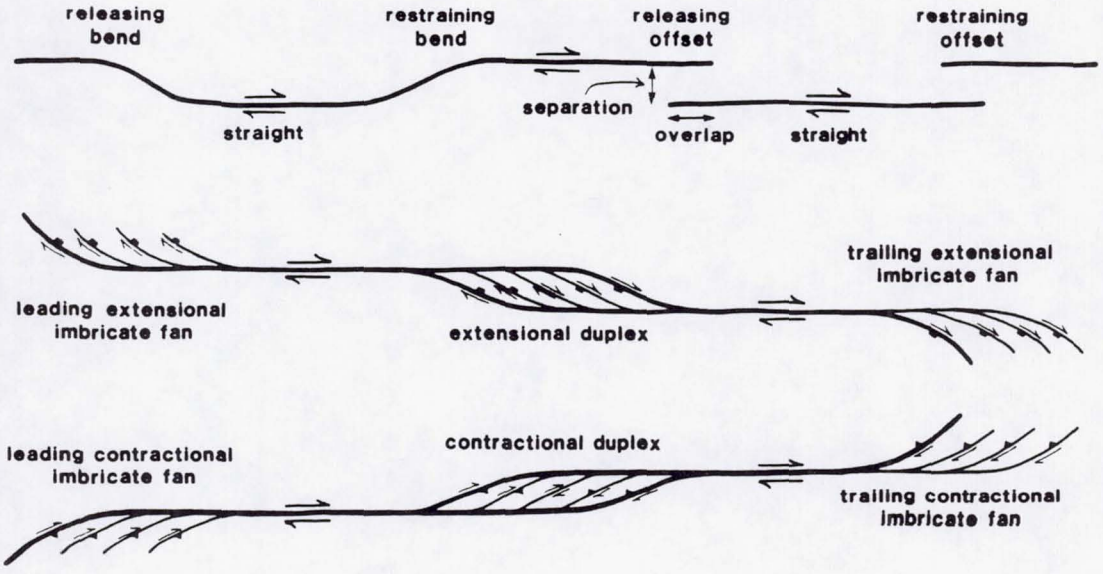
releasing bend
restraining bend
releasing offset
restraining offset
separation
overlap
straight
straight
trailing extensional imbricate fan
leading extensional imbricate fan
extensional duplex
leading contractional imbricate fan
contractional duplex
trailing contractional imbricate fan

B

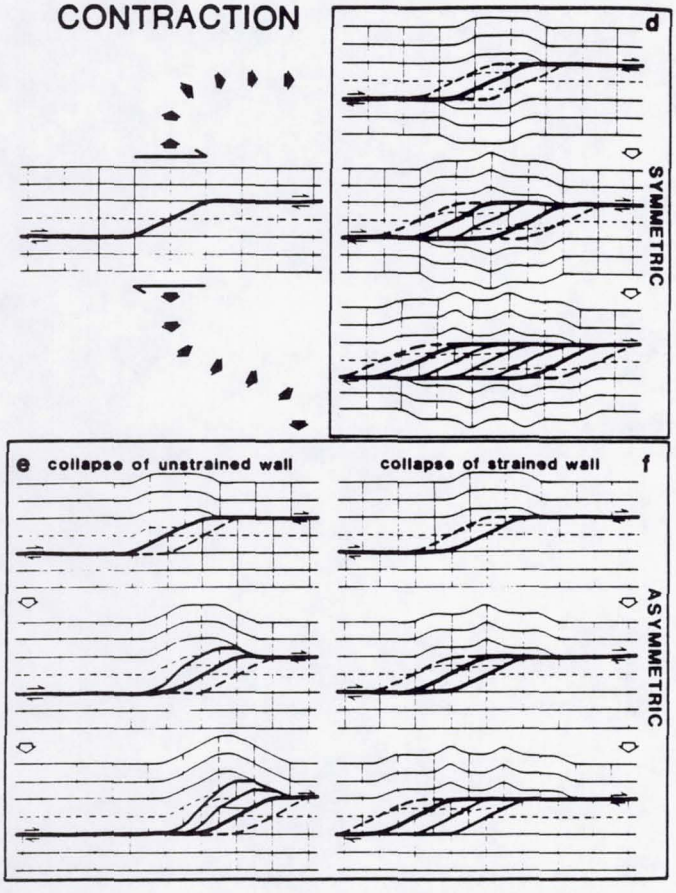
CONTRACTION
d
SYMMETRIC
e collapse of unstrained wall
collapse of strained wall
f
ASYMMETRIC

the Avawatz monzodioritic body as it "ramped up" along the Mule Spring fault. Furthermore, the north-directed thrusting observed along the northern Avawatz Mountains is consistent with the theoretical direction of maximum compressional stress which Segall and Pollard (1980) determined experimentally from elastic crack theory.

Thrust faults in the northern Avawatz Mountains and the northern end of the Arrastre Spring fault to the south, have dip angles and orientations which are also in accordance with the first model. In the model of Woodcock and Fischer (1986), faults beneath a left-stepping offset in a right-lateral fault zone are inward-dipping and may converge at depth into a single shear zone. The Death Valley fault zone segments along the northern Avawatz Mountains dip southwest while the northern end of the Arrastre Spring fault dips northeast back underneath the Avawatz Mountains (Spencer, 1981). The Avawatz Mountains can therefore be considered a horst-like structure that has a fault geometry similar to that of a left-stepping offset

The second, "thin-skinned" model invokes deformation in the upper few kilometers of crust to produce a bend in the southern Death Valley fault zone. In this case, the eastward movement of the Mojave block against the Death Valley fault zone causes an eastward deflection and southward flattening of the fault segments along the leading edge near the intersection. The fault configuration proposed by Woodcock and Fischer (1986) for a restraining bend in a right-lateral strike-slip system is very similar to what is observed in the northern Avawatz Mountains (Figure 20B). If this model is correct, a shallow-dipping detachment fault is necessary under the Avawatz Mountains in order to maintain three-dimensional strain. One possibility is that the somewhat steeply dipping faults located along the northern mountain-front converge into a sub-horizontal, upper-crustal discontinuity below the Avawatz Mountains. Brady (1986) interpreted data from a gravity survey as indicating that a sub-horizontal discontinuity is present 2 km beneath the Avawatz Mountains. He interpreted the discontinuity to be the plane of the Mule Spring fault which flattens beneath the monzodioritic mountain core.

Based on this sub-horizontal discontinuity, the low-angle, imbricate style of thrusting observed in the southeastern Avawatz Mountains and the

westward flattening of the low-angle, reverse-slip segment of the Death Valley fault zone exposed along the eastern mountain front, we believe that the second "thin-skinned" model is more consistent than the first model which would require offset of the southern Death Valley fault zone to greater depths.

CONCLUSIONS

Analysis of the processed images and detailed field investigations have provided significant information concerning the late-Pliocene and Quaternary evolution of the intersection between the Garlock and Death Valley fault zones. The images were used to detect patterns of sedimentation and age relationships on the alluvial fans and to determine the geometry, styles of deformation, and timing of movements on major and minor faults in the study area. The field investigation usually confirmed the inferences drawn from the images and provided additional tectonic and geomorphologic data about the Quaternary deformation of the region.

INTERSECTION OF THE GARLOCK AND DEATH VALLEY FAULT ZONES

With regard to the kinematics of the intersection of the Garlock and Death Valley fault zones, the primary conclusions of this study are:

1) The Garlock fault zone terminates as an east-vergent reverse fault in the eastern Avawatz Mountains and does not continue east of the southern Death Valley fault zone.
2) There is a minimum of 25-30 km of late Tertiary and Quaternary, right-lateral separation across the southern Death Valley fault zone.
3) The Soda-Avawatz fault zone is most likely a right-lateral, strike-slip or oblique-slip fault similar in style to the Death Valley fault zone.
4) The Soda Lake lineaments are probably caused by Quaternary movement on northwest-striking, lateral faults
5) The northern Bristol Mountains contain at least four major, parallel, northwest-striking lateral faults having probable right-lateral separation.

6) The southern Death Valley fault zone, the Soda-Avawatz fault zone, the Soda Lake lineaments, and the faults of the northern Bristol Mountains form a discontinuous belt of shears and related structures having a similar style and orientation. This belt probably extends at least 35 km south of the Bristol Mountains where it connects with similar structures in the Granite Mountains fault zone described by Dokka (1988). The belt is herein designated as the Eastern Mojave shear zone.
7) The Eastern Mojave shear zone is a major Neogene tectonic feature of the eastern Mojave province and it represents the boundary between domains having very different tectonic styles.

ALLUVIAL FANS OF THE AVAWATZ MOUNTAINS

With regard to the dynamics of the development of the alluvial fans of the Avawatz Mountains, the primary conclusions are:

1) Initial tectonic uplift probably occurred in the southeastern Avawatz Mountains.
2) The greatest amount of uplift has occurred in the northeastern Avawatz Mountains.
3) The Avawatz Mountains were uplifted essentially in place after being translated east about 8 km along the Mule Spring fault.
4) West-dipping thrust faults, surfacing along the eastern Avawatz Mountains, flatten at depth beneath the range.
5) Lower Sheep Creek canyon was uplifted sometime after the Avawatz monzodioritic rock of the upper canyon, resulting in a northward enlargement of the Avawatz Mountains.
6) Very little or no subsidence has occurred in the alluvial region adjacent to the northern flank of the Avawatz Mountains.
7) Uplift of the alluvial fans has occurred after late-Pleistocene time.
8) Holocene uplift is on-going although at a slower rate than during Plio-Pleistocene times as suggested by evidence for rapid early alluviation which has gradually declined to its present slower rate.

OUTSTANDING PROBLEMS

There are several unresolved problems regarding the Eastern Mojave shear zone:

1) The shear zone is a structural element of regional importance, but little is known about its relation to the tectonic evolution of the Basin and Range and Mojave provinces.
2) The slip and chronology of the individual faults in the Soda-Avawatz and Bristol Mountains fault zones are uncertain.
3) Although there is abundant evidence for Quaternary deformation along the shear zone, the potential for earthquakes is unknown.

REFERENCES CITED

Basset, A.M. and D.H. Kupfer, 1964, A geologic reconnaissance in the southeastern Mojave Desert, California: California Division of Mines and Geology, Special Report 83.

Bird, P. and R.W. Rosenstock, 1984, Kinematics of present crust and mantle flow in southern California: Geological Society of America Bulletin, v. 95, p. 946-957.

Bishop, C., 1963, Geologic Map of California, Needles Sheet: California Division of Mines and Geology Map, 1:250,000 scale.

Bonilla, M.G., 1979, Historic faulting-map patterns, relation to subsurface faulting, and relation to pre-existing faults, *in* Proceedings of Conference VIII, Analysis of actual fault zones in bedrock: U.S. Geological Survey Open File Report 79-1239, p. 36-65.

Brady, R.H. III, and B.W. Troxel, 1981, Eastward termination of the Garlock fault in the Avawatz Mountains, San Bernardino County, California: Geological Society of America Abstracts with Programs, v. 13, p. 46.

Brady, R.H. III, 1986, Cenozoic geology of the northern Avawatz Mountains in relation to the intersection of the Garlock and Death Valley fault zones, San Bernardino County, California [Ph.D. dissertation]: Davis, California, University of California, 292 p.

_____ 1986a, The eastward continuation of the Garlock fault zone: A geological paradox: Geological Society of America Abstracts with Programs, Cordilleran Section, v. 18, n. 2, p. 88-89.

_____ 1984, Neogene stratigraphy of the Avawatz Mountains between the Garlock and Death Valley fault zones, southern Death Valley, California: Implications as to late Cenozoic tectonism: Sedimentary Geology, v. 38, p. 127-157.

Bull, W.B., 1978, Geomorphic tectonic activity classes of the southern front of the San Gabriel Mountains, California: United States Geological Survey Contact Report 14-08-001-G-394, Menlo Park, California, 100 p.

_____ 1968, Alluvial fans: Journal of Geology, v. 16, p. 101-106.

Bull, W.B. and C.M. Menges, 1977, Geomorphic evidence for Holocene faulting in the central Mojave Desert, California: Geological Society of America Abstracts with Programs, v. 9, p. 915.

Burbank, D.W. and D.P. Whistler, 1987, Temporally constrained tectonic rotations derived from magnetostratigraphic data; implication for the initiation of the Garlock fault, California: Geology, v. 15, p. 1172-1175.

Burchfiel, B.C. and J.H. Stewart, 1966, "Pull-apart" origin of the central segment of Death Valley, California: Geological Society of America Bulletin, v. 77, p. 439-442.

Butler, P.R., 1984, Fluvial response to on-going tectonism and base-level changes, lower Amargosa River, southern Death Valley, California: Sedimentary Geology, v. 38, p. 107-125.

Butler, P.R., B.W. Troxel and K.L. Verosub, 1988, Late Cenozoic history and styles of deformation along the southern Death Valley fault zone, California: Geological Society of America Bulletin, v. 100, p. 402-410.

Carter, B.A., 1971, Quaternary displacement on the Garlock fault, California: American Geophysical Union Transactions, EOS, v. 52, p. 350.

Clark, M.M., 1973, Map showing recently active breaks along the Garlock and associated faults, California: U.S. Geological Survey Miscellaneous Geological Investigations Map I-741.

Clayton, J.A., 1988, Quaternary tectonism of Sheep Creek alluvial fan deposits, Avawatz Mountains, southern Death Valley, *in* Gregory, J.L. and E.J. Baldwin, eds., Geology of the Death Valley region: Annual Field Trip Guidebook #16, South Coast Geological Society, p. 224-239.

Crippen, R.E., R.G. Blom and J.R. Heyada, 1987, Directed band ratioing for the retention of perceptually-independent topographic expression in chromaticity-enhanced imagery: International Journal of Remote Sensing, (in press).

Davis, G.A., 1977, Limitations on displacement and southward extent of the Death Valley fault zone, California: California Division of Mines and Geology Special Report 129, p. 12-33.

Davis, G.A. and B.C. Burchfiel, 1973, Garlock fault, an intracontinental transform structure, southern California: Geological Society of America Bulletin, v. 84, p. 1407-1422.

Dibblee, T.W., 1980, Geologic structure of the Mojave Desert, *in* Fife, D.L. and A.R. Brown, eds., Geology and Mineral Wealth of the California Desert: South Coast Geological Society, Dibblee Volume, p.69-100.

Dokka, R., 1988, Synthesis of middle and late Cenozoic tectonic history of the Mojave Desert block: Geological Society of America Abstracts with Programs, Cordilleran Section, v. 20, n. 3, p. 156.

_____ 1983, Displacements on late Cenozoic strike-slip faults of the central Mojave Desert, California: Geology, v. 11, p. 305-308.

Freund, R., 1971, The Hope Fault, a strike-slip fault in New Zealand: New Zealand Geological Survey, Bulletin n.s. 86, 49 p.

_____ 1974, Kinematics of transform and transcurrent faults: Tectonophysics, v. 21, p. 93-134.

Gillespie, A.R., 1980, Digital techniques of image enhancement, *in* Siegal, B. and A. Gillespie eds., Remote Sensing in Geology: John Wiley, New York, p. 139-226.

Gillespie, A.R., A.B. Kahle and R.E. Walker, 1986, Color enhancement of highly correlated images. I. Decorrelation and HSI contrast stretches: Remote Sensing of Environment, v. 20, n. 3, p. 209-235.

Golembek, M.P. and L.L. Brown, 1988, Clockwise rotation of the western Mojave Desert: Geology, v. 16, p. 126-130.

Grose, L.T., 1959, Structure and petrology of the northeast part of the Soda Mountains, San Bernardino County, California: Geological Society of America Bulletin, v. 70, p. 1509-1548.

Hewett, D.F., 1956, Geology and mineral resources of the Ivanpah quadrangle, California and Nevada: United States Geological Survey Professional Paper 275, 172 p.

_____ 1955, Structural features of the Mojave Desert region: Geological Society of America Special Paper, v. 62, p. 377-390.

_____ 1954, General geology of the Mojave Desert region, California, *in* Jahns, R.H., ed., Geology of Southern California: California Division of Mines and Geology Bulletin 170, c. 2, p. 5-20.

Hill, M.L. and B.W. Troxel, 1966, Tectonics of Death Valley region, California: Geological Society of America, Bulletin, v. 77, p. 435-438.

Hoeppener, R., E. Kalthoff and P. Scrader, 1969, Zur physikalischen Tektonik: Bruchbildung bei verschiedenen Deformationen im Experiment, Geol. Rundsch., v. 59, p. 179-193.

Honeycutt, T.K., L.L. Malinconico and J.E. Marzolf, 1986, Geophysical study of the Soda-Avawatz fault zone in the Soda Mountains: Evidence for east vergent thrusting: Geological Society of America Abstracts with Programs, Cordilleran Section, v. 18, n. 2, p. 118.

Hooke, R. LeB., 1967, Processes on arid-region alluvial fans: Journal of Geology, v. 75, p. 438-460.

Jahns, R.H. and L.A. Wright, 1960, The Garlock and Death Valley fault zones in the Avawatz Mountains, California (abs): Geological Society of America Bulletin, v. 71, p. 2063.

Jennings, C.W., 1961, Geologic Map of California, Kingman Sheet: California Division of Mines and Geology Map, 1:250,000 scale.

Jennings, C.W., J.L. Burnett and B.W. Troxel, 1962, Geologic Map of California, Trona Sheet: California Division of Mines and Geology Map, 1:250,000 scale.

Kahle, A.B. and A.F.H. Goetz, 1983, Mineralogic information from a new airborne thermal infrared multispectral scanner: Science, v. 222, p. 24-27.

Lensen, G.J., 1958, A method of graben and horst formation: Journal of Geology, v. 66, p. 579-587.

Michael, E.D., 1966, Large lateral displacement on the Garlock fault, California, as measured from offset fault systems: Geological Society of America Bulletin, v. 77, p. 111-114.

Noble, L.F. and L.A. Wright, 1954, Geology of the central and southern Death Valley region, California, *in* Jahns, R.H., ed., Geology of Southern California: California Division of Mines and Geology Bulletin 170, c. 2, p. 143-160.

Palluconi, F. and J. Meeks, 1985, "Thermal infrared multispectral scanner (TIMS): An investigator's guide to TIMS data": Jet Propulsion Laboratory Publication 85-32, Jet Propulsion Laboratory, Pasadena, California.

Plescia, J.B. and T.L. Henyey, 1982, Geophysical character of the proposed eastern extension of the Garlock fault and adjacent areas, eastern California: Geology, v. 10, p. 209-214.

Ritter, J.B., 1985, Late Quaternary piedmont stratigraphy of the Salt Spring Hills area, eastern Mojave Desert, California, *in* Hale, R.G., ed.,

Quaternary lakes of the Eastern Mojave Desert, California, Field Trip Guide: Pacific Cell, Friends of the Pleistocene, p. 101-112.

Schumm, S.A., 1973, Geomorphic thresholds and complex response of drainage systems, *in* Morisawa, M., ed., Fluvial Geomorphology: Publications in Geomorphology, New York State University, Binghamton, New York, p. 299-310.

Segall, P. and D.D. Pollard, 1980, Mechanics of discontinuous faults: Journal of Geophysical Research, v. 85, n. B8, p. 4337-4350.

Sharp, R.V. and M.M. Clark, 1972, Geologic evidence for previous faulting near the 1968 rupture on the Coyote Creek fault: U.S. Geological Survey Professional Paper 787, p. 131-140.

Shipman, H. and J.B. Adams, 1987, Detectability of minerals on desert alluvial fans using reflectance spectra: Journal of Geophysical Research, v. 92, n. B10, p. 10,391-10,402.

Smith, G.I. and K.B. Ketner, 1970, Lateral displacement on the Garlock fault, southeastern California, suggested by offset sections of similar metasedimentary rocks: United States Geological Survey Professional Paper 700-D, p. 1-9.

Smith, G.I., 1962, Large lateral displacement on the Garlock fault, California, as measured from offset dike swarm: American Association of Petroleum Geologists Bulletin, v. 46, p. 85-104.

Spencer, J.E., 1981, Geology and geochronology of the Avawatz Mountains, San Bernardino County, California [Ph.D. dissertation]: Massachusetts Institute of Technology, Cambridge, Massachusetts.

Stewart, J.H., 1967, Possible large right-lateral displacement along fault and shear zones in Death Valley-Las Vegas area, California and Nevada: Geological Society of America Bulletin, v. 78, p. 131-142.

Troxel, B.W., 1968, Possible relationship in faults in the Mojave Desert to the San Andreas fault (abs.), *in* Geologic Problems of San Andreas Fault System Conference: Stanford University Publications in Geological Science, v. 11, p. 181-182.

_____ 1970, Anatomy of a fault zone, southern Death Valley, California: Geological Society of America Abstracts with Programs, Cordilleran Section, v. 2, n. 2, p. 154.

Troxel, B.W., L.A. Wright and R.H. Jans, 1972, Evidence for differential displacement along the Garlock fault zone, California: Geological Society

of America Abstracts with Programs, Cordilleran Section, v. 4, n. 3, p. 250.

Troxel, B.W., R.H. Jans and P.R. Butler, 1979, Quaternary and Tertiary history of offsets along the easternmost segment of the Garlock fault zone: Geological Society of America Abstracts with Programs, Cordilleran Section, v. 11, n. 3, p. 132.

Troxel, B.W. and P.R. Butler, 1979, Tertiary and Quaternary fault history of the intersection of the Garlock and Death Valley fault zones, southern Death Valley, California: unpublished report submitted to U.S. Geological Survey, Menlo Park, California, 29 p.

Weldon, R. and E. Humphreys, 1986, A kinematic model of southern California: Tectonics, v. 5, p. 33-48.

Wells, S.G., L.D. McFadden, J.C. Dohrenwend, T.F. Bullard, B.F. Feilberg, R.L. Ford, J.P. Grimm, J.R. Miller, S.M. Orbock and J.D. Pickle, 1984, Late Quaternary geomorphic history of Soda Mountains piedmont and Silver Lake playa area: Geological Society of America Annual Meeting Guidebook, n. 14, p. 69-87.

Wernicke, B., J.E. Spencer, B.C. Burchfiel and P.L. Guth, 1982, Magnitude of crustal extension in the southern Great Basin: Geology, v. 10, p. 499-502.

Woodcock, N.H. and M. Fischer, 1986, Strike-slip duplexes: Journal of Structural Geology, v. 8, n. 7, p. 725-735.

Wright, L.A. and B.W. Troxel, 1967, Limitations on right-lateral strike-slip displacement, Death Valley and Furnace Creek fault zones, California: Geological Society of America Bulletin, v. 78, p. 933-950.

Wright, L.A., J.K. Otton and B.W. Troxel, 1974, Turtleback surfaces of Death Valley viewed as phenomena of extensional tectonics: Geological Society of America, Geology, v. 2, n. 2, p. 53-54.

Wright, L.A., 1988, Role of strike-slip faulting in the Cenozoic evolution of the Death Valley-Amargosa desert region, California-Nevada: (in press).

PLATES

Plate 1. Thematic Mapper image of alluvial fans along the northern Avawatz Mountains. Decorrelation stretched bands 1, 5 and 7 are displayed as blue, green and red, respectively, using statistical analysis on data selected from areas covered by alluvium. This image displays maximum discrimination between alluvial fan surfaces of different ages and reveals uplifted fanglomerate units within the mountain-front. Westward overlap of recent sedimentation on adjacent fans indicates the direction of the modern depositional slope.

ORIGINAL PAGE
COLOR PHOTOGRAPH

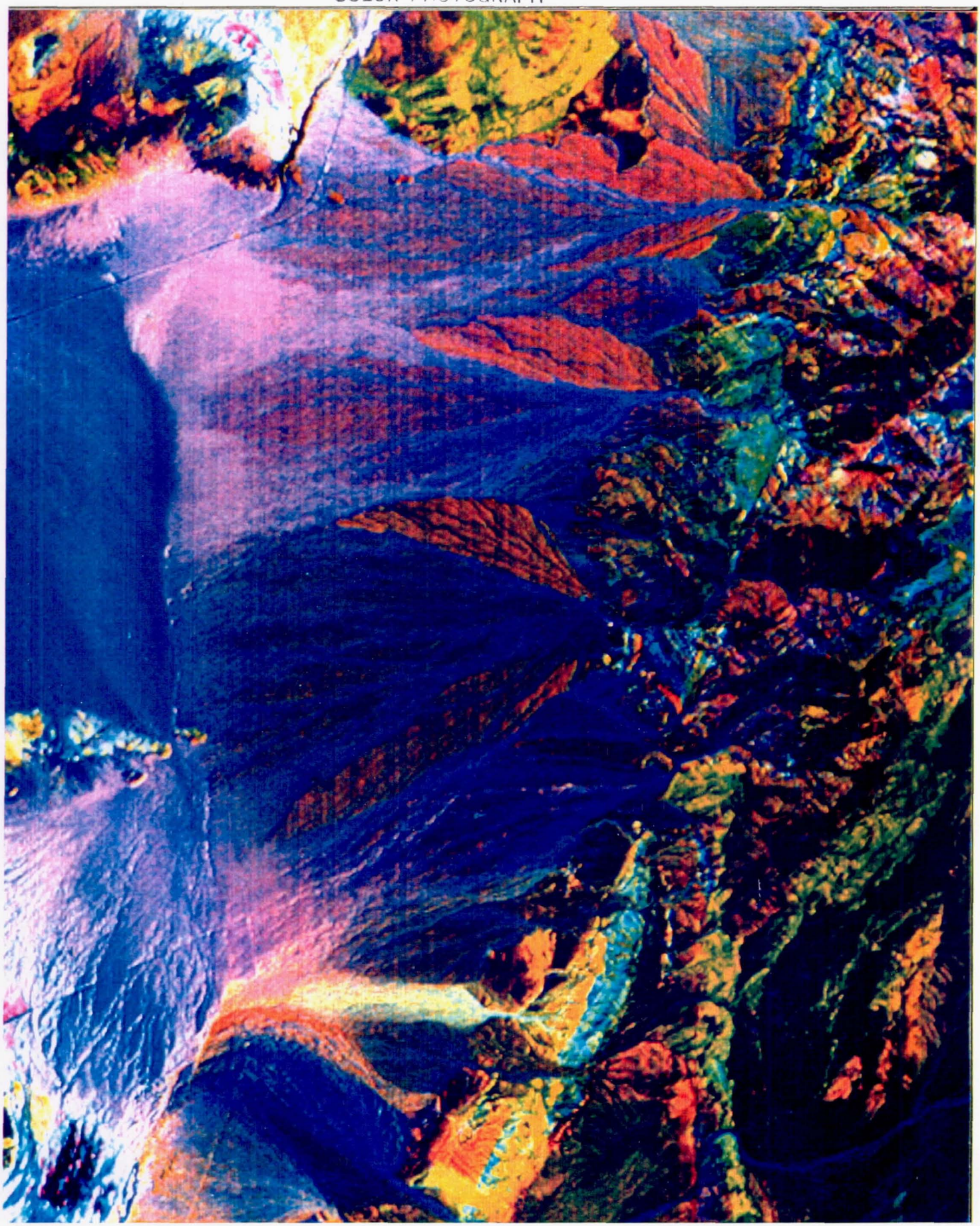

Plates 2. SPOT panchromatic image showing tonal differences of alluvial fan surfaces from Sheep Creek alluvial fan. Arrow points to an exhumed fan surface (Qf3) younger than previously thought.

ORIGINAL PAGE
COLOR PHOTOGRAPH

Plate 3. Thematic Mapper image of the northeast corner of the Avawatz Mountains. The image was processed with a Hue-Saturation-Intensity transformation using bands 1, 4 and 7 displayed as blue, green and red, respectively. Arrows point to arcuate-shaped fault scarp indicating the presence of a low-angle reverse-slip fault dipping southwest beneath the mountain range.

ORIGINAL PAGE
COLOR PHOTOGRAPH

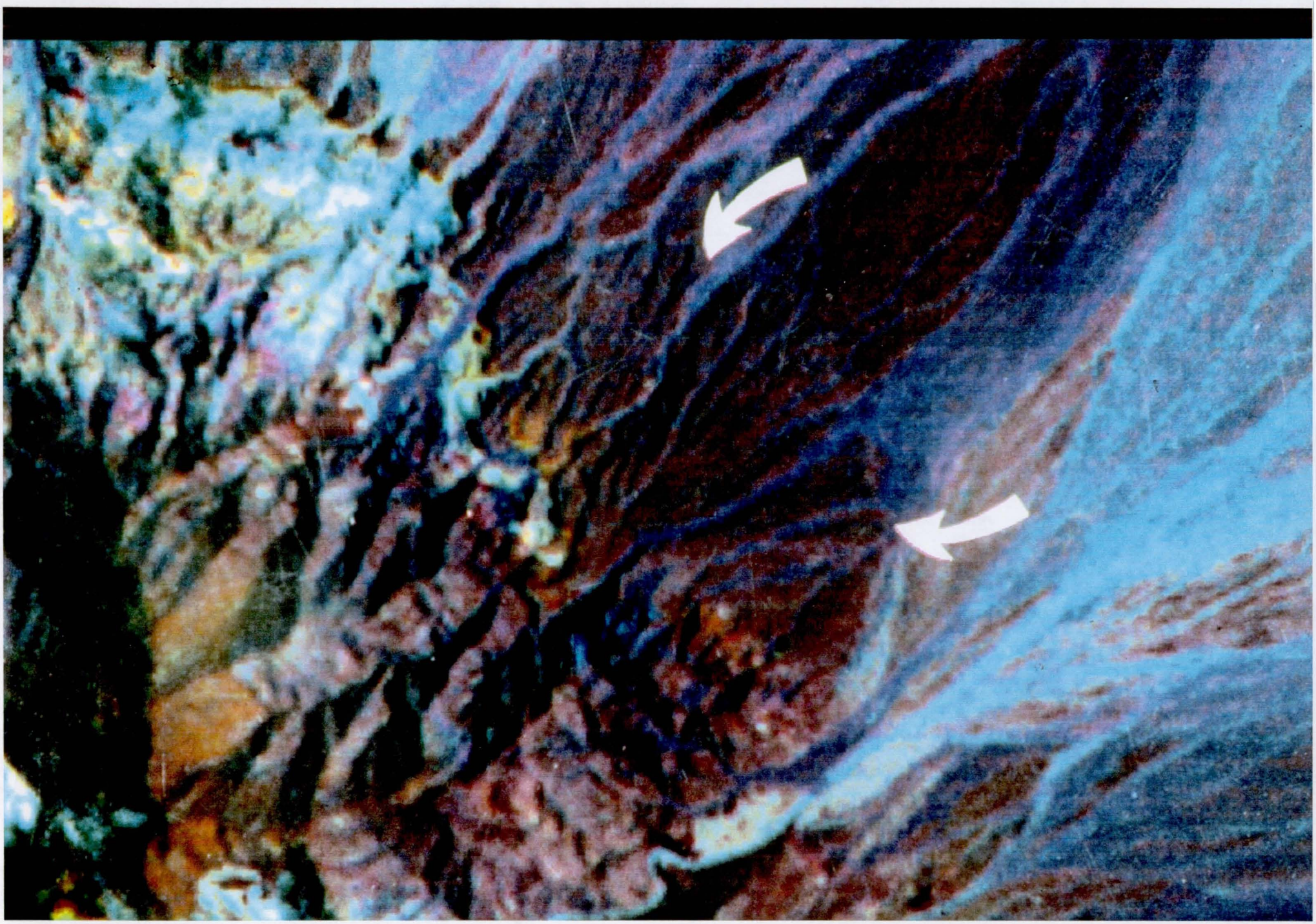

Plate 4. Thematic Mapper decorrelation stretched image of eastern part of Kingston Wash. Bands 4, 5 and 7 are displayed as blue, green and red, respectively.

ORIGINAL PAGE
COLOR PHOTOGRAPH

Plate 5. SPOT panchromatic image of the Soda Mountains area.

ORIGINAL PAGE
COLOR PHOTOGRAPH

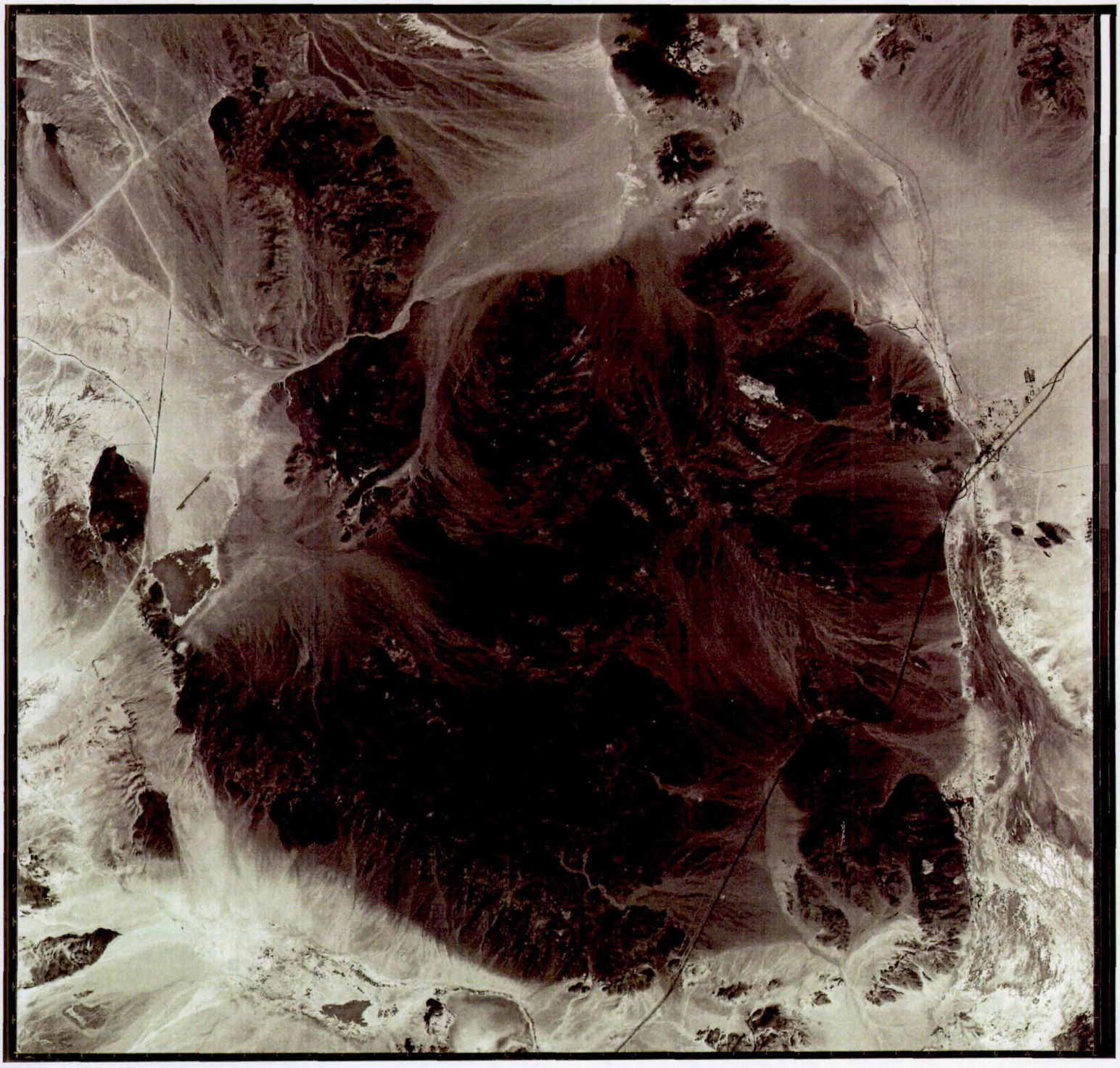

Plate 6. Thematic Mapper image of Soda Mountains area. Decorrelation stretched bands 4, 5 and 7 are displayed as blue, green and red, respectively.

ORIGINAL PAGE
COLOR PHOTOGRAPH

Plate 7. Thematic Mapper decorrelation stretched image of area around Ivanpah Valley. Bands 4, 5 and 7 are displayed as blue, green and red, respectively.

ORIGINAL PAGE
COLOR PHOTOGRAPH

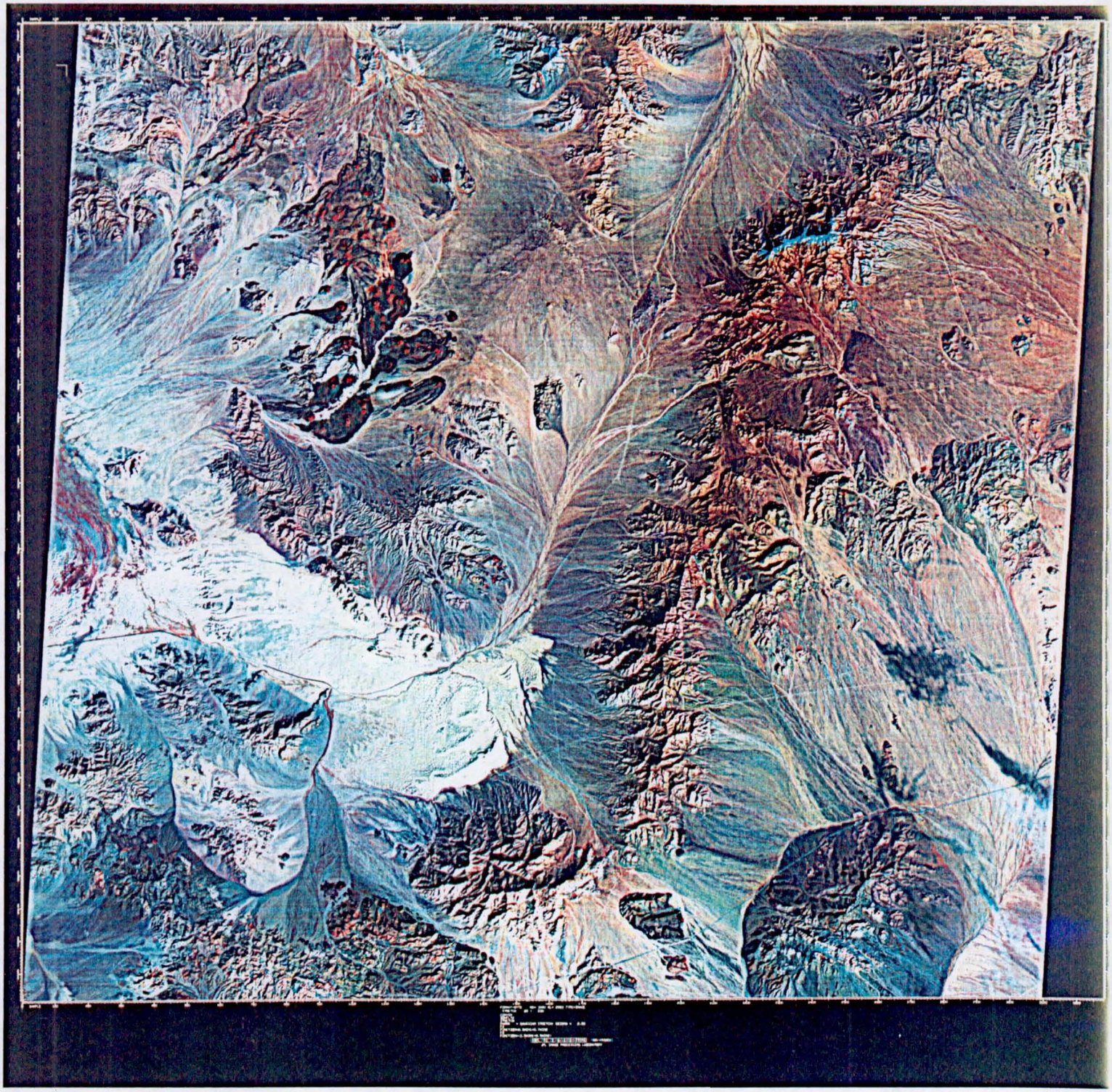

APPENDICES

APPENDIX I. Radiometric ages.

University of Arizona
Isotope Geochemistry Laboratory
Date of Report: March 21, 1988

Project: Death Valley Fault Study
RH Brady/R. Luther
Cal. State Univ. Fresno

Sample Number
UAKA 88-23 Originator's - BM 88-6B

Sample Information
Hornblende, biotite-hornblende vitric tuff
Tuff interbedded within braided fluvial and lacustrine deposits. It lies below two major unconformities and is part of informal "Sandy Wash Formation".

Location Information
Northern Bristol Mountains, San Bernardino County, California
Longitude 35 0' 36" North
Latitude 116 0' 19" East

Analytical Data

% Potassium		Radiogenic Ar pm/g		% Atm. Ar		Reported
Data	Mean	Data	Mean	Data	Mean	Date +/- Err
0.422	0.425	19.38	19.31	16.3	19.2	26.0 +/- 0.6
0.429		19.30		20.3		
0.425		19.38		19.9		
		19.19		20.3		

Sample Number
UAKA 88-24 Originator's - BM 88-13

Sample Information
Groundmass feldspar concentrate, aphanetic, vesicular basalt
Lower part of informal "Sandy Wash Formation" in a disarticulated sedimentary basin cut by NW striking high angle faults. These faults could possibly be southern continuation of the Southern Death Valley fault zone between Mojave and Basin & Range structural provinces.

Location Information
Northern Bristol Mountains, San Bernardino County, California
Longitude 35 0' 12" North
Latitude 116 0' 37" East

Analytical Data

Potassium		Radiogenic Ar pm/g		% Atm. Ar		Reported
Data	Mean	Data	Mean	Data	Mean	Date +/- Err
1.509	1.524	71.34	70.96	28.9	28.9	26.7 +/- 0.6
1.518		70.97		28.9		
1.531		70.60		28.8		
1.536		70.91		28.9		

University of Arizona
Isotope Geochemistry Laboratory

Project:

Date of Report:

Sample Number

UAKA 88-25 Originator's - OHS 87-10

Sample Information

Biotite, vitric tuff
A prominent marker bed in the upper part of the informal owl Hole Spring Formation" that represents the last lacustrine phase prior to coarse clastic infilling of a syntectonic basin along the Garlock Fault.

Location Information

Owlshead Mountains, San Bernardino County, California
Longitude 35 38' 10" North
Latitude 116 41' 22" East

Analytical Data

Potassium		Radiogenic Ar pm/g		% Atm. Ar		Reported
Data	Mean	Data	Mean	Data	Mean	Date +/- Err
6.677	6.676	72.68	73.09	65.1	64.9	6.31 +/- 0.21
6.646		70.77		66.2		
6.704		75.04		64.4		
		74.09		64.8		
		72.89		64.1		

United States Department of the Interior

GEOLOGICAL SURVEY

Geologic Division
Branch of Western Regional Geology
345 Middlefield Road M/S 975
Menlo Park, California 94025

July 8, 1988

Alan Cregan
c/o Roland Brady
Department of Geology
California State University
Fresno, California 93740-0001

Dear Alan:

Charlie Meyer has completed electron-microprobe analyses of one of your samples (SAFZ #6) of the five samples you submitted to us in March this year.

This sample matches best with one of several tephra layers erupted from the Long Valley-Mono Glass Mountain area east of the central Sierra Nevada (Bishop, Glass Mountain D, and Bailey ash beds, ranging in age from about 0.7 to 1.2 Ma). The Bishop ash bed, 0.74 Ma, is probably the best match.

The remaining samples will be done in about two months.

Sincerely,

Andrei

Andrei Sarna-Wojcicki
Geologist

SAMPLE: T163-3 SAFZ-6

PT	BEAM COUNTS	NA COUNTS	9 SD	MG COUNTS	8 SD	AL COUNTS	3 SD	SI COUNTS	7 SD	K COUNTS	2 SD	CA COUNTS	6 SD	TI COUNTS	5 SD	MN COUNTS	1 SD	FE COUNTS	4 SD
1	25599	1613	40	171	13	1371	37	25464	160	8064	90	966	31	32	6	79	9	417	20
2	25701	1622	7	147	17	1352	13	25197	189	8284	155	987	15	25	5	85	4	409	6
3	25679	1678	35	168	13	1377	13	25188	157	8124	114	1033	34	30	4	77	4	417	5
4	25667	1603	33	176	13	1303	34	24898	231	8103	97	1040	36	30	3	57	12	482	34
5	25655	1467	78	174	11	1346	29	25182	200	8284	104	953	39	29	3	78	11	395	34
6	25641	1600	70	172	10	1366	27	25032	190	8503	164	993	35	35	3	71	10	413	30
7	25630	1616	64	185	11	1300	32	24784	224	7725	242	979	33	24	4	84	10	369	34
8	25622	1564	61	182	11	1375	31	25513	252	8286	229	1024	32	29	4	68	9	402	32
9	25617	1583	57	175	11	1320	31	25416	251	8487	239	953	33	41	5	78	9	402	30
10	25612	1575	54	171	10	1397	33	25545	263	8783	289	993	32	28	5	59	10	390	29
11	25612	1567	52	157	11	1374	32	25114	251	8355	276	1047	34	30	5	91	11	449	30
12	25607	1588	50	181	11	1349	31	25004	247	8320	263	966	34	28	5	69	10	419	29
13	25607	1636	49	165	10	1348	30	24912	249	7812	283	945	35	20	5	85	10	409	28
14	25608	1481	56	184	10	1337	29	24996	244	8454	278	1064	39	33	5	74	10	438	27
15	25600	1504	58	193	11	1312	29	24774	256	8006	276	978	38	21	5	67	10	415	26
16	25597	1569	56	161	11	1366	29	25110	247	8122	268	949	38	19	6	65	10	376	27

LINES DELETED: 7 10

AVE. BEAM CURRENT/SEC = 1281

DATA REDUCED USING $B-AL: *GL9M

ON SPECIMEN: T163-3 SAFZ-6

$B-AL VERSION 1.0

OXIDE FORM.	WEIGHT% (OXIDE)	STD.DEV. (%)	HOMO. INDEX	FORMULA	K-RATIO	UNKN PEAK (COUNTS)	UNKN BKGD (COUNTS)	COUNTING TIME(SEC)	STD PEAK (COUNTS)	STD BKGD (COUNTS)	COUNTING TIME(SEC)	STANDARD FILENAME
NA2O	3.707	3.63	1.489	0.000	0.95245	1576.9	31.7	20.00	1653.8	31.5	20.00	%RGSC
MGO	0.032	73.42	0.903	0.000	0.00843	171.8	147.5	20.00	3034.3	147.6	20.00	%RGSC
AL2O3	11.826	3.77	0.660	0.000	0.89992	1349.7	4.4	20.00	1499.5	4.5	20.00	%5831
SIO2	72.832	0.89	1.381	0.000	0.98657	25128.5	66.8	20.00	25470.4	67.5	20.00	%5831
K2O	4.095	1.65	2.194	0.000	1.12302	8229.0	144.9	20.00	7353.8	155.3	20.00	%RGSC
CAO	0.413	4.91	1.302	0.000	0.08111	992.6	255.2	20.00	9369.8	277.8	20.00	%RGSC
TIO2	0.055	63.30	1.123	0.000	0.00050	28.8	18.0	20.00	21460.3	27.8	20.00	%TIO2
MNO	0.039	65.33	1.058	0.000	0.00039	74.9	57.3	20.00	45035.4	111.4	20.00	%MN2O
FEO	0.628	7.13	1.248	0.000	0.09795	417.5	91.1	20.00	3434.3	101.6	20.00	%RGSC

TOTAL 93.628 NO. OXYGENS = 0 NO. ITERS. = 2 AVE. ATOMIC NO. = 10.95

14-MAY-88 17:42:53

Listing of 50 analyses used in the comparison of COMP. NO. 1941 SAMPLE NO. SAFZ-6 T163-3

	C.No	Sample Number	Date	SiO2	Al2O3	Fe2O3	MgO	MnO	CaO	TiO2	Na2O	K2O	Total/R	Sim. Co	
1	1941	SAFZ-6 T163-3	5/14/84	77.73	12.62	0.74	0.03	0.04	0.44	0.06	3.96	4.37	99.99	1.0000	
2	1920	A6741.3 T154-11	2/24/86	77.75	12.57	0.72	0.05	0.06	0.44	0.12	3.92	4.39	100.02	0.9923	Bishop?
3	449	6sW3, T3-7		77.59	12.74	0.74	0.03	0.05	0.45	0.07	3.88	4.44	99.99	0.9884	Bishop
4	1278	PICO-39A (2) BULK T20-5	7/1/85	77.77	12.51	0.75	0.03	0.07	0.45	0.07	3.89	4.47	100.01	0.9859	Bailey
5	1306	R-1-87 T143-6	6/24/87	77.52	12.67	0.75	0.03	0.03	0.45	0.05	3.93	4.56	100.01	0.9841	Bishop?
6	145	J6-239, T43-4		77.40	12.81	0.74	0.03	0.04	0.44	0.06	4.20	4.27	99.99	0.9835	Bishop?
7	274	PICO-39A(2), T20-6		77.47	12.75	0.75	0.03	0.04	0.46	0.05	3.95	4.49	99.99	0.9834	Bailey
8	276	PICO-41A, T6-6		77.38	12.94	0.73	0.03	0.05	0.42	0.04	4.01	4.39	99.99	0.9825	Bailey-like
9	1969	FLV-4-WP T143-7	8/24/87	77.93	12.49	0.74	0.05	0.04	0.44	0.06	3.73	4.53	100.01	0.9823	Bishop?
10	577	LLB-1, T52-6	03/25/83	77.37	12.62	0.74	0.04	0.04	0.43	0.06	4.04	4.65	99.99	0.9821	Pre Bishop
11	1279	BT-6 (2) BULK T20-2	7/1/85	77.75	12.43	0.73	0.03	0.05	0.44	0.05	3.82	4.65	100.00	0.9799	Bishop
12	273	PICO-39A(1), T5-6		77.32	12.99	0.75	0.04	0.05	0.46	0.05	3.90	4.44	100.00	0.9796	
13	100	ELSI-1, T2-9,		77.42	12.85	0.75	0.02	0.03	0.46	0.05	4.10	4.31	99.99	0.9789	
14	254	PICO-143, T36-4		76.45	12.91	0.76	0.04	0.01	0.42	0.06	3.93	4.43	99.01	0.9780	
15	953 D4-06			77.71	12.70	0.73	0.03	0.04	0.42	0.07	3.80	4.50	100.00	0.9775	
16	444	e3CU-26(3), T1, N-3SW-2, P		77.64	12.88	0.74	0.03	0.02	0.46	0.07	3.72	4.43	99.99	0.9766	etc.
17	51	BT-7, T20-1		77.54	12.60	0.76	0.03	0.03	0.45	0.05	3.86	4.66	99.98	0.9767	
18	144	JAMBA-389, T2-12		77.42	12.87	0.74	0.04	0.02	0.47	0.05	4.10	4.28	99.99	0.9763	
19	1926	FLV-1-CS T145-4	6/24/87	77.63	12.72	0.73	0.03	0.04	0.47	0.07	3.80	4.45	99.99	0.9759	
20	279	PICO-73, T39-3		77.29	12.83	0.79	0.03	0.04	0.45	0.06	4.03	4.46	100.00	0.9751	
21	1276	BT-7 (2) BULK T20-1	7/1/85	77.63	12.48	0.74	0.03	0.05	0.42	0.07	3.87	4.71	100.00	0.9745	
22	1280	BT-7 BULK 200SEC LTS T20-1	7/1/85	77.57	12.48	0.73	0.02	0.05	0.43	0.07	3.88	4.76	100.01	0.9741	
23	1923	LTH-DH-15-32.5 T75-10	6/23/84	77.78	12.45	0.74	0.04	0.03	0.43	0.05	3.77	4.71	100.00	0.9738	
24	562	BT-10, T62-10	08/26/83	77.47	12.75	0.73	0.03	0.03	0.43	0.07	3.77	4.72	100.00	0.9713	
25	53	BT-6(2), T20-2		77.48	12.68	0.71	0.03	0.02	0.45	0.06	3.85	4.72	100.00	0.9712	
26	60	BHA-3, T15-10		77.56	12.72	0.76	0.03	0.03	0.47	0.05	3.83	4.56	100.01	0.9709	
27	1394	YUC-1-87 T150-11	11/9/87	77.28	12.91	0.73	0.04	0.05	0.44	0.07	3.74	4.75	100.01	0.9704	
28	441	23-24-10B, T2-15		77.25	12.90	0.76	0.06	0.05	0.48	0.06	3.92	4.51	99.99	0.9702	
29	271	PICO-23, T2-11		77.26	12.87	0.77	0.04	0.05	0.42	0.07	3.89	4.61	100.00	0.9701	
30	563	BT-6, T62-15	08/26/83	77.64	12.67	0.74	0.03	0.03	0.43	0.07	3.86	4.75	100.00	0.9701	
31	1865	JT-0307-1 T150-3	11/9/87	77.34	12.69	0.76	0.03	0.07	0.46	0.06	3.81	4.59	100.01	0.9697	
32	1906	JT-41186-1 T150-4	9/11/87	77.34	12.89	0.76	0.03	0.07	0.46	0.06	3.81	4.59	100.01	0.9697	
33	1604	R-26-Y1 T154-5	11/25/86	77.73	12.52	0.70	0.04	0.04	0.44	0.05	3.75	4.66	100.00	0.9697	
34	346	TL-111, T46-2		77.24	12.85	0.75	0.04	0.01	0.45	0.07	3.81	4.76	100.00	0.9694	
35	1950	FRIANT 9A T74-4	6/22/84	77.42	12.57	0.71	0.03	0.00	0.44	0.07	3.86	4.91	100.01	0.9694	
36	1356	2490850Z T107-2	6/30/85	78.16	12.15	0.76	0.03	0.04	0.44	0.07	3.72	4.63	100.00	0.9690	
37	1827	FLV-2-CS T145-5	6/24/87	77.61	12.81	0.72	0.05	0.09	0.47	0.06	3.73	4.47	100.01	0.9687	
38	1044	Y1473-10C T75-11	6/23/84	77.53	12.50	0.74	0.03	0.07	0.41	0.04	3.89	4.80	100.00	0.9683	
39	1772	In201A T141-14	5/27/87	77.84	12.60	0.72	0.05	0.04	0.43	0.06	3.62	4.62	100.00	0.9679	
40	264	PICO-75(3), T36-7		76.59	12.86	0.72	0.04	0.04	0.42	0.05	4.13	4.15	99.01	0.9679	
41	26	BT-1, T6-13		77.36	12.91	0.80	0.03	0.03	0.43	0.05	3.85	4.57	99.99	0.9671	
42	277	PICO-43, T30-5		76.85	12.90	0.73	0.03	0.03	0.47	0.05	3.93	4.02	99.01	0.9670	
43	268	PICO-74, T30-5		76.55	12.99	0.74	0.03	0.04	0.42	0.07	4.12	4.05	99.01	0.9665	
44	1355	2490850I T107-1	6/30/85	78.06	12.27	0.76	0.04	0.04	0.44	0.07	3.64	4.67	99.99	0.9661	
45	67	BT-14, T15-3		77.53	12.65	0.74	0.03	0.04	0.42	0.06	3.71	4.91	99.99	0.9656	
46	65	D77-2A, T31-6		77.39	12.66	0.73	0.03	0.05	0.45	0.07	3.72	4.89	99.99	0.9650	
47	40	BT-1101, T15-12		77.47	12.75	0.74	0.03	0.04	0.41	0.04	3.76	4.76	100.00	0.9643	
48	1828	FLV-3-CS T145-6	6/24/87	77.66	12.69	0.73	0.05	0.09	0.43	0.05	3.68	4.56	100.01	0.9641	
49	374	T6CU-6, T14-1		77.47	12.84	0.73	0.03	0.04	0.41	0.05	3.76	4.67	100.00	0.9636	
50	452	813051, T35-5		76.52	12.77	0.74	0.04	0.02	0.46	0.07	3.87	4.72	99.01	0.9630	

POWCUS COMP NO. 1942 DATE OF UPDATE: 5/16/86
SAMPLE IDs: DA-3PO-M-1 T163-2
ELEM. IN CALC. Na, Al, Si, K, Ca, Fe

50 BEST MATCHES:

APPENDIX II. Measured sections and clast counts, Owl Hole Spring formation.

APPENDIX 2. Measured sections through Cenozoic strata of the northern Avawatz Mountains.

Table 1. Abbreviations and key to composition diagram used in Figure 2A-D.

ABND- abundant
AGGLOM- agglomerate
AIRFLL- airfall
ALTD- altered
ALUV- alluvial
ANG- angular
APPROX- approximately
ASSEMB- assemblage
BD- bed
BDD- bedded
BDDG- bedding
BDS- beds
BIOT- biotite
BIOTURB- bioturbated
BLDR- boulder
BLDRY- bouldery
BNTH- beneath
BRDD- braided
BRN- brown
BRNG- bearing
BTWN- between
BX- breccia
CALC- calcareous
CAV- cavernous
CBL- cobble
CEL- celestite
CBLY- cobbly
CG- coarse grained
CGL- conglomerate
CHNL- channel
CHNLD- channeled
CHNLS- chanels
CHRT- chert
CHRTY- cherty
CLN- clean
CLST- clast
CLSTC- clastic
CLSTCS- clastics
CLSTS- clasts
CLYEY- clayey
CLYST- claystone
CM- centimeter
CMPLX- complex
CNTCT- contact
COALESD- coalesced
COMN- common
COMNLY- commonly
CRB- carbonate
CRSNS- coarsens
CRUDLY- crudely
CSNG- coarsening
CSNS- coarsens
CTR- center
CYN- canyon
DECRS- decreases
DEFD- deformed
DEPS- deposits
DESSIC- dessication
DIAG- diagenesis
DIAM- diameter
DIAMICT- diamictite
DIFUS- diffused
DISCONT- discontinuous
DK- dark
DNSE- dense
DOM- dominated
DSTL- distal
EFFLOR- effloresence
EQ- equal
ESP- especially
EVAP- evaporite
FG- fine grained
FLDBSN- floodbasin
FLDPLN- floodplain
FLO- flow
FLOS- flows
FLOTNG- floating
FLUCT- fluctuating
FLUV- fluvial
FM- from
FMWK- framework
FNING- fining
FNS- fines
FRMWK- framework
GNS- gneiss
GNUL- granule
GR- grained
GRDD- graded
GRDNG- grading
GRDS- grades
GRN- green
GRY- gray
GYPSIF- gypsiferous
HB- hornblend
HLT- halite
HLTIC- halitic
INCRS- increases
INDSTNCT- indistinct
INTBDD- interbedded
INTBDS- interbeds
INTRVNING- intervening
IRREG- irregular
LAC- lacustrine
LAM- laminated
LAT- laterally
LENSNG- lensing
LIMON- limonite
LMY- limy
LNS- lens
LNSES- lenses
LOWR- lower
LRGST- largest
LS- limestone
LVNDR- lavander
MD- Monzodiorite
MDCRX- mudcracks
MDFLO- mudflow
MED- medium
MEGABX- megabreccia
MG- medium grained
MICAC- micaceous
MIDLE- middle
MIDPRXML- mid-to-proximal
MINR- minor
MIXD- mixed
MNLY- mainly
MNO- Mn oxides
MRGN- margin
MRKER- marker
MROON- maroon
MSTLY- mostly
MMV- Mesozoic metavolcanic
MTX- matrix
OBLIT- obliterated
OBS- obscure
OLYNG- overlying
OM- Owlshead Mts.
OSCL- oscillation
OTCRPS- outcrops
PARALL- parallel
PBL- pebble
PBLS- pebbles
PBLY- pebbly
PLNR- planar
PLYA- playa

Table 1. (Con't.)

PNK- pink
PONDING- ponding
PORUS- porous
PRNTS- prints
PROG- prograding
PRPL- purple
PRT- part
PRTNG- parting
PRTNGS- partings
PRXML- proximal
QTZ- quartz
RCH- rich
RECDNG- receeding
REMOBLZD- remobilized
REWKD- reworked
RK- rock
RKSLIDE- rockslide
RPLMX- ripplemarks
RTCSTS- rootcasts
RWKD- reworked
RX- rocks
SCATTRD- scattered
SCOURD- scoured
SEQ- sequence
SHALO- shallow
SHL- shale
SHPD- shaped
SHRP- sharp
SHTFLD- sheetflood
SHTS- sheets
SIL- siliceous
SLT- silt
SLTIER- siltier
SLTST- siltstone
SLTY- silty
SND- sand
SNDIER- sandier
SNDY- sandy
SORTD- sorted
SPRSE- sparse
SS- sandstone
STND- stained
SUBANG- subangular
SUBRND- subrounded
SUPRTD- supported
THK- thick
THKBDD- thick-bedded
THKNG- thickening
THKNS- thickens
THN- thin
THNING- thinning
THNLY- thinly
THNS- thins
THRUOUT- throughout
TRX- tracks
TUFFAC- tuffaceous
TUFFS- tuffs
TURBS- turbidites
TV- Tertiary volcanic
UNCONF- unconformity
UPPR- upper
UPTO- up to
V- very
VCG- very coarse grained
VERTBRT- vertebrate
VIT- vitreous
VOL- volume
VOLC- volcanic
WHT- white
WKLY- weakly
WX- weathers
XBDS- crossbeds
XLN- crystalline
XTL- crystal
YELO- yellow
ZN- zone
ZNS- zones

Figure 1.
Key to conglomerate clast composition diagrams.

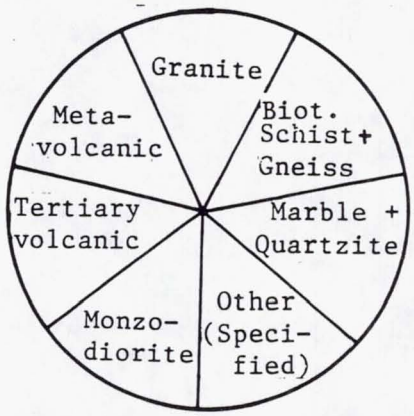

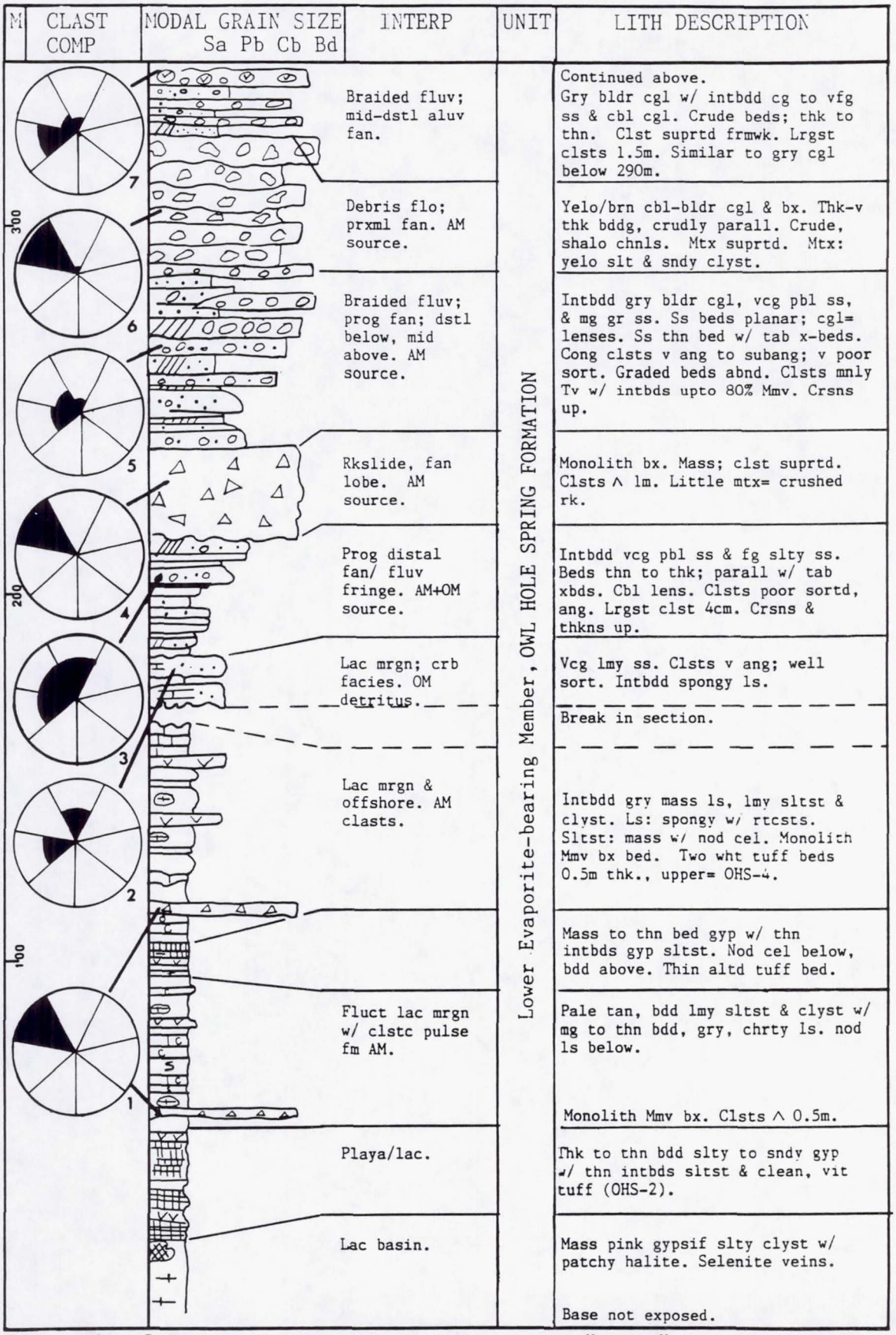

Figure 2A. Columnar section from south side of "wedge", Owl Hole Spring.

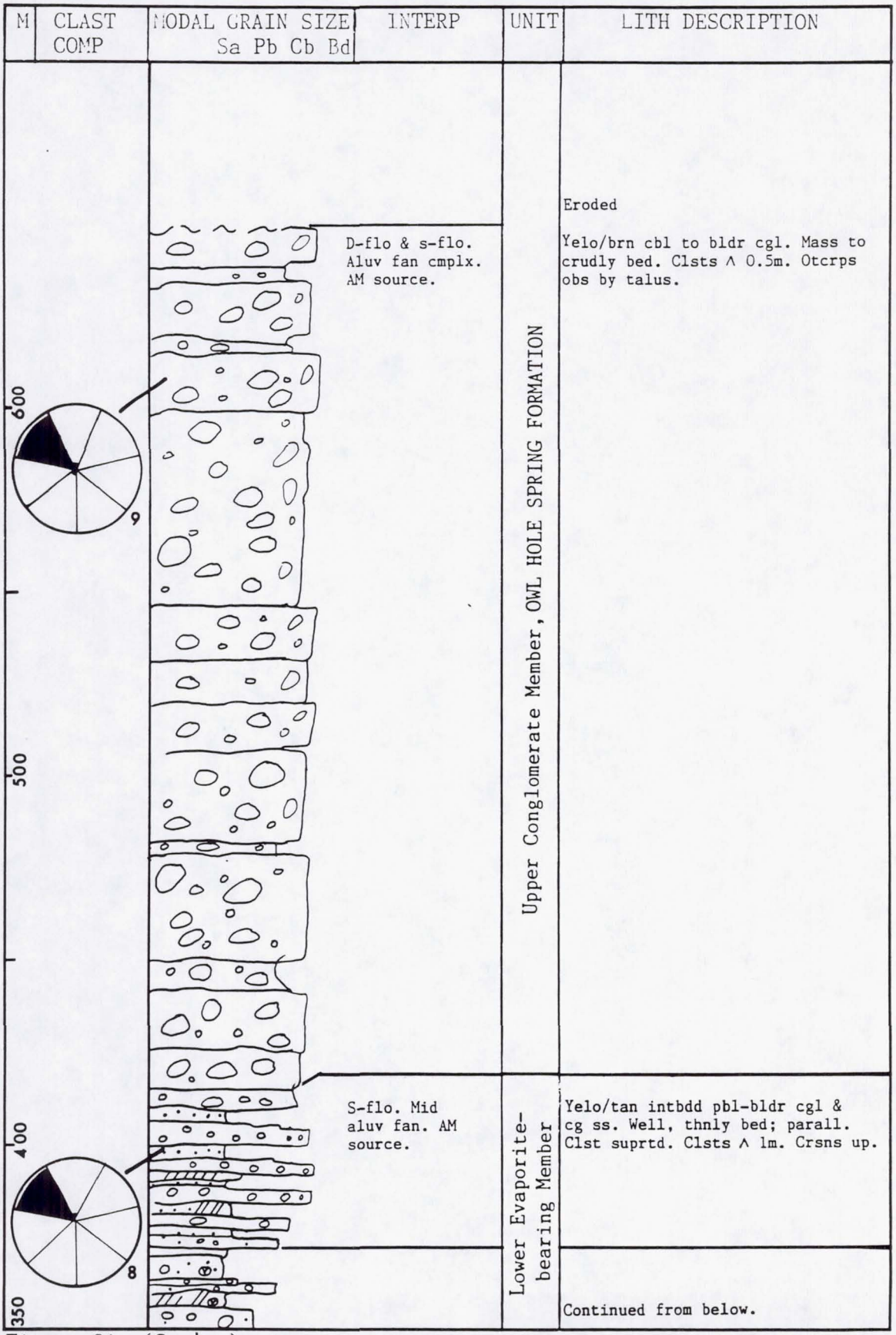

Figure 2A. (Con't.)

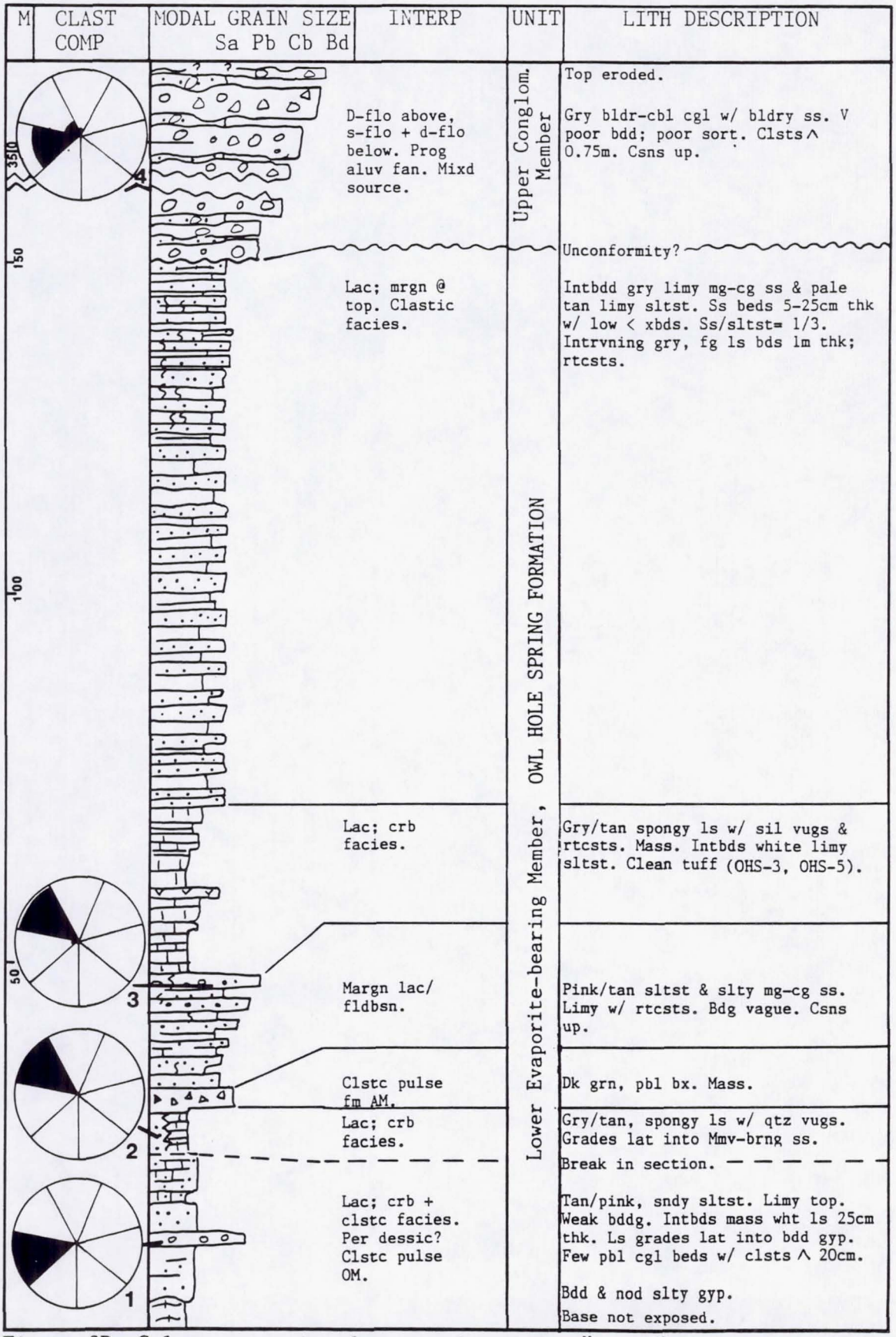

Figure 2B. Columnar section from north side of "wedge", Owl Hole Spring.

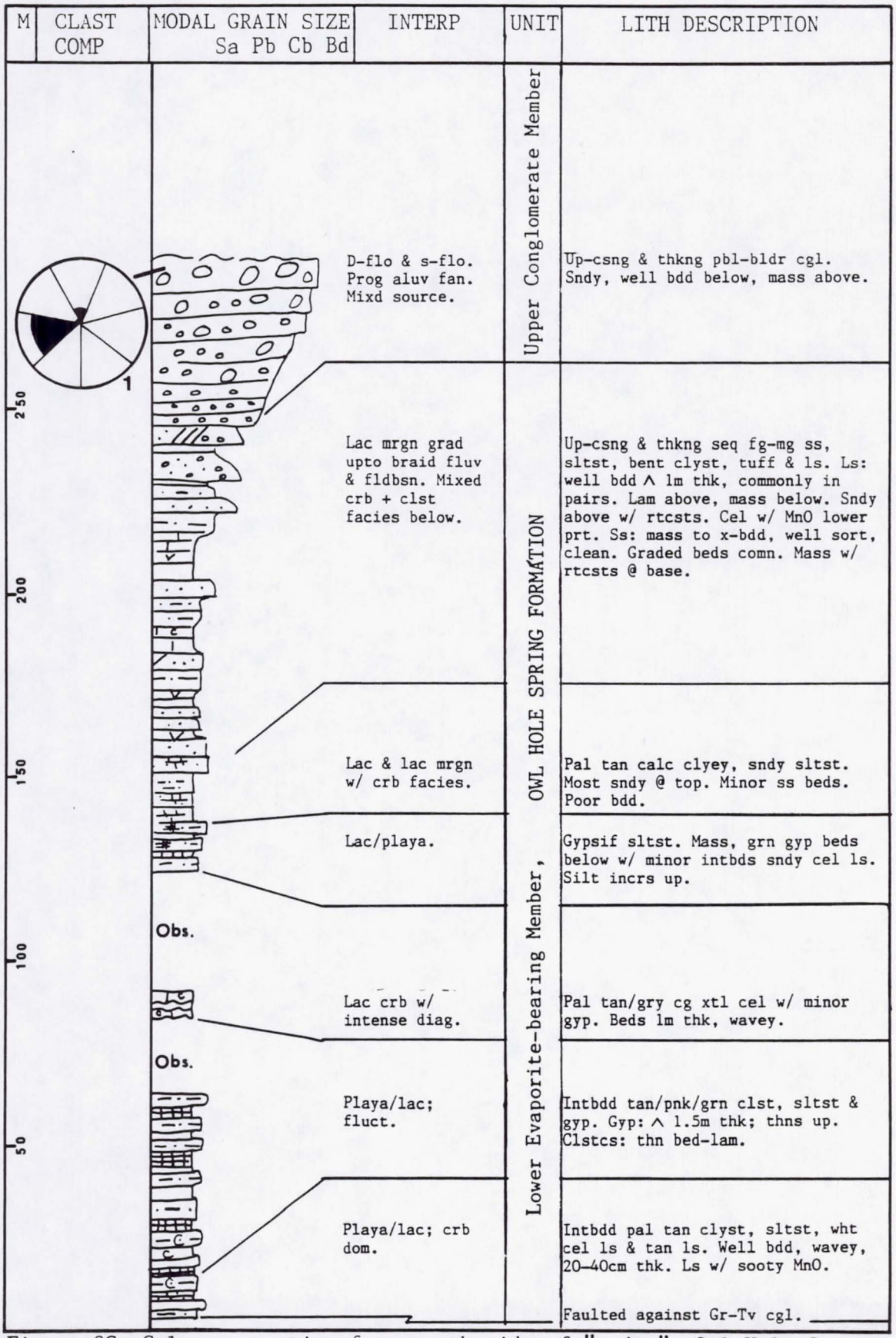

Figure 2C. Columnar section from north side of "wedge", Owl Hole Spring.

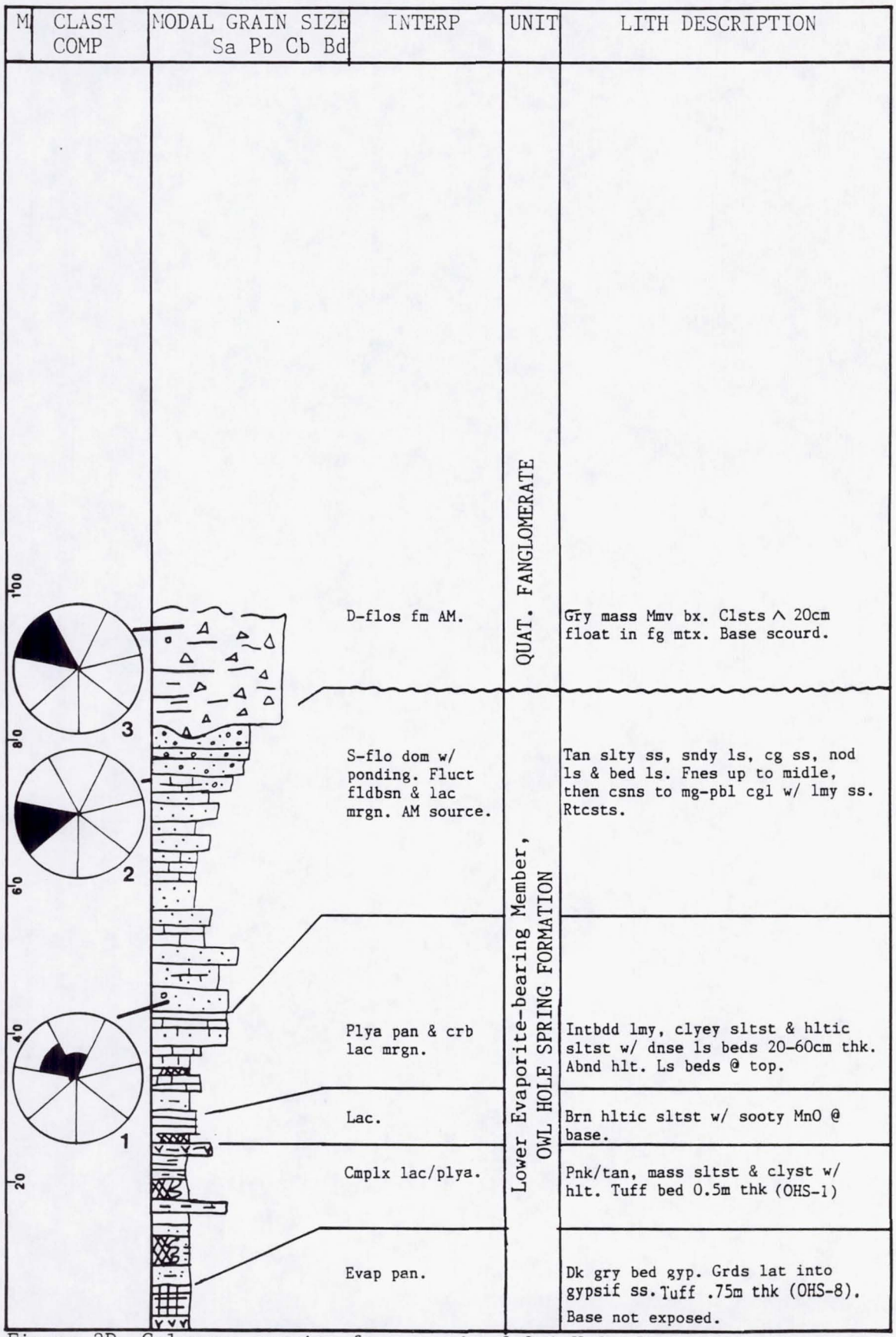

Figure 2D. Columnar section from south of Owl Hole Spring.

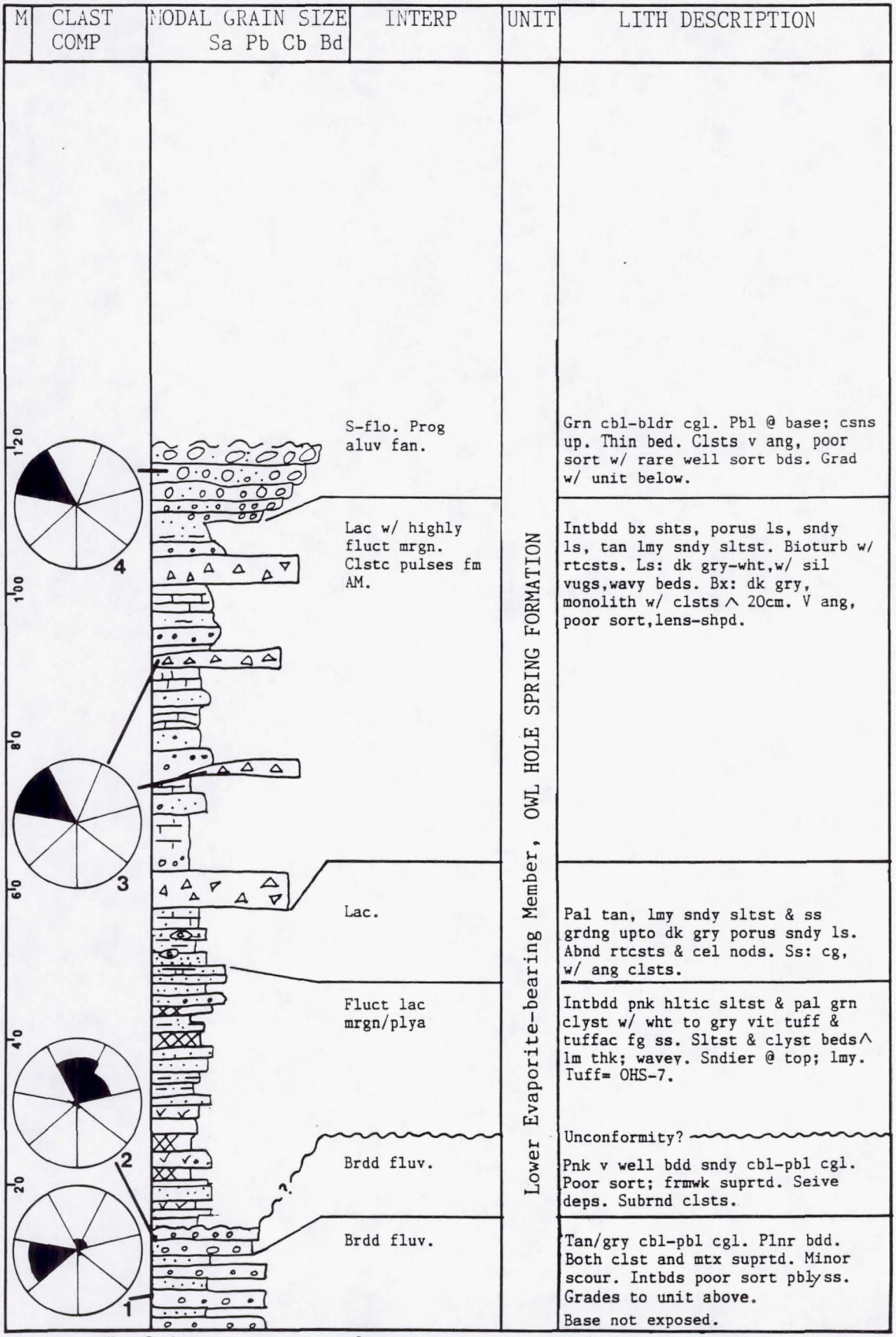

Figure 2E. Columnar section from south side of Owl Lake Road.

APPENDIX III. Gravity study of the Soda-Avawatz fault zone.

GRAVITY PROFILE OF THE SODA-AVAWATZ FAULT ZONE

INTRODUCTION

The purpose of this study is to attempt to determine whether there is geophysical evidence for a continuation of the Soda-Avawatz fault zone from the Soda Mountains to the Avawatz Mountains beneath the intervening alluvial valley. The Avawatz Mountains are separated from the Soda Mountains to the south by a broad, alluvial valley 6 km across (Fig. 1). The Death Valley and Garlock strike slip fault zones meet in the northeastern Avawatz Mountains, and each seems to terminate at this intersection. Structural relations between fault blocks at this intersection are complex and controversial (Davis and Burchfiel, 1973; Plescia and Henyey 1982; Brady, 1986). The Soda-Avawatz fault zone in the Soda Mountains, has variously been considered as a right-lateral fault (Grose, 1959), a down-to-the-west, normal fault (Davis, 1977), and a wrench fault having superimposed east-directed thrusting (Honeycutt *et al.*, 1986). These disputes could be at least in part resolved, if it could be determined whether the Soda-Avawatz fault zone is physically continuous with the faults in the Avawatz Mountains.

This study will test the extent of faults under alluvial cover using four gravity lines oriented perpendicular to the proposed fault continuations. A total of 285 gravity stations have been occupied along four lines at 0.1 mile intervals in order to obtain high resolution gravity data necessary for detecting these faults. The station elevations for Bouger and free air corrections have been measured to within six inches using a laser transit, and the value of the observed gravity was measured using a Texas Instruments Worden gravimeter. The collected data were reduced to the Complete Bouger Anomaly. The location and character of the proposed continuations were determined using two-dimensional computer modelling (Talwani 1959). The Soda Mountains and the Avawatz Mountains have each been mapped in detail (Grose, 1959;

Figure A3-1. Index map showing location of gravity line and Soda-Avawatz fault zone.

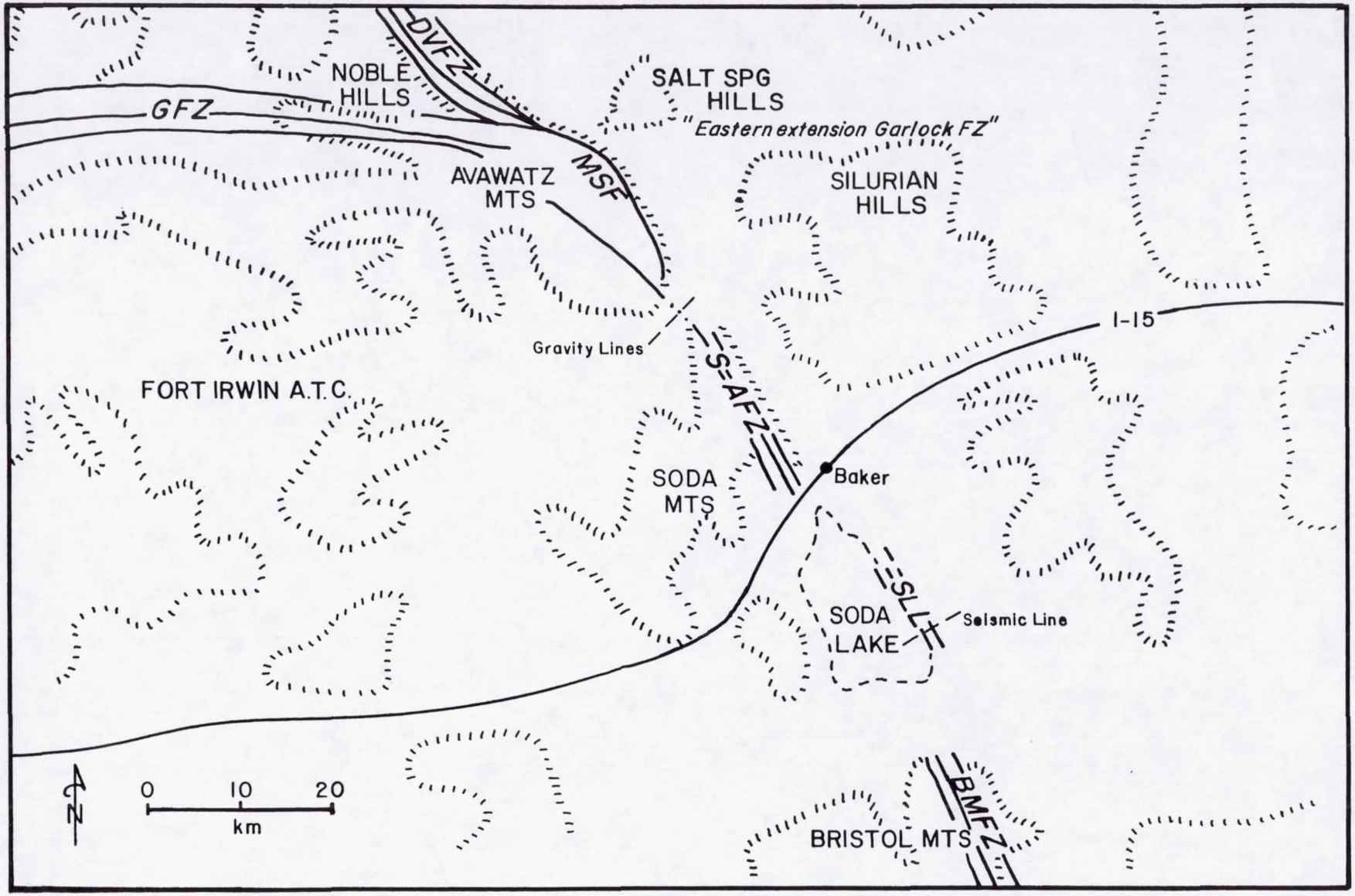
DVFZ
NOBLE HILLS
GFZ
SALT SPG HILLS
"Eastern extension Garlock FZ"
AVAWATZ MTS
MSF
SILURIAN HILLS
I-15
Gravity Lines
S-AFZ
FORT IRWIN A.T.C.
SODA MTS
Baker
SODA LAKE
S-LL
Seismic Line
BMFZ
BRISTOL MTS
N
0
10
20
km

Brady, 1986; Spencer, 1981), providing the structural control necessary for meaningful data interpretation.

RESULTS OF THE GRAVITY STUDY

The Southern Illinois University gravity modelling program on an IBM PC computer was used to analyze the data. Figure 2 shows the observed gravity anomaly for line C plotted as a function of station distance in kilometers. After subtracting the regional background, the anomaly due to the local geology varies from +2.19 milligals to -13.8 milligals. The lower half of the diagram shows the model for the cross sectional geometry of the alluvial basin (alluvium density = 2.2 g/cm^3; bedrock density = 2.67 g/cm^3). The models calculated anomaly is compared with the observed anomaly in the top half of the diagram.

The model in Figure 2 is a simple, tilted-block, assymetrical basin, which is typical of Basin and Range structural style; the theoretical anomaly produced by this geometry is inconsistent with the gravity anomaly observed in the study area. Figure 3 however, shows a model similar to Figure 2, but with significant bedrock relief wherein the theoretical gravity matches the observed gravity profile. The similarity between the theoretical and observed anomalies indicates that there is significant relief of the bedrock beneath the alluvial cover in the study area.

Figure 4 is a block fault model which resembles the cross-section of a typical strike-slip fault zone. The splinters caught between multiple strands of such a fault zone have been faulted up or down as horsts and graben. The southern Death Valley fault zone in the northern Avawatz Mountains contains six, sub-parallel, nearly vertical branches in a 2.5 km wide zone (Brady, 1986); it is possible that the fault has similar character in the study area. The model in Figure 4 indicates that the observed gravity anomaly may be interpreted in terms of a strike-slip fault zone. The structure in this area may consist of a tilted block, assymetrical basin that

Figure A3-2. Gravity model for simple, tilted-block, assymetrical basin. Observed gravity profile (dashed) does not match theoretical curve.

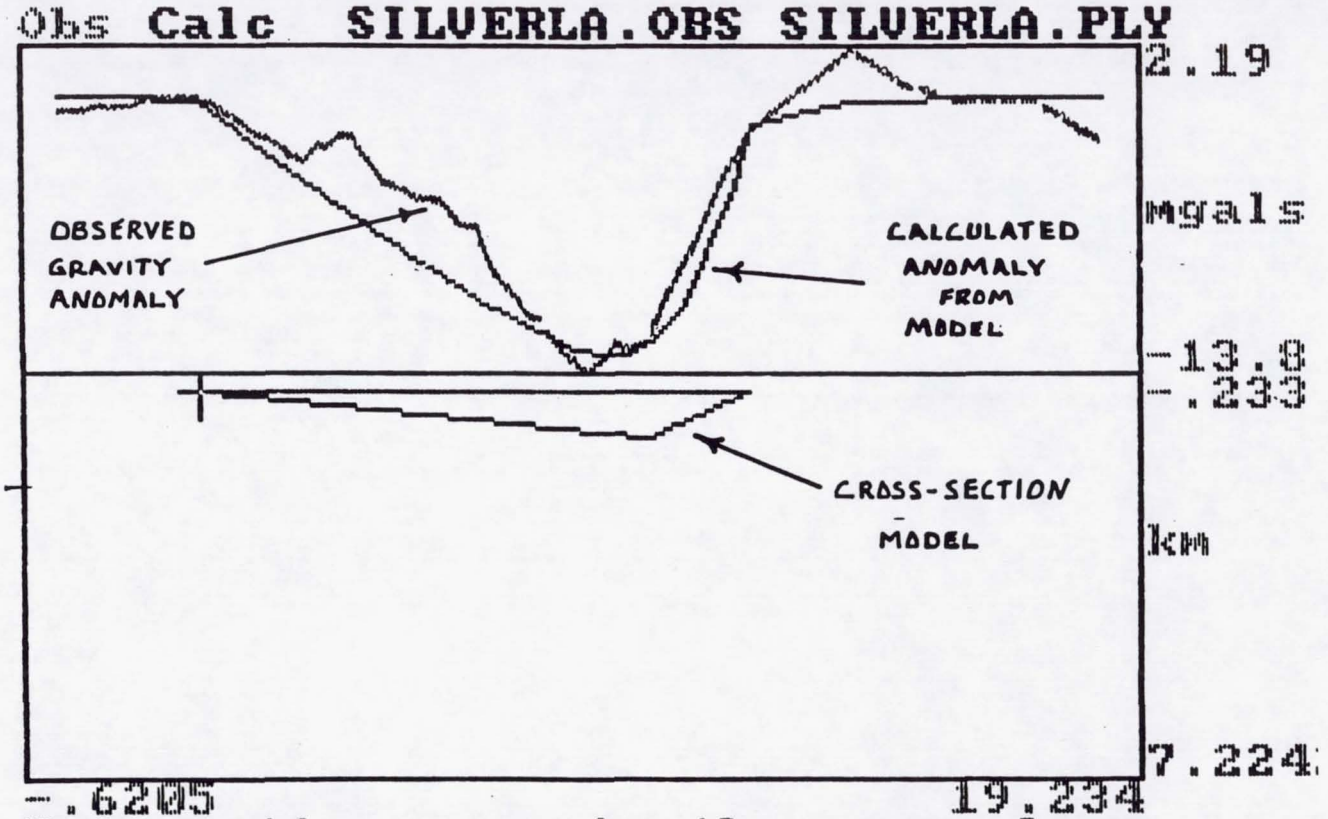

Two vertices are in the same place
Check vertices 1 and 2 in polygon: 1
Ver Exag:1

Figure A3-3. Gravity model for tilted basin having basement relief. Note moderate fit between observed (dashed) and theoretical curves.

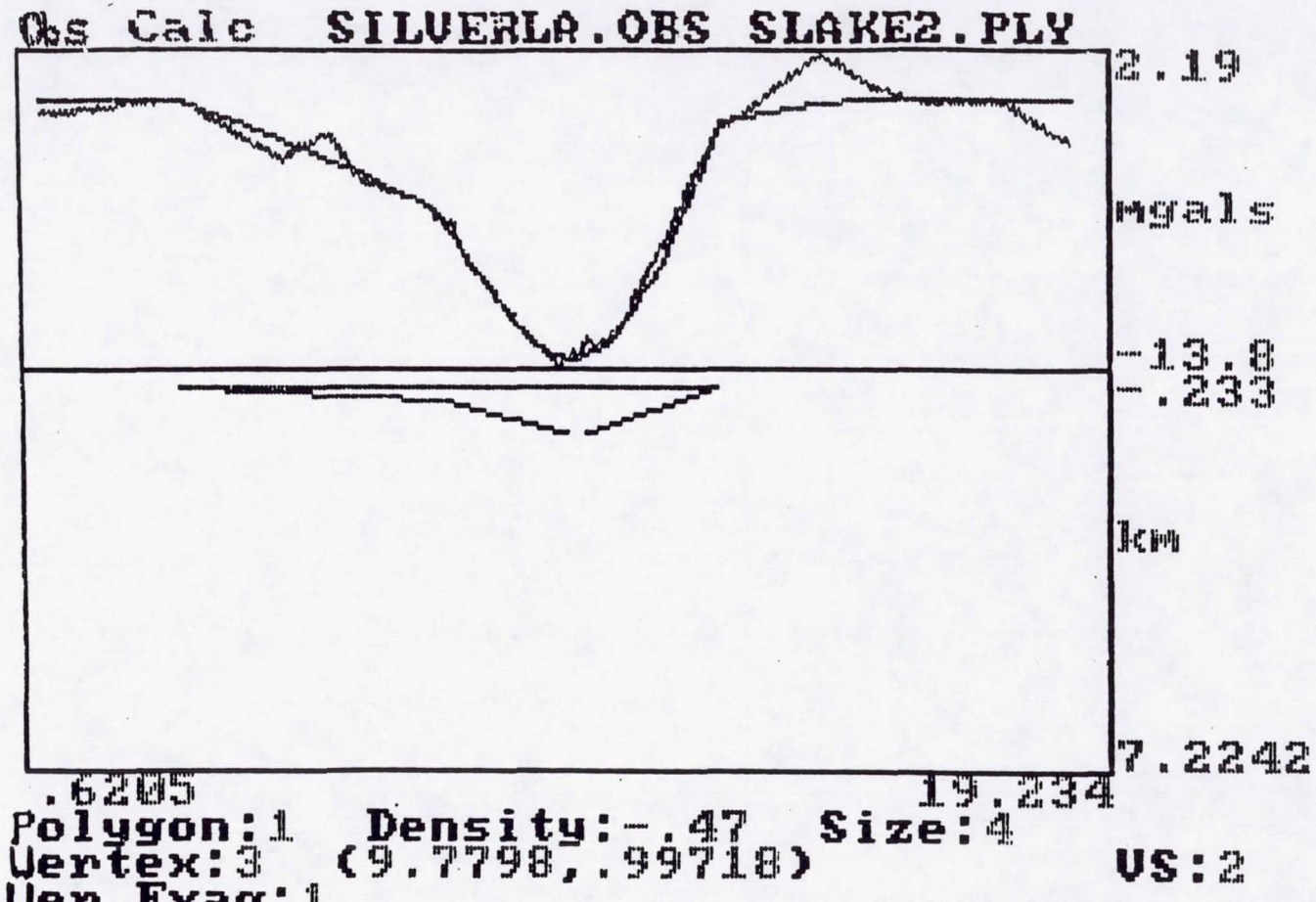

Figure A3-4. Gravity model over basin having irregular subsurface topography typical of strike-slip fault zones. Note fit between observed (dashed) and theoretical curves.

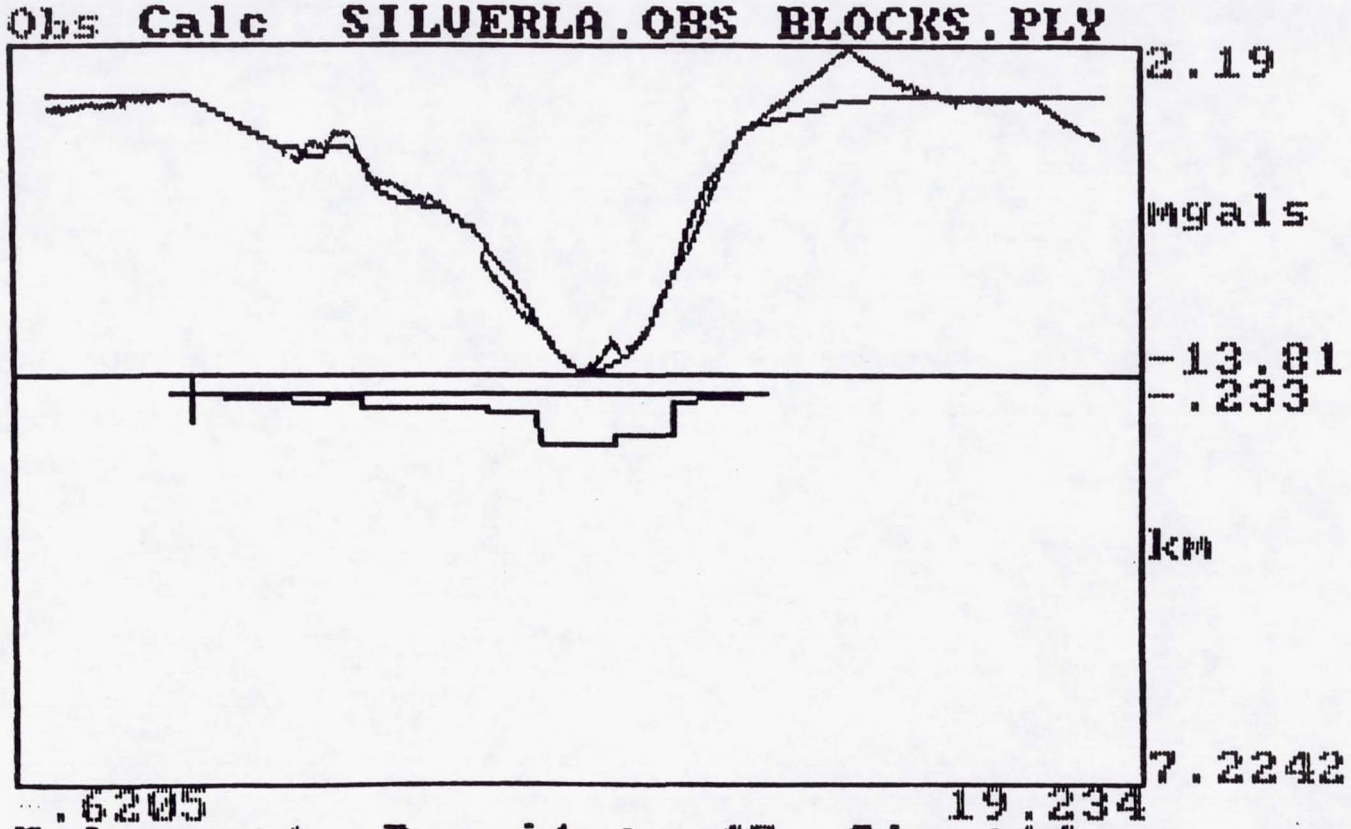

has been overprinted by strike-slip movement on multiple strands, such as by the southern Death Valley fault zone.

CONCLUSIONS

1) The basement beneath the alluvial cover between the Avawatz and Soda Mountains has considerable relief.
2) The genesis of the relief is inconsistent with having been formed by a block tilting such as would be formed by a simple, normal fault.
3) A linear trough exists between the ranges and trends parallel to the Soda-Avawatz fault zone.
4) The irregular basement topography is consistent with having formed by sub-parallel, northwest-striking, lateral faults.
5) The axis of the basement topographic low is 4 km west of the topographic low of the overlying alluvial cover.

APPENDIX IV. Seismic study of the Soda Lake lineaments.

Results of Soda Lake Seismic Refraction Survey, February 1988

Bill Robin
Submitted June, 1988

Abstract

A seismic refraction survey across two north-south trending botanical lineaments, approximately 25 km south of Baker, CA (map 1) reveals lateral velocity changes on the order of 500 m/s corresponding to changes in depth to a shallow refractor. These changes are located approximately 8 meters west of station 14', between stations 59 and 62, and between 8 meters east of station 64 and station 66 (plate 1). Smaller lateral variations in the refractor's velocity which did not correspond to changes in refractor depth were also found.

Introduction:

Between February 26 and 28, 1988, a series of geophysical surveys were performed in order to verify the existence of a postulated N-S trending strike-slip fault zone on the eastern edge of Soda Lake, California. Evidence for the existence of this fault zone was found in aerial photos showing a series of botanical lineaments, and from extrapolation of strike-slip faulting in mountains both north and south of the area.

A seismic refraction survey, in conjunction with gravity and magnetic surveys, was done on an east-west line approximately 25 km south of Baker, California. The seismic line stretched from the foot of the Little Cow Hole mountains approximately 2100 meters to the west onto the playa of Soda Lake. The data collected in the seismic survey was processed using a delay time technique known as the ABC method (Sjogren, 1984).

These surveys were done for Dr. Roland Brady of California State University, Fresno. This paper presents the results of the seismic survey.

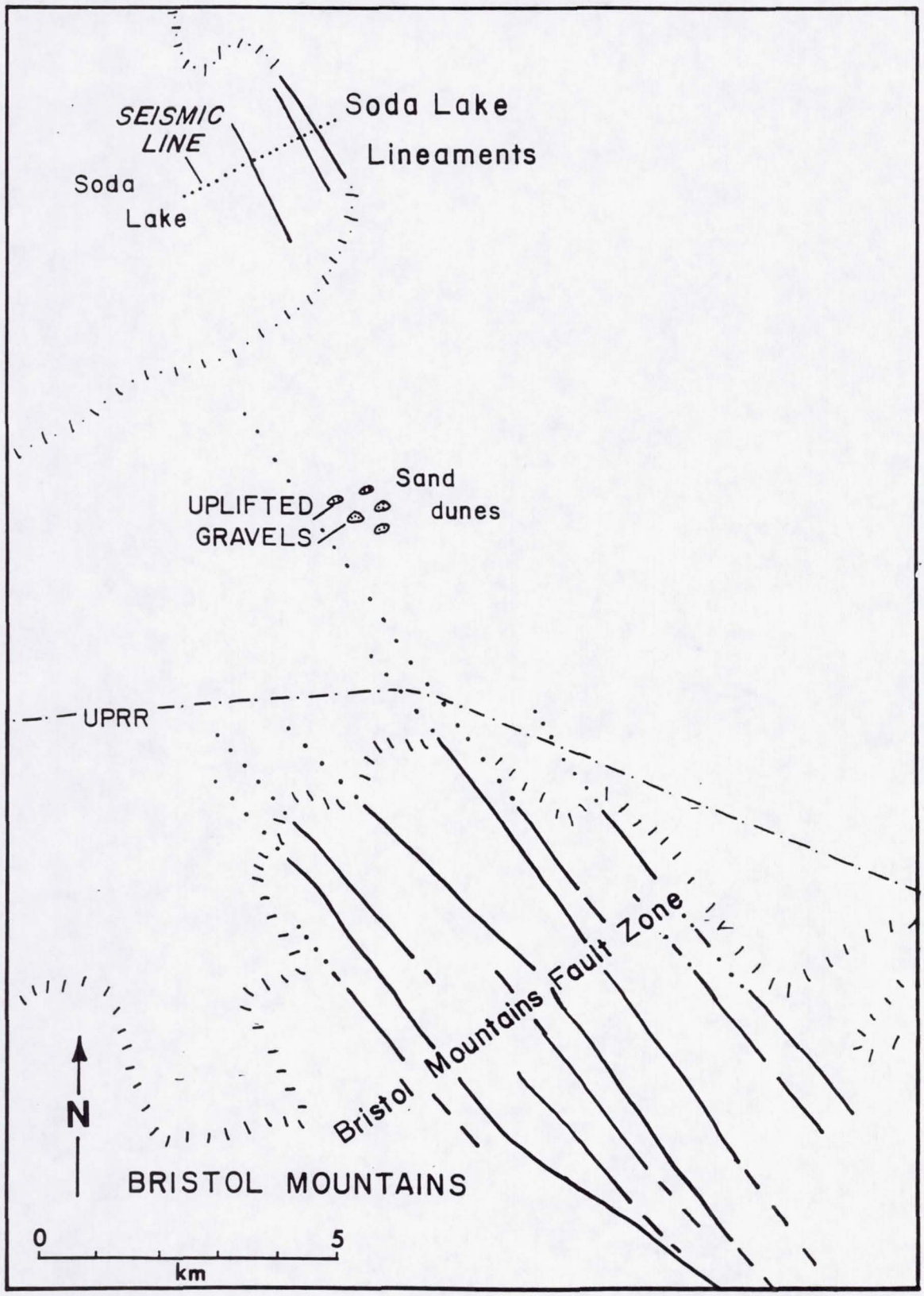

Map 1. Location of seismic refraction survey, Soda Lake lineaments, California.

Instrumentation:

The seismic data was recorded with an E.G.& G. Geometrics ES-1225 12 channel digital seismograph. A Zenith ZFL-181 Laptop computer was used to store the data on 3.5" diskettes, and for later processing of the data. Geospace 8Hz, 20D geophones were used to receive the seismic signals. A single string of 6 geophones was laid out in a star pattern each station on the line (fig. 1). The seismograph was connected to 12 of these stations, 6 on either side, by 2 cables. These 12 stations constituted a recording spread. The string of geophones at each station were connected to the cables at takeouts 100 feet apart. A 12 gauge 'Buffalo Gun' was used as the energy source (Pullan & MacAulay, 1987) (fig. 2). All shot points and geophone stations were located with a theodolite surveying system. Labor was supplied by the Winter, 1988 Advanced Geophysics class at California State University, Bakersfield.

Field Techniques:

The seismic survey was divided into two parts (plate 1). The main part of the survey was 1100 meters long, not including shotpoints located off the ends of the first and last recording spreads. This portion of the survey was located on the eastern boundary of the lake bed so that it would cross one of the botanical lineaments in the area. A 375 meter long 'tail' was shot further to the west, in line with the main portion of the survey. This part of the survey was centered on another botanical lineament on the playa lake

Figure 1 : Star pattern geophone layout

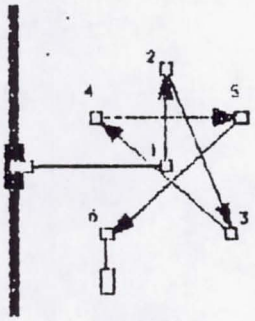

Figure 2: Buffalo Gun modified from Pullan & MacAulay, 1987. Can be assembled from Threaded pipe fittings and bar stock.

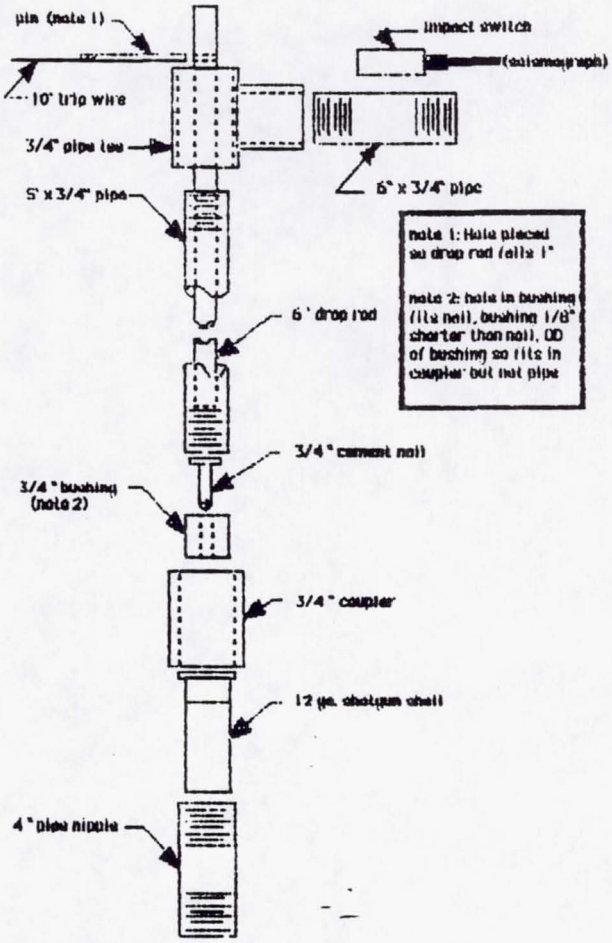

Figure 3 : Layout of two consecutive geophone spreads. Note overlap of one geophone station..

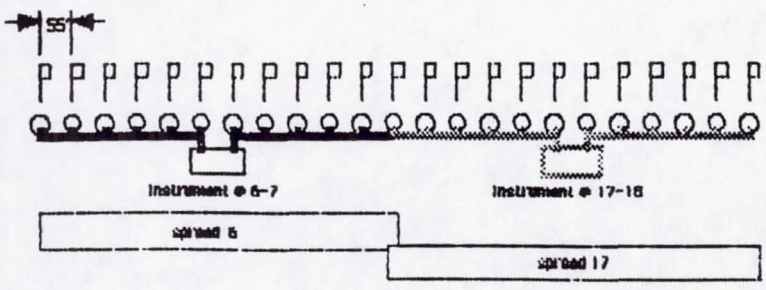

which corresponded to a break in slope of a trend in the gravity data (R. Negrini, personal communication, 1988).

The 'Buffalo Gun' was employed at shotpoints located at regular intervals along the main part of the survey (plate 1). An impact switch attached to the gun triggered the seismograph when the gun was detonated. The length of the cable connecting the seismograph to the impact switch limited the maximum offset possible. The time spent in handling this cable also limited the speed at which the survey could be done.

On the main portion of the seismic survey, the maximum offset was initially 301.83 meters (990 feet). The large signal to noise ratio of the data allowed an increase of the maximum offset to 385.67 meters (1265 feet), the length of the shot cable connecting the impact switch on the energy source to the seismograph.

Geophone stations were placed at 16.77 meter (55 foot) intervals on the main part of the survey. At each of these stations, the geophones were laid out in a star pattern 2 meters across. The last geophone station of each of these spreads was used as the first geophone station of the next recording spread (plate 1, note 1). This was done in order to insure that any errors in timing could be identified when data was recorded on the next spread from the same shotpoint.

In order to maintain the maximum offset distance on the main portion of the survey, the shotpoints used on the first and second recording spreads differed from those used on the

third and fourth spreads, and on the fifth and sixth spreads (plate 1, notes 2, 3, 4). This arrangement led to unnecessary problems during the processing of the data. It is recommended that a consistent set of shot points be used in future surveys.

The 'tail' portion of this survey was located about 400 meters west of the main portion of the survey (plate 1). A station interval of 33.54 meters (110 feet) was used here. Since the connections for the geophones on the cables were 30.5 meters (100 feet) apart, the geophone pattern was expanded to 6 meters across so that this difference in length could be made up. Shotpoints were located 33.54 meters (110 feet) off either end of the single recording spread used (plate 1).

Data Processing & Analysis:

The travel-time curves constructed from the data collected in this survey suggest that one, shallow refracting surface is present. These curves indicate that this refracting surface is irregular and that the thick lake sediments underneath have lateral velocity changes. These travel-time curves did not have shallow sloping segments corresponding to high velocities typical of basement rocks. Only sparse information about the thin weathering layer over this interface could be determined from the data.

In order to accurately locate the lateral velocity changes in the lower layer, a delay-time processing technique was selected. Such techniques allow the calculation of the

depth and velocity of refractors beneath each geophone station. The delay-time method used here is known as the ABC method (Sjogren, 1986). This method requires arrival times from fore- and backshots, originating from the same refracting surface, at each geophone station (fig. 4). The seismic waves from the fore- and backshot originate from two different points on the refractor and converge at the receiving station. These refracting points are separated by a distance dependent upon the depth of the refractor and the velocities of the overburden and refractor. It is assumed that the refractor is dipping less than 20 degrees and that the refracting surface may be approximated by a line connecting the refracting points. It is also assumed that there are no velocity inversions, and that the rocks are reasonably homogeneous. Although the ABC method requires refractors with gentle relief, the same is not required of the surface topography since only a single receiving station is used.

Processing seismic refraction data with the ABC method requires the four steps listed below (plate 1).

1. Complete travel-time curves for arrivals from each refractor are constructed.
2. Velocity analysis curves may be constructed from the travel-time curves. This gives the velocity structure of the subsurface.
3. Time sections for each refractor may also be constructed from the travel-time curves. This gives the amount of time required to travel from the surface to a given refractor.

Figure 4: Raypaths used in the ABC method of processing seismic refraction data. The foreshot is located at P and the backshot at Q. The wave generated at P follows PXAB to the reciever and the wave generated at Q follows QYCB. The reciprocal time is the time it takes a wave to follow PXYQ.
The delay-time is:

$$T = \frac{PXAB + QYCB - PXYQ}{2}$$

This is the time required to travel perpendicularly from a point M on the refractor to the reciever at B.

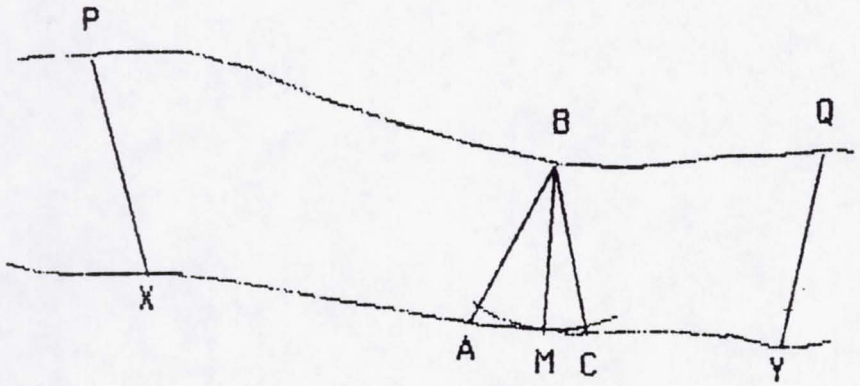

4. A depth section may be constructed from the information contained in the velocity analysis curves and the time sections. This is a cross-section of the seismic expression of the geology

Appendix 1 outlines these tasks in more detail. A discussion of sources of error is discussed in Appendix 2.

Conclusions:

A velocity of 370 m/s was chosen for the overburden on the main portion of this survey. This velocity was based upon a single downhole measurement. Considering the looseness of the soil where the measurement was taken, this is probably a minimum velocity. The velocity of the overburden chosen for the 'tail' of this survey was based upon the slope of the line connecting each shotpoint with its neighboring receiving station. The steepest of these lines gave a velocity of 620 m/s for the overburden. This is the lowest velocity found in this manner on this portion of the survey. It is either a maximum value or the true velocity of the overburden was measured. Since the overburden was more consolidated on the 'tail', this value was taken to be the maximum over the entire area. There is a 40% difference between the maximum and minimum velocities of the overburden, giving rise to an uncertainty in the depth of about 40% (appendix 2).

This survey may be divided into 8 zones which will be discussed in turn. The first seven zones lie on the main portion of the survey, and are numbered from west to east. These zones correspond to the lateral velocity variations

found in the lower layer. The final zone to be considered will be the 'tail'. This discussion was divided in this manner because each zone has different a different character in regards to error (table 1). The sources of these errors is discussed in appendix 2.

The first zone is located at the western end of the main part of the survey. This is the widest zone, extending from station 8 to station 46 (plate 1). The overburden on this interval thins uniformly to station 23 and the error in depth is very small. After this point the refracting surface mimics the surface topography and the error is much larger. Water began appearing in the shot holes around station 36, near the edge of a dried up marsh.

The second zone lies between stations 46 and 52. The refracting surface roughly mimics the surface topography in this zone. Water was found at the bottom of shotholes on this interval.

The third zone lies between station 52 and station 59. The thickness of the overburden here slopes gently to the west. This interval ends with a step of about 1.4 meters. This is supported by perturbations in the time-distance plot and by the behavior of the time section at station 59 (plate 1, notes 5, 6). Although the scatter in the time section is large around this point, the individual curves which were averaged together to construct the final plot are more or less parallel. This implies that the step is real but its actual depth may be different than that computed for

TABLE 1. ERROR BOUNDS OF COMPUTATIONS

ZONE	LOCATION (m) Note 1	ERROR % Ti +, -	V1 m/s	V2 m/s	TOT. ERROR % Note 2	MAX. HI m	MIN. HI
1	1207 to 1843 (+10, -0)	+26.5 -26.0	370	1648 +19, -48	+26.5 -26.0	4.15 +2.69, -2.62	1.36 + .88, -
2	1843 (+10, -0) to 1943	+35.8 -33.9	370	1831 +49, -31	+35.8 -33.9	1.74 + .62, - .59	.91 + .33, -
3	1943 to 2060 (+0, -16)	+45.1 -37.8	370	1757 +6, -7	+45.1 -37.8	2.62 +1.18, - .99	.91 + .41, -
4	2060 (+0, -16) to 2110 (+0, -8)	+51.8 -40.0	370	1442 +75, -89	+51.8 -40.0	3.64 +1.89, -1.46	1.77 + .80, -
5	2110 (+0, -8) to 2152 (+8, -8)	+49.2 -27.9	370	1974 +12, -12	+49.2 -27.9	3.72 +1.83, -1.04	2.79 +1.33, -
6	2152 (+8, -8) to 2177	+33.4 -23.9	370	1442	+33.4 -23.9	3.31 +1.11, - .79	3.18 +1.06, -
7	2177 to 2294	+17.6 -13.7	370	1917 +83, -84	+17.6 -13.7	3.58 + .63, - .49	2.69 + .47, -
8	436 to 805, divide at 596 (+8, -8)	+29.7 -26.6	620 +0, -250	1609 on west, 1778 on east	+29.7 -73.6 on west, -72.6 on east	16.3 +4.84, - 12.0 (on west end)	9.9 +2.94, -7. (on east e

Note 1: Horizontal line distance from the western end (plate 1)

Note 2: The total error is the sum of each individual error

it. Water was found in the shot holes on this interval.

The forth zone is an interval of relatively low velocities between stations 59 and 62. The error in depth here is at a maximum (table 1), but the character of the time section is the same as in zone 3. Water was found in the shot holes on this interval.

The fifth zone extends from station 62 to station 64.5. This zone represents the westernmost edge of rocks with notably higher velocities. This interval begins at the eastern edge of the marsh, and no water was found in the shot holes.

The existence of a narrow sixth zone found between stations 64.5 and 66 is uncertain. Perturbations of the time distance plots support the existence of this zone (plate 1). However, the small scale of this zone relative to the receiving station interval and the lack of correlation with features in the time and depth sections throw some doubt upon its existence. More importantly, of the two overlapping velocity analysis curves in this area, one shows the feature quite clearly while the other doesn't. The error on this interval is moderate (table 1).

The easternmost zone on the main part of the survey is located from stations 66 to 73, the end of the line. The lower layer has a relatively high velocity, similar to that in zone 5. The overburden in this zone begins to thin to the east, consistent with the proximity to the Little Cow Hole mountains. The error on this interval is relatively small

(table 1).

The final zone to be considered is that corresponding to the 'tail' which was shot at the western end of the main portion of the survey (plate 1). This interval extends from stations 19' on the west to 8' on the east. A botanical lineament trending approximately north-south bisects the recording spread (between stations 12' and 13'). A lateral change in velocity was observed to the west of station 14'. This corresponds to the western edge of a rise in both the time and depths sections. The higher velocity in the lower layer corresponds to the shallower, eastern end of the refractor. Due to the sparseness of data collected in this area, error bounds were estimated from that of all data collected in the survey. In addition, the maximum error possible from an incorrect the overburden velocity was included in the error bounds for this interval (table 1).

References:

Dobrin, M.B., 'Introduction to Geophysical Prospecting': 1976, Mc-Graw Hill, 630pp.

Palmer, D., 'The Generalized Reciprocal Method of Seismic Refraction Interpretation': 1980, Society of Exploration Geophysicists, 104pp.

Pullan, S.E., H.A. MacAulay, An In-Hole Shotgun Source for Engineering Seismic Surveys: 1987, Geophysics, V.52, pp.985-996

Sjogren, B., 'Shallow Refraction Seismics': 1984, Chapman and Hall, 268pp.

Appendix 1:

To process seismic refraction data using the ABC delay time method four tasks must be performed. The first of these is to construct complete travel time curves for each refracting surface. Next, velocity analysis curves and time sections are computed and plotted. From the results of the previous tasks, a depth section may be constructed.

The plotted travel-time curves from the raw data help to identify the refractors present. In order to construct a complete travel-time curve for a refractor, arrivals on neighboring curves are shifted in time so that they overlap with equivalent arrivals on the curve of interest (fig. A-1) (plate 1, note 8). This is done for both fore- and backshots. The extent to which this shifting is necessary depends upon the number of refractors present and the spacing of the shot points.

With complete travel-time curves for each refractor, the velocity structure of the subsurface may be determined. The velocity analysis used in this project was the 'Mean-Minus T' method (Sjogren, 1986). Fore- and backshot arrivals for a given refractor at each recording station are used to construct a velocity curve (eqn. 1).

$$1. \quad Tv = \frac{Tf - Tb}{2}$$

Each point is plotted and connected to the next. Inspection of the completed plot will reveal line segment(s) whose inverse slope is the apparent velocity of the refractor.

Figure A-1. Arrival times of seismic waves from different shots at a reciever differ by a constant (ΔT) related to the refractor velocities and the difference in the distances the wave has travelled. This difference may be expressed as:

$$\Delta T = (AB-CX)/V1 + (BX)/V2$$

After the waves have passed X they travel the same path and so, take the same amount of time. Seismic arrivals from different shots and the same refractor at the same array of geophones differ by this constant, ΔT. In order to construct a complete travel time curve of arrivals from a given refractor, it is necessary to add or subtract ΔT from arrival times from neighboring shots. In this report, this process is called shifting.

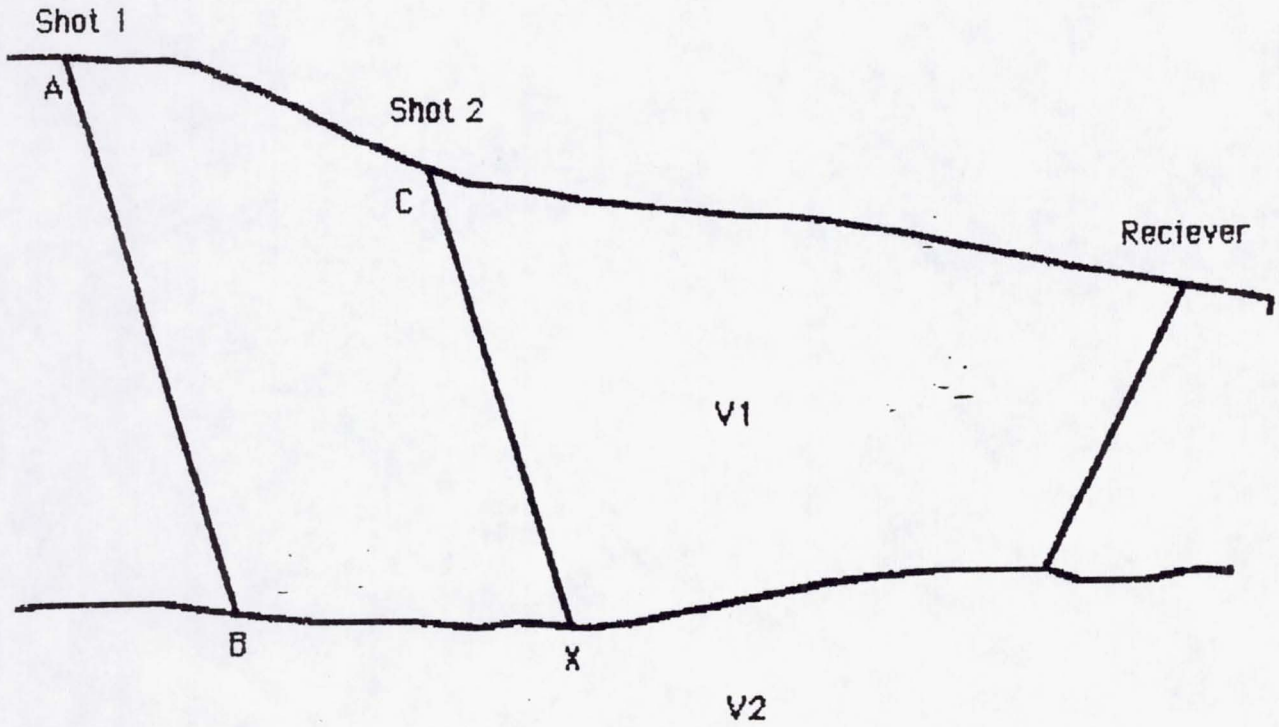

Best fit lines are not used to find the velocities since subtle lateral velocity changes may go unnoticed. The lateral velocity changes are located by the breaks in slope of the velocity analysis function. In order to compute the true velocity of a refractor, the dip must be known. For refractors dipping less than 20 degrees, the error between computed and true velocity is less than 5%.

Time sections are constructed in the same way as velocity analysis curves. The same fore- and backshots are used, but instead of finding the difference between arrival times, they are added and the reciprocal time is subtracted from the sum, giving the two-way delay-time (eqn. 2).

2. $Ti = Tf + Tb - Tr$

These delay-times are then plotted for each geophone location. This plot is a distorted profile of the refractor.

The travel-time curves which provide the data used to construct the velocity analysis curves and the time sections should overlap to some extent. In this way, differences in velocities and delay-times for a given point may be averaged and error bounds determined.

Before a depth section can be computed, a velocity for the thin overburden must be selected. In order to find this velocity, different, more empirical methods may be employed. The most accurate technique is to record the arrival at the surface of a deeply buried shot. This was done at one shot point in the center of the main portion of this survey. This velocity was used for the overburden on the main portion of

the survey. However, data was not usually recorded on the channel at the shot point for the sake of record clarity. This technique may still be used if deeply buried shots are not avalible. By moving successive shots laterally from a recording station, similar computations may be made. The recording stations used should be as close to a point as possible in order to obtain sharp, accurate readings. A single geophone rather than a string of geophones is ideal.

The maximum velocity of the weathering layer may be approximated by connecting the shot point to neighboring recieving stations in the travel-time curves. The steepest slope is the lowest velocity. This gives a maximum value for the overburden velocity, unless the actual value was measured.

It was assumed that the weathering layer over the length of this survey was more or less homogeneous and there were no sudden, large lateral variations in its velocity. Such lateral changes will result in errors in the computed depth of the refractor (appendix 2). However, the lateral velocity changes in the lower layer and any correlation with its depth are of interest here. If the above assumption is true, an inaccurate choice of surface layer velocities will only result in a constant error in the depth of the refractor, not in a change in the refractor's shape.

Finally, the depth section may be constructed. Using the appropriate velocities for the overburden and the refracting layer and the delay times computed for each point,

the depth perpendicular to the refractor may be computed (eqn. 3).

$$3. \quad Hi = \frac{Ti*V1*V2}{2*(V2**2 - V1**2)**1/2}$$

Although the dip of the refractor is unknown, the computed depth may be plotted as a loci of points (a portion of a circle with a radius Hi). After plotting several points in this manner, the dip of the refractor may be measured. If more accuracy is desired, this dip may be used to recompute the refractor velocities. Then a new depth section may be plotted.

Appendix 2:

The resolution of a seismic survey is ultimately limited by by the physical processes of sound waves traveling through real earth materials. The resolution is degraded further by experimental errors. These errors include uncertainties in the measurement of arrival times and velocities, and uncertainties in the horizontal location of anomalies. The sources of these errors will be discussed here.

The accuracy to which subsurface features could be located horizontally in this study was limited in two ways. The most obvious of these was due to the separation between the recieving stations. A lithologic boundry occuring between two stations could only be located to within a few meters (table 1). Another limitation was imposed by the method used to process the data and the critical angle of refraction (eqn. 4). This is the vertical angle from the

$$4. \quad Ic = \sin^{-1}\left(\frac{V1}{V2}\right)$$

refractor and the surface. The reciever and the two refracting points from the fore- and backshots form an isoceles triangle. The base of this triangle defines the limit of horizontal resolution (fig. 4). Features smaller than the length of the base of this triangle (eqn. 5) will

$$5. \quad d = 2*Hi*\tan(Ic)$$

not be detected no matter what the geophone station interval is.

Errors in the depths computed in a seismic refraction survey may be attributed to uncertainties in the delay-times and velocities of the refractors present. Since this study involved two layers, two velocities and one set of delay times will be considered. By taking the derivative of the expression for the depth (eqn. 3) with respect to each of these independant variables, we find that the percent error in depth (Hi) is proportional to the percent error in each of the independant variables.

The percentage of change in the delay-time (Ti) results in the same percentage of change in the computed depth to the refractor (Hi) (eqn. 6). In this study there were two

$$6. \quad \frac{dHi}{Hi} = \frac{dTi}{Ti}$$

sources of error in the delay-time. The most important of these stemmed from differences in the depths of successive shots at a given shotpoint. A minor error was introduced by

the rate at which the data was sampled by the seismograph.

Each time the buffalo gun was detonated, the hole in which it was buried grew deeper. Although one shot was usually sufficent for recording on a given spread of geophones, the same shotpoint was used for recording on up to three other spreads. A change of a foot in shot depth introduced a change of about 1 ms in the arrival time recorded at the same receiver. This resulted in "seam faulting" (plate 1, note 1), scatter in velocity analysis curves (plate 1, note 7), and parallel delay time curves in the time section (plate 1, note 6). These timing errors may be removed by adjusting the shotpoints to some common datum (Dobrin, 1976). Static corrections of this sort require knowledge of the overburden velocities. In order to reduce the number of computations, this error was delt with by using the simple average of overlapping values.

A small error in the delay-time was introduced by the rate at which the incoming data was sampled. For the seismograph used, this rate is related to the length of the seismic record for a shot. The shot record is sampled 1000 times regardless of the record length. The record length used in this survey was 500 ms, so the data was sampled every .5 ms. This sample rate may be decreased to a minimum of .1 ms by shortening the record length to 100 ms.

Errors in the selection of velocities may also lead to errors in the computed depth of the refracting layer. The largest error of this type is that associated with an

incorrect selection of the overburden velocity. Assuming that the velocity of the refractor is much larger than that of the overburden, the percent error in depth will approch that in the overburden velocity (eqn. 7). Using the same

$$7. \quad \frac{dHi}{Hi} = \frac{dV1}{V1}\left[\,1 + \frac{V1^{**}2}{V2^{**}2 - V1^{**}2}\,\right]$$

assumption, any error in the velocity of the refractor results in a negligible percentage of error in the depth of the refractor (eqn. 8).

$$8. \quad \frac{dHi}{Hi} = \frac{dV2}{V2}\left[\,1 - \frac{V2^{**}2}{V2^{**}2 - V1^{**}2}\,\right]$$

Glossary:

Delay-Time: The amount of time required for a seismic wave to travel perpendicularly from a refractor to a reciever at the surface. Twice this quantity is approximated by equation 2.

Geophone String: In this survey, six geophones were connected in series, forming a string of geophones. This increases the amplitude (gain) of the signal recieved well over that of an individual geophone.

Offset: This refers to the distance between a shot point and the geophones which record the shot. The maximum offset is largest distance from a shot to the recording station furthest away. The maximum offset used in this survey was 1265 feet. The maximum depth attainable in a refraction survey is usually between 1/3 and 1/4 of this distance.

Reciprocal Time: The time it takes a seismic wave to travel from a shot at point A to a reciever at point B, and for it to travel from a shot at B to a reciever at A. These times should be the same.

Recording Spread: An array of geophone stations connected to the seismograph by an electrical cable. Each of these stations consists of some pattern of geophones which provide data to a single recording channel of the seismograph. The seismograph used in this study was capable of recording on 12 channels, so a recording spread of 12 stations was used.

Shotpoint: The location at which the energy source is detonated and the seismic wave generated. A foreshot is located on one side of a recording spread, a backshot on the other side; chioce of which side is which is arbitrary.

APPENDIX V. Measured sections through Tertiary strata, northern Bristol Mountains (see Figure in text for locations).

Composite Section at Loc. 6

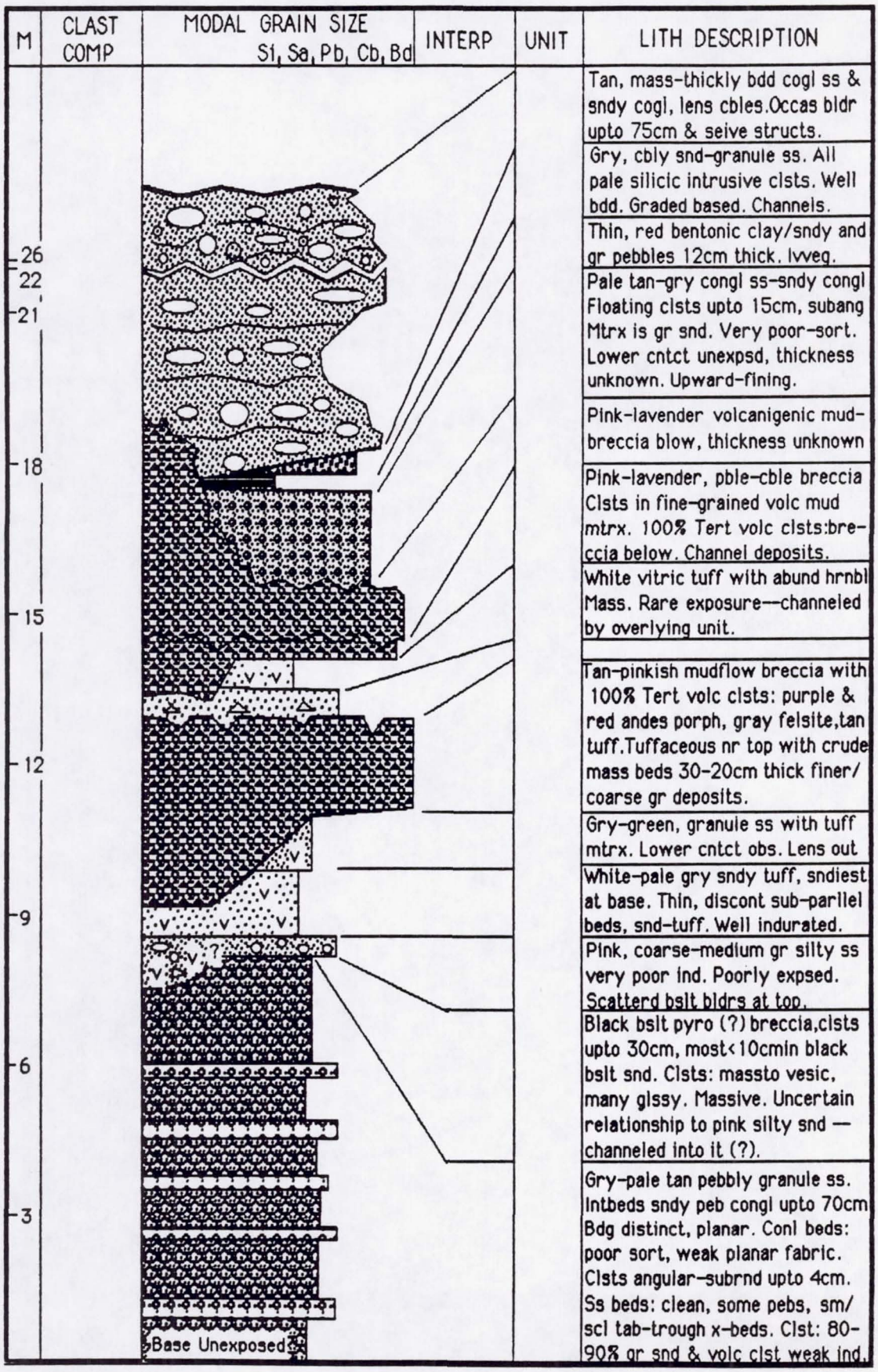

Sequences Exposed at Loc. 18

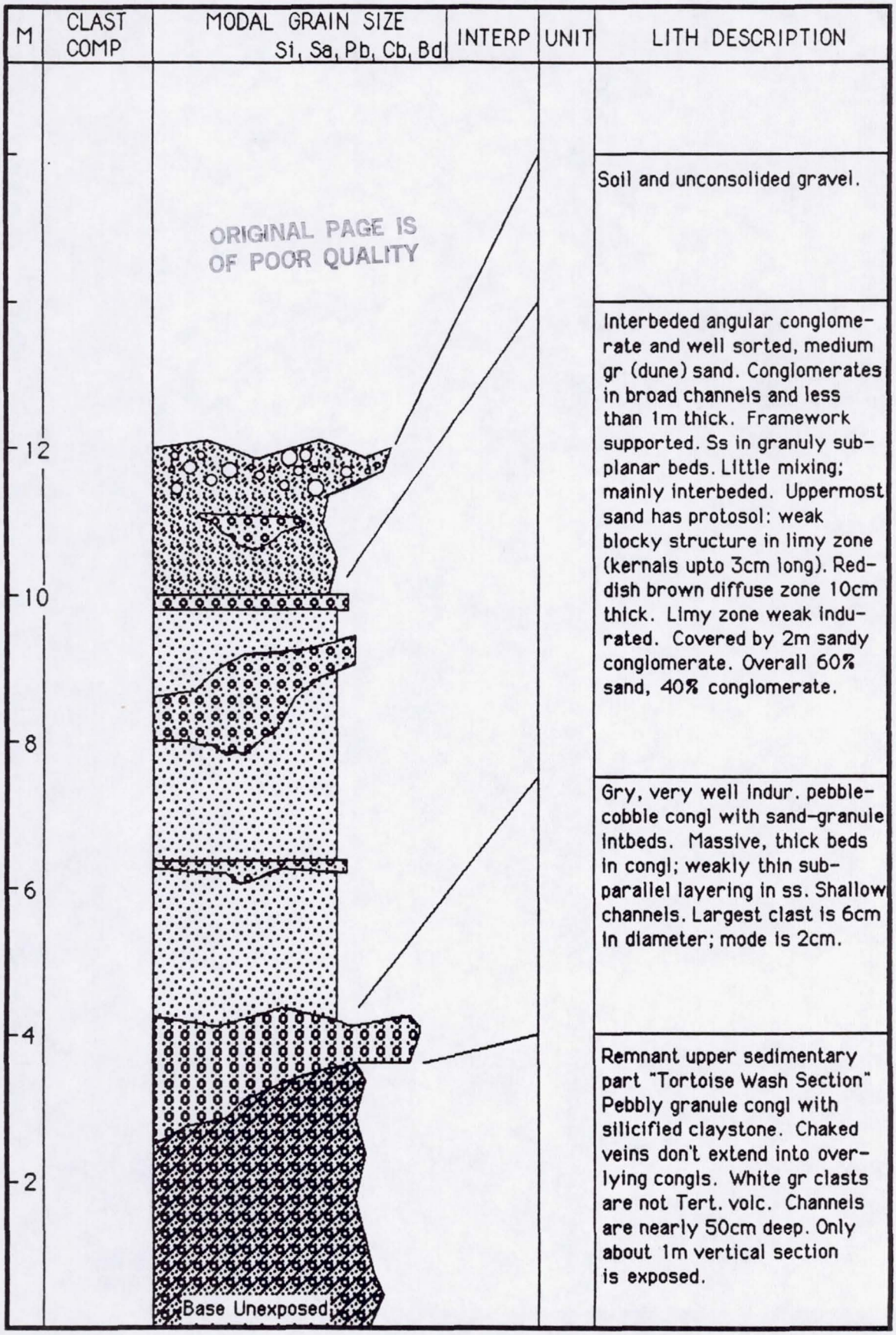

Stratigraphic Relationship at Location 19

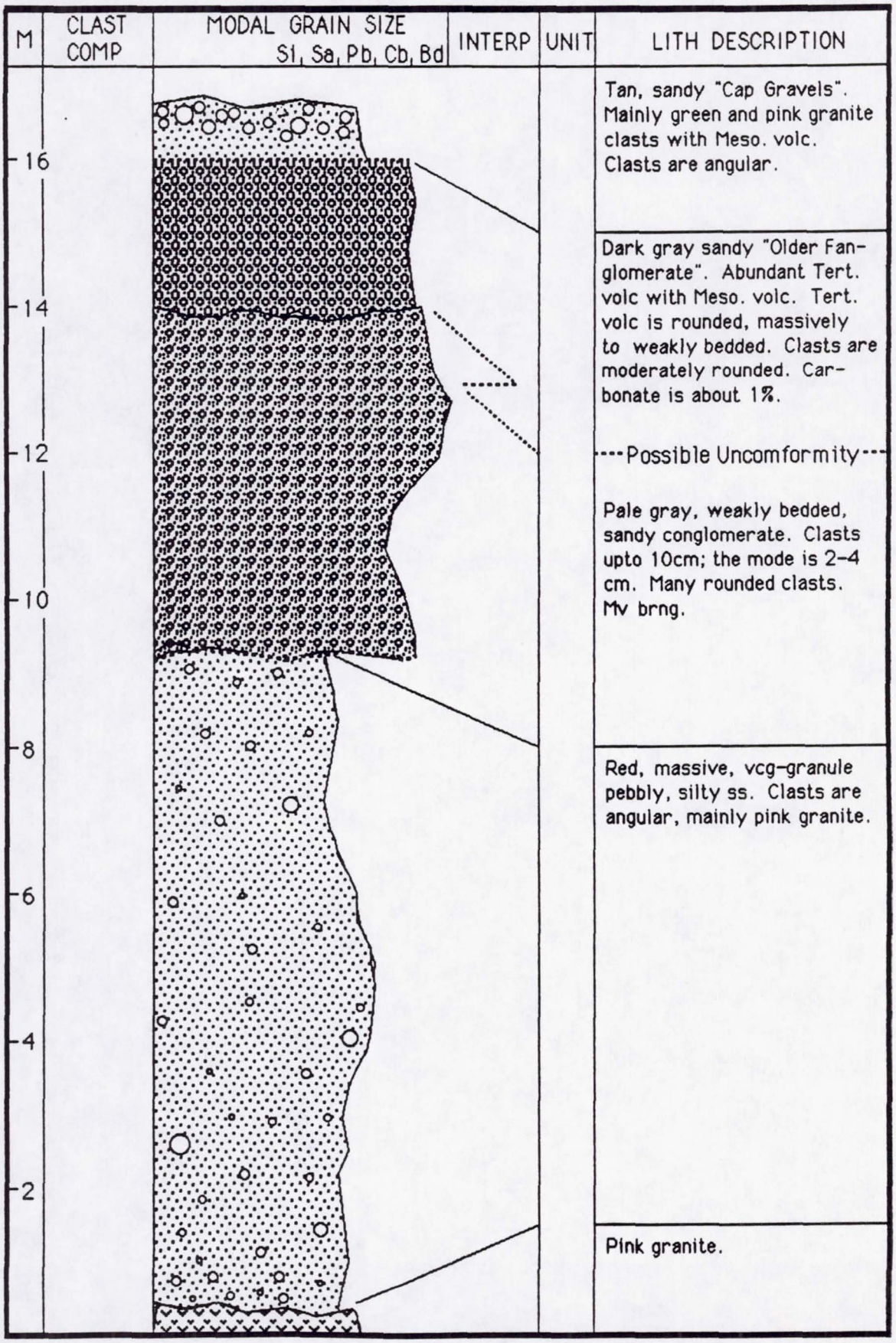

Schematic Section at Loc. 32

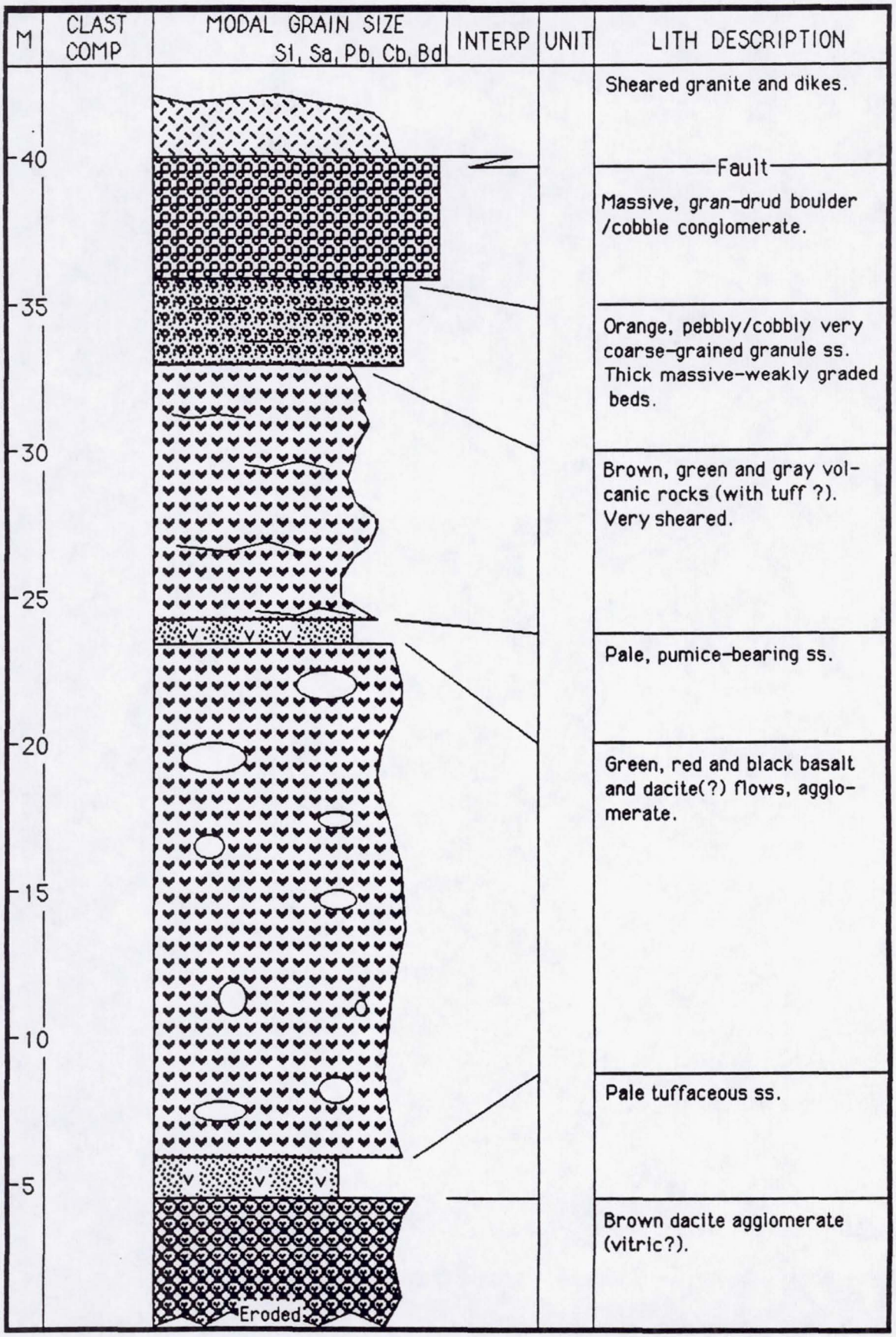

APPENDIX VI. Conglomerate clast counts in Tertiary strata, northern Bristol Mountains (see Figure in text for locations).

EXPLANATION:

GGR = Green granitic
PGr = Pink granitic
Gn = Gneiss
Ft = Felsite (including weskly metamorphosed)
Bt = Basalt
Mv = Metavolcanic
WS = White aphanitic intrusive
Car = Carbonate
Qtz = Quartzite
Otr = Other (includes vein quartz, epidote, metasedimentary rocks)